TRENDS IN SCIENCES 2025; 22(8): 9855
https://doi.org/10.48048/tis.2025.9855
REVIEW ARTICLE

Mitigating Corrosion in Downhole Environments of Oil and Gas Operations: Mechanisms, Challenges, and Control Strategies

Ezz Ahmed[1], Jianguo Liu[1,2] and Jing Liu[1,*]

[1]Department of Chemical and Materials Engineering, University of Alberta, Edmonton, Canada
[2]Shandong Key Laboratory of Oil & Gas Storage and Transportation Safety, College of Pipeline and Civil Engineering, China University of Petroleum (East China), Qingdao, China

([*]Corresponding author's e-mail: jing.liu.arrow@ualberta.ca)

Received: 24 January 2025, Revised: 1 March 2025, Accepted: 10 March 2025, Published: 10 June 2025

Abstract

As oil and gas exploration and production extend into deeper and more challenging environments, the prevalence of acid gases in high-temperature, high-pressure conditions intensifies corrosion risks. This review examines corrosion mechanisms in downhole environments, focusing on the impact of CO_2, H_2S, and O_2, as well as key forms of degradation, including pitting, crevice, under-deposit, stress corrosion cracking, and erosion-corrosion. Corrosion control strategies such as inhibitors, surface coatings, and material selection are analyzed, highlighting their effectiveness and limitations. Additionally, the role of advanced dissolvable tools in enhancing operational efficiency and reducing post-fracture cleanup, their controlled corrosion mechanism, and application case studies are discussed. Despite significant progress, gaps remain in understanding gas interactions, corrosion behavior in extreme conditions, and the long-term performance of mitigation strategies. Future research should focus on refining corrosion prediction models, optimizing material performance, and evaluating economic feasibility, development, and practical use of advanced technologies to ensure reliable and cost-effective downhole operations.

Keywords: Corrosion, High temperature, Downhole environments, Corrosion control techniques, Dissolvable tools

List of abbreviations

Abbreviation	Term
APB	Acid-Producing Bacteria
CCS	Critical Crevice Solution
CCUS	Carbon Capture, Utilization, and Storage
CFV	Critical Flow Velocity
CO2-EOR	Carbon Dioxide Enhanced Oil Recovery
CRA	Corrosion-Resistant Alloy
CS	Carbon Steels
DFP	Dissolvable Frac Plugs
DI	Deionized Water
Ecorr	Corrosion Potential
Erp	Repassivation Potential
HA	Hexamethylenetetramine
HIC	Hydrogen Induced Cracking
HSLA	High Strength Low Alloy Steels
HT/HP	High Temperatures/Pressures
NTG	N-(5,6-diphenyl-4,5-dihydro-[1,2,4] triazin-3-yl)-guanidine
PANI	Waterborne Polyaniline

PBR	Polished Bore Receptacle
PTFE	Polytetrafluoroethylene
SAGD	Steam-Assisted Gravity Drainage
SCC	Stress Corrosion Cracking
SDBS	Sodium dodecylbenzenesulphonate
SRB	Sulfate-Reducing Bacteria
UDC	Under-Deposit Corrosion

Introduction

Corrosion, defined as the detrimental degradation of a material through interactions with its environment [1], is a significant challenge in the upstream oil and gas sector, often leading to unforeseen costs and environmental repercussions. Aqueous phases in production fluids amplify the risk and severity of corrosion, impacting the industry's equipment and materials. Traditionally, carbon steels (CS), favored for their affordability and accessibility, have been extensively used in hydrocarbon extraction infrastructure, despite their susceptibility to corrosion due to their high electrochemical activity [2].

The annual corrosion cost in oil and gas production, estimated at $1.372 billion, notably includes $463 million attributed to downhole tubing expenses [3]. As exploration extends into harsher downhole environments, characterized by high temperatures/pressures (HT/HP), corrosive gases, and acids, the corrosion challenge intensifies. The evolving conditions demand ongoing operational adaptations, tool redesigns, and material revisions to combat corrosion effectively. **Figure 1** encapsulates the common corrosion root causes and types prevalent in downhole settings, illustrating a breakdown of failure types and their associated frequencies, derived from a limited industry-wide survey in the 1980s [4]. CO_2 and H_2S-related failures account for 46 % of the total failures observed, underscoring their corrosive nature in industrial settings. Each type of corrosion observed in a downhole setting will be discussed in later sections.

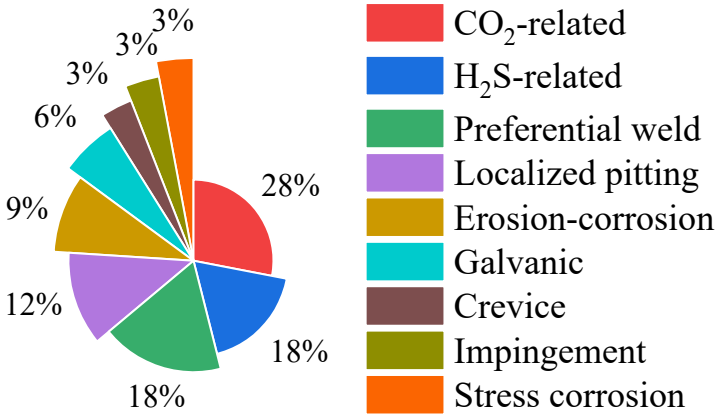

Figure 1 Corrosion-related issues and failure instances encountered in the oil and gas industry [4].

A recent and refined data pulled out from PHMSA (Pipeline and Hazardous Materials Safety Administration) and Government Canada related to corrosion failures and incidents in pipelines is presented in **Figure 2** for the period from 2008 to 2024 [5,6]. The data indicates that corrosion is a major cause of pipeline failures, accounting for an average of 11.5 and 18.7 % of the total failures in Canada and the USA, respectively.

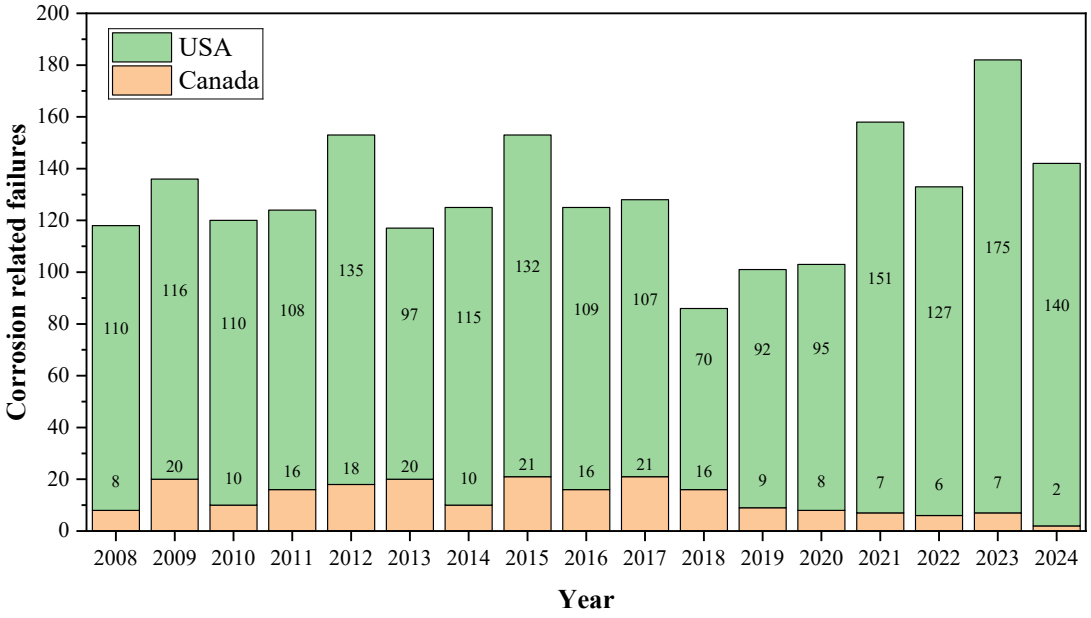

Figure 2 Data for corrosion-related failures in pipelines for the period from 2008 to 2024 in Canada and USA [5,6].

In downhole environments, where aqueous phases mingle with corrosive gases, acids, and brines, corrosion susceptibility escalates under HT/HP conditions. The operating temperatures typically range between 130 (266) and 250 °C (482 °F), coupled with pressures often exceeding 2 MPa (approximately 290 psi) [7,8]. These extreme conditions not only exacerbate corrosion severity but also modify the corrosion mechanisms experienced. Notably, downhole failures stem from the interplay of multiple corrosion and wear processes and their synergistic effects [9]. The presence of CO_2 and H_2S in condensed water phases exacerbates corrosion challenges across oil and gas operations, from production to stages [10]. CO_2, dissolved in water, forms corrosive carbonic acid, while H_2S, acting as a weak acid, releases hydrogen ions, furthering corrosive effects. Oxygen, though not typically present in producing formations, infiltrates during drilling, intensifying corrosion in conjunction with CO_2 and H_2S [11].

Apart from natural downhole aggressors, introduced chemicals like acids and brines during well completion and production significantly influence steel corrosion. Chloride ions, commonly found in brines, are notorious for localized corrosion and stress corrosion cracking (SCC) of downhole facilities [12]. Various oil recovery techniques, involving corrosive species injection, further exacerbate steel corrosion [13-15]. However, oil and gas products can act as organic corrosion inhibitors, mitigating steel corrosion [16,17]. The interplay of these factors, alongside HT/HP and stresses during drilling or production, complicates downhole corrosion analysis and prevention and hinders accurate prediction of corrosion type and rate in lab tests. To mitigate failures, understanding and controlling critical parameters such as reactive gas partial pressures, system pressures, temperatures, chloride content, oxygen levels, aqueous phase properties, and synthetic brine compositions are paramount.

Controlling corrosion rates can often be more cost-effective than attempting complete prevention, given the near-impossibility of eradicating corrosion. The initial step in managing corrosion-related failures is identifying the specific corrosion type. Downhole environments commonly experience pitting corrosion, stress corrosion cracking, crevice corrosion, corrosion under deposits and scales, and erosion-corrosion [18]. Corrosion in these settings often coincides with the formation of iron sulfide (FeS) scale, especially in the presence of H_2S, leading to decreased production and tubing plugging [19]. This FeS scale, originating from the corrosion of carbon steel, lacks the protective properties of a passive film and can even foster localized corrosion, hastening structural failure [20,21]. Furthermore, downhole structures are susceptible to erosion-corrosion due to the continuous impact of multi-

phase fluids containing solid particles [22]. This erosion-corrosion issue costs the oil and gas industry millions annually in efforts to prevent and rectify downhole sand control failures [23].

To combat downhole corrosion, various techniques are employed, including corrosion inhibitors [24], coatings [25], corrosion-resistant alloys (CRAs) [26], and non-metallic composites [27]. Despite the prevailing trend of combating and minimizing corrosion, there exists a niche where controlled and favorable corrosion is harnessed. This approach diverges from the conventional norm of corrosion prevention, showcasing how intentional and strategic corrosion can serve as a valuable tool in advanced technologies, such as dissolvable downhole tools. These dissolvable tools, such as balls and frac plugs, dissolve entirely under downhole conditions after their operational lifespan, eliminating the need for retrieval and enhancing operational efficiency [28]. A dedicated section in this paper will delve further into the principles and applications of this technology, providing a detailed discussion.

Over the past decade, the publication trends reflect a consistent and significant focus on downhole corrosion research. From 2014 to 2024, an average of 67 publications annually addressed downhole corrosion, 60 focused on sour corrosion, and 36 explored sweet corrosion, as depicted in **Figure 3**. These numbers highlight the sustained efforts to advance understanding and address challenges in this critical field. The higher focus on sour corrosion research may be attributed to its more aggressive nature, leading to severe material degradation, particularly in HT/HP environments. Additionally, sour environments often require specialized materials and mitigation strategies due to the presence of H_2S, which poses safety and operational challenges. In contrast, sweet corrosion, while still significant, generally results in less severe damage, possibly explaining the relatively lower number of studies. These trends suggest a prioritization of research efforts based on industry needs and the severity of corrosion related risks.

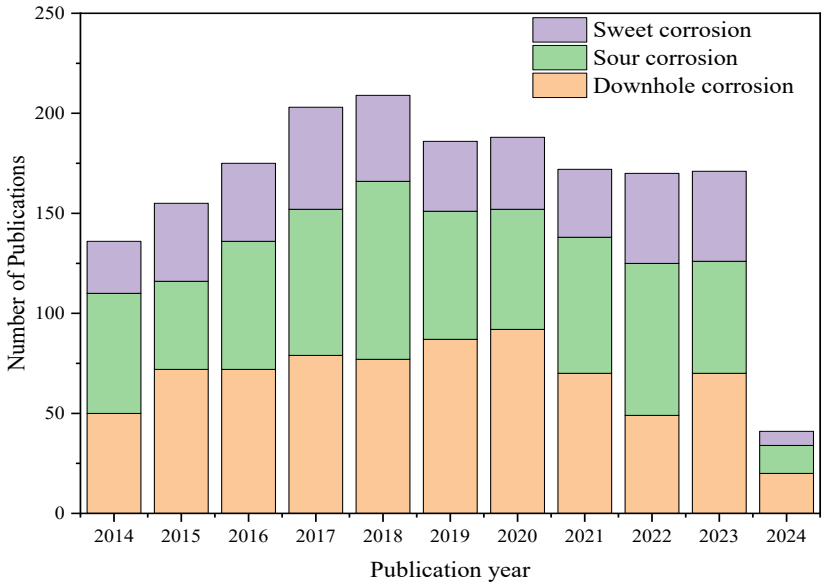

Figure 3 Recent publication records on corrosion issues in downhole environments over the past decade. Data obtained from Scopus (2014 - 2024) searching for downhole corrosion, sour corrosion, and sweet corrosion.

Previous studies have extensively addressed corrosion challenges in oil and gas environments, focusing on a wide range of themes, including corrosion monitoring and controls, i.e., well integrity, [29-35], sour corrosion challenges [36-39], sweet corrosion [35,40-46], and microbial-induced corrosion [47-55]. Thus far, the findings emphasize the importance of continued research and improvement specifically targeting corrosion issues in the oil and gas industry. Choi *et al.* [56] emphasized the critical role of wellbore

integrity, highlighting the risks of casing steel corrosion under CO_2 sequestration conditions and the importance of cement quality in mitigating leakage. Solovyeva *et al.* [29] provided insights into the advancement in corrosion protection, discussing the potential of smart coatings, nanomaterial-based solutions, and environmentally friendly inhibitors to address harsh operational demands. Olorundaisi *et al.* [57] explored the application of High Strength Low Alloy Steels (HSLAs) in pipelines, showcasing the benefits of alloying with chromium and surface treatments to enhance corrosion and wear resistance in petrochemical settings. Additionally, Askari *et al.* [46] examined internal corrosion and cracking in oilfield pipelines, categorizing risks in both sweet and sour service environments and discussing specific corrosion mechanisms and case studies, while Khan *et al.* [58] reviewed various electrochemical techniques for corrosion monitoring in surface and downhole applications, highlighting ongoing challenges and prospects.

Our work stands apart by synthesizing these perspectives and extending the scope to address HT/HP downhole environments, where the effects of CO_2, H_2S, and O_2 pose unique challenges on metallic structures. The discussion extends to various forms of corrosion encountered in downhole environments, offering insights into their implications on pipeline failure. Moreover, we evaluate the countermeasures of current corrosion control strategies identifying their strength and limitations. Uniquely, our work also touches on favorably controlled corrosion through advanced dissolvable alloys, exploring their potential in downhole operations, particularly in enhancing efficiency and reducing post-fracture clean-up in unconventional oil and gas wells. By synthesizing these themes, our review bridges existing knowledge gaps and provides insights to advance corrosion management in challenging operational settings.

Corrosive gases in downhole environments

CO_2 corrosion

CO_2, often referred to as "sweet gas," is a common component in downhole environments. The concentration of CO_2 in wells can vary from 0.5 to 7.5 % depending on geographical factors [2,27,59]. It plays a dual role in oilfield operations: While naturally occurring, CO_2 contributes to corrosion challenges, injected CO_2 is a critical component of Enhanced Oil Recovery (EOR) and Carbon Capture, Utilization, and Storage (CCUS) processes. CO_2-EOR, which increases oil extraction by 15 - 20 %, involves injecting CO_2 into the subsurface to reduce the viscosity and interfacial tension of crude oil, enhancing mobility and recovery [60]. While CO_2-EOR supports sustainability goals by utilizing captured CO_2, its net sequestration potential varies depending on operational practices. Studies indicated that approximately 40 - 60 % of the injected CO_2 is produced with the oil, whereas standalone CCUS processes are designed for permanent storage, aiming for near-total sequestration [61-64]. This distinction highlights that while CO_2-EOR contributes to carbon sequestration, its effectiveness in long-term CO_2 reduction depends on retention rates and project-specific parameters. Both techniques support environmental efforts by utilizing captured CO_2, aligning with global sustainability goals.

Despite its operational benefits, CO_2 poses significant risks to downhole equipment. In the presence of water, CO_2 dissolves to form carbonic acid (H_2CO_3) which initiates "sweet corrosion." This type of corrosion affects materials like CS commonly used in oilfield infrastructure, resulting in degradation that can compromise the integrity of wells and pipelines. Effective management of CO_2-induced corrosion is essential to ensure the longevity and safety of oilfield operations.

Mechanism of CO_2 corrosion

When CO_2 dissolves into formation water, it initiates the corrosion of metals, particularly CS. Dissolved CO_2 undergoes hydration and ionization, releasing hydrogen ions and leading to a decrease in pH. This process, illustrated in Reactions (1) - (3), forms carbonic acid (H_2CO_3), a key driver of CO_2 corrosion. The anodic and cathodic reactions, outlined in Reactions (4) - (6), involve the reduction of hydrogen ions and carbonate to hydrogen gas, further facilitating the corrosion process [42,65,66]. The mechanism is illustrated in **Figure 4**.

$$CO_2 + H_2O \rightleftharpoons H_2CO_3 \quad (1)$$

$$H_2CO_3 \rightleftharpoons H^+ + HCO_3^- \quad (2)$$

$$HCO_3^- \rightleftharpoons H^+ + CO_3^{2-} \quad (3)$$

Anodic reaction: $Fe \rightarrow Fe^{2+} + 2e^-$ (4)

Cathodic reaction: $2H^+ + 2e^- \rightarrow H_2$ (5)

$$H_2CO_3 + 2e^- \rightarrow CO_3^{2-} + H_2 \quad (6)$$

One critical component of CO_2 corrosion is iron carbonate ($FeCO_3$), which forms a protective layer on steel surfaces as illustrated in Reactions (7) [42,67]. $FeCO_3$ precipitates due to its low solubility and can significantly reduce the corrosion rate if the layer is dense and adherent. This primary corrosion product forms a protective film on the metal surface, which can mitigate further corrosion and reduce the overall corrosion rate [68,69]. The formation of $FeCO_3$ was also proposed to take place in a 2-stage reaction, Reactions (8 and 9), where iron bicarbonate ($Fe(HCO_3)_2$) is formed from ferrous ions and bicarbonate ions. The formed $Fe(HCO_3)_2$ decomposes to $FeCO_3$ that precipitates on the metal surface.

$$Fe^{2+} + CO_3^{2-} \rightarrow FeCO_3 \quad (7)$$

$$Fe^{2+} + 2HCO_3^- \rightarrow Fe(HCO_3)_2 \quad (8)$$

$$Fe(HCO_3)_2 \rightarrow FeCO_3 + CO_2 + H_2O \quad (9)$$

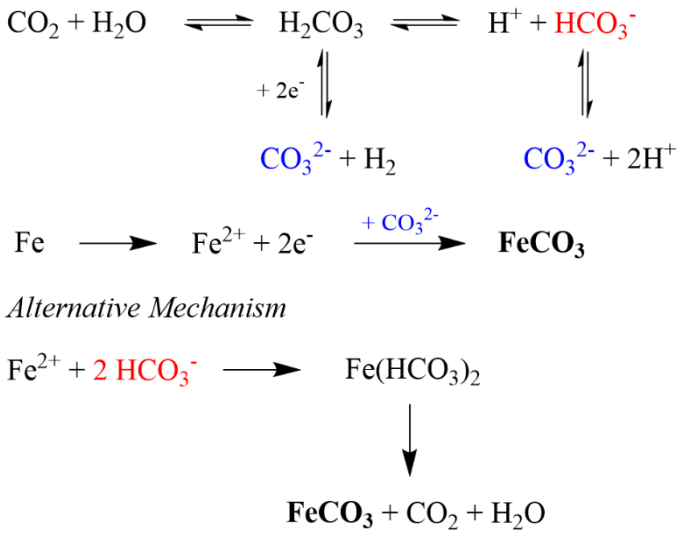

Figure 4 Mechanism of CO_2-induced corrosion.

Figure 5 shows the influence of chloride concentration and temperature. In **Figure 5(a)**, a parabolic trend was observed when the corrosion rate of N80 carbon steel was studied under varying Cl^- concentrations from (0 to 150) g/L [70]. A slight increase in Cl^- concentration significantly influenced the corrosion rate, peaking at 25 g/L after which it drops as Cl^- concentration increases. **Figure 5 (b)** shows the corrosion rate as a function of the temperature of T95, C110, and Q125 carbon steels [71]. The highest corrosion rate was observed at 38 °C, while at 71 and 107 °C, the corrosion rate decreased as protective layers became more stable. The chloride concentration and temperature have similar effects, where the corrosion rate generally decreases as their values increase. This results in reducing the solubility of CO_2 and $FeCO_3$, which promotes the formation of the protective layer. It is important to note that at elevated temperatures localized corrosion and pitting become more prominent due to the possible formation of porous and non-uniform corrosion scales.

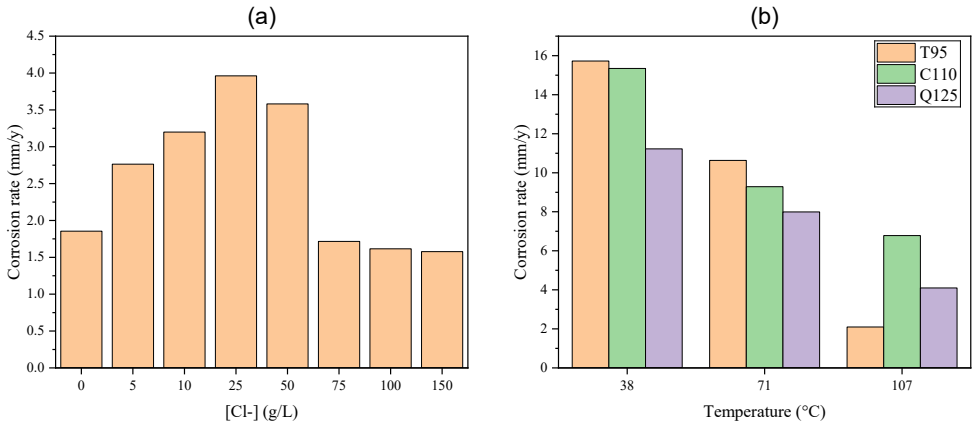

Figure 5 Influence of chloride concentration and temperature on the corrosion rate of carbon steels. (a) The impact of chloride concentration on the corrosion rate of N80 at 20 MPa pCO_2 and 100 °C after 72 h exposure [70], and (b) the impact of temperature on the corrosion rate of T95, C110, and Q125 carbon steels at 20.7 MPa pCO_2 and 2 % NaCl after exposure for 168 h [71].

The protectiveness of this scale depends on multiple factors, including the steel's composition and microstructure, as well as environmental parameters such as CO_2 partial pressure and pH. Controlled formation conditions promote a dense and adherent $FeCO_3$ scale, effectively mitigating further corrosion. Conversely, rapid precipitation can lead to porous and loosely adherent films, which are less protective [69,72]. While the influence of these factors is reviewed elsewhere [73,74]. **Table 1** summarizes their effects on the corrosion behavior and protective layer in CO_2 environments.

Table 1 Summary of factors influencing corrosion behavior and protective layer formation in CO_2 environments.

Factor	Effect on corrosion behavior and protective layer	Reference
pH	Higher pH promotes the formation of bicarbonate and carbonate salts, decreasing $FeCO_3$ solubility and enabling protective layer formation.	[75–77]
Alloying elements	Cr, Mo, and Ni improve $FeCO_3$ film stability by refining microstructure and reducing film porosity. Microalloying elements like V and Ti can improve overall performance by refining the microstructure and forming stable carbides.	[57,73,78]
Oxygen Content	$FeCO_3$ films are unstable in oxygenated environments. Oxygen promotes oxidation of Fe^{2+} to Fe^{3+}, destabilizing films, and increasing cathodic reaction rates.	[79-81]
Iron Content	Adequate Fe^{2+} concentration is necessary for $FeCO_3$ precipitation. The growth rate depends on temperature and supersaturation levels.	[77,82,83]
Flow Velocity	High flow velocities hinder $FeCO_3$ film formation, remove existing films, or retard growth, increasing corrosion rates. Erosion-corrosion and localized corrosion are significant concerns.	[84-87]
CO_2 Partial Pressure	Increased CO_2 pressure lowers pH, increasing corrosion product solubility and enhancing H^+ ion availability, leading to higher uniform corrosion rates.	[76,88-91]
Temperature	The corrosion rate increases at low temperatures (<60 °C), but protective $FeCO_3$ films form more readily at higher temperatures. Film failure can lead to localized corrosion, particularly in conditions similar to oil and gas pipelines.	[75,77,86,89,92-94]

Factor	Effect on corrosion behavior and protective layer	Reference
Surface roughness	Higher surface roughness increases the surface area, accelerating the corrosion process. It also disturbs uniform film formation, leading to weaker, less protective $FeCO_3$ layers.	[95,96]
Water Content	Water reacts with CO_2 to form carbonic acid, which is highly corrosive to carbon steel. Dehydrating CO_2 before transportation is critical to mitigate this risk.	[97-101]
Presence of SO_2	SO_2 reduces pH and increases H^+ ion concentration, leading to an elevated corrosion rate in CO_2 pipelines.	[102-105]

Role of CO_2 solubility in corrosion

A key factor in CO_2-induced corrosion is its solubility in brine. CO_2 solubility is influenced by temperature and pressure, which significantly impact the corrosion environment. It decreases with increasing temperatures, leading to a less aggressive corrosion environment due to reduced carbonic acid formation (Reactions (1) - (3)) [42]. Conversely, increasing pressure enhances CO_2 solubility, intensifying the corrosion environment. **Figure 6** illustrates an example of CO_2 solubility in deionized and brine water at pressures of 1 - 2 MPa across various temperatures [64]. The balance of these effects underlies operational decisions in oilfield production to minimize corrosion risks.

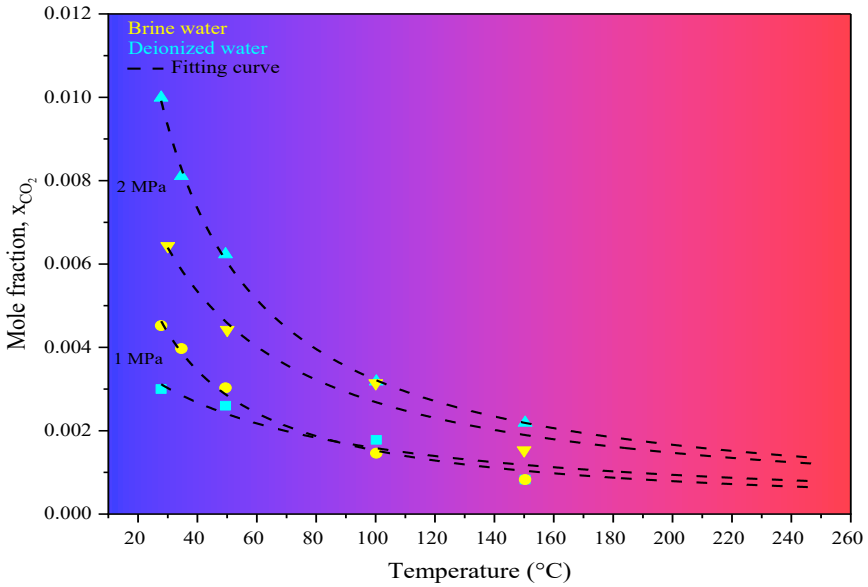

Figure 6 Mole fraction of gaseous CO_2 (1 and 2 MPa) dissolved in DI and brine water at different temperatures [106].

Finally, it is important to note that in the absence of water, no hydration of CO_2 or metal ions occurs, effectively halting the electrochemical corrosion process. Dry CO_2, whether under low pressures or supercritical conditions, does not provide the necessary water molecules to support corrosion reactions [99,107]. This highlights the critical role of water presence in governing CO_2-induced corrosion in downhole environments.

CO_2 corrosion in downhole environments

In downhole environments, CO_2 can occur as a gas or supercritical phase. Supercritical CO_2 is a unique phase of carbon dioxide, occurring above its critical temperature of 31.1 °C and critical pressure of 7.38 MPa. In this state, CO_2 behaves as both a gas and a liquid, having high density and diffusivity. This environment is particularly relevant in applications such as CCUS and EOR.

Al-Hashem *et al.* [108] studied the corrosion of L80 steel in simulated oil well conditions at various temperatures and pressures with saturated pure CO_2. They reported a maximum corrosion rate of 1.8 mm/y at 6.89 MPa (1,000 psi) CO_2 pressure and 90 °C. Similar trends were observed for N80 steel in CO_2-saturated formation water for 168 h, with the corrosion rate increasing as temperature increased up to 60 °C and 5 MPa, achieving a maximum weight-loss corrosion rate of 10 mm/y [92]. Whittaker *et al.* [109] also observed a maximum corrosion rate of 1.75 mm/y for CS in a steam-assisted gravity drainage (SAGD) brackish water system at 90 °C.

Various alloys have been investigated under supercritical CO_2 conditions, further illustrating the influence of CO_2 partial pressure (pCO_2), pressure, and temperature on the corrosion rate. Elgaddafi *et al.* [91] studied the corrosion behavior of C110 carbon steel under varying pCO_2 and at 38 °C and different total pressures (20.68, 41.37 and 62.05 MPa). At low overall pressure, the corrosion rate of C110 increased with increasing pCO_2, owing to the enhanced dissolution of CO_2 in the brine, which raised the acidity and lowered the pH. At 38 °C and 100 % pure pCO_2, the corrosion rate reached its maximum of 14.21 mm/y at 20.68 MPa and the corrosion was uniform. The corrosion rate was notably reduced with increasing pressure. A behavior described by the formation of a protective scale, inhibiting the corrosion process. In another study, they reported the average corrosion rates of T95, C110, and Q125 carbon steels at 38 °C and 41.37 total pressure, with ~50 % pCO_2 [110]. The obtained values were 14.6, 12.8 and 3.0 mm/y for T95, C110, and Q125 carbon steel, respectively. Q125 carbon steel exhibited high corrosion resistance, owing to the presence of manganese, nickel, and chromium.

The effect of CO_2 corrosion on chromium-containing steels was investigated by Trasatti *et al.* [111]. A similar behavior was observed when pCO_2 was increased from 1.0 to 1.4 MPa at 100 °C. The average corrosion rate of 9.78Cr and 8.53Cr increased from 0.13 to 0.32 and from 0.6 to 0.59 mm/y, respectively, when CO_2 partial pressure increased. In addition, they reported the corrosion rate of 8.95Cr, 8.93Cr, and AISI 410, having values of 0.17, 0.16, and 0.013 mm/y, respectively, at 150 °C and 1.4 pCO_2.

Hassani *et al.* [112] assessed the CO_2 corrosion behavior of AISI 1018, 13Cr (S41000), and 5Cr (A182) in the gas phase (3 MPa) and supercritical phase (8 MPa) at 60 °C. Regarding corrosion resistance, 13Cr steel exhibited excellent corrosion resistance (~0.1 mm/y) followed by 5Cr steel (~6 mm/y) and carbon steel (~20 mm/y) at 3 and 8 MPa pCO_2. This observed behavior is in agreement with the previously discussed formation of the Cr-containing corrosion product layer, which acts as a diffusion barrier, blocking corrosion species from reaching the metal surface and reducing the corrosion rate. The decrease in the corrosion rate of chromium steels was also observed when the pCO_2 increased from 3 to 8 MPa, while the opposite was observed for carbon steel, which was explained by the higher solubility of CO_2 leading to lower pH.

A similar observation was found in Kermani *et al.* [113] study of the corrosion performance of 3Cr steels and L80 steel in 10 % NaCl at 0.1 MPa CO_2 and 50, 80 and 120 °C. At 50 °C the corrosion rates for 3Cr-A and 3Cr-B (see Appendix A for their respective compositions) are lower (2.9 and 4.0 mm/y, respectively) compared to L80 steel (8.5 mm/y). The trend continues at 80 and 120 °C, with both 3Cr-A and 3Cr-B demonstrating lower corrosion rates, owing to the formation of Cr-enriched protective layers on 3Cr steel samples. It is worth mentioning that at 120 °C, the corrosion rate of 3Cr steels decreased to 0.32 and 0.41 mm/y for 3Cr-A and 3Cr-B, respectively, compared to the continuous increase of corrosion rate for L80 carbon steel from 8.5 mm/y at 50 °C to 13 mm/y at 120 °C. This behavior is in agreement with Hassani *et al.* [112] findings. **Table 2** summarizes the performance of various alloys in sweet corrosion at different conditions.

The Cr-enriched protective layers formed on Cr-containing steels play a crucial role in mitigating corrosion, primarily by acting as a diffusion barrier that limits the penetration of aggressive species. These layers are typically composed of chromium oxides and mixed with iron carbonate phases, which enhance the overall stability of the steel surface. In CO_2 corrosion, an additional anodic reaction takes place, relating to the formation of $Cr(OH)_3$ when the steel matrix contains Cr [114]. The amorphous $Cr(OH)_3$ possesses a dense structure, reducing the diffusion channels and porosity in the corrosion film. Under downhole conditions of 50 °C, 8 MPa, and 1 MPa pCO_2, the corrosion product of

2Cr steels has a dense morphology, with corrosion film thickness of 41.4 and 13.1 μm for static and dynamic conditions [115]. The Cr-enriched inner layer acts as a barrier, limiting the penetration of Cl^- ions to the metal matrix. This reduction in anion concentration at the film-metal interface helps suppress the metal corrosion.

Environmental and operational factors play a critical role in corrosion behavior, influencing the formation and stability of protective layers on carbon steel surfaces. While a summary of these factors was presented in **Table 1**, this section focuses exclusively on the influence of corrosive gases encountered in downhole environments. The following subsections will discuss the roles of H_2S and O_2, providing a detailed examination of their impact on corrosion mechanisms.

Table 2 Performance summary of various alloys under sweet corrosion conditions.

Material	Temperature (°C)	pCO_2 (MPa)	Corrosion rate (mm/y)	Exposure time (h)	Electrolyte	Ref.
N80	100	1.7	2.40	72	0.35 M NaCl	[116]
X65	120	0.7	34.30	24	0.08 M [Cl^-]	[2]
3Cr80	90	0.4	1.13	168	0.55 M [Cl^-]	[117]
3Cr-A	50	0.1	2.90	144	10 % NaCl	[113]
3Cr-A	80	0.1	1.10	144		
3Cr-A	120	0.1	0.32	144		
3Cr-B	50	0.1	4.00	144		
3Cr-B	80	0.1	1.20	144		
3Cr-B	120	0.1	0.41	144		
L80	50	0.1	8.50	144		
L80	80	0.1	7.60	144		
L80	120	0.1	13.00	144		
9A (9.78Cr)	100	1.0	0.13	720	1.71 M NaCl pH 4.2	[111]
9A (9.78Cr)	100	1.4	0.32	720		
9B (8.95Cr)	150	1.4	0.17	720		
9C (8.93Cr)	150	1.4	0.16	720		
9D (8.53Cr)	100	1.0	0.60	720		
9D (8.53Cr)	100	1.4	0.36	720		
AISI410	150	1.4	0.01	720		
CS (AISI 1018)	60	3.0	14.86	48	1.18 NaCl, pH 6.3	[112]
CS (AISI 1018)	60	8.0	18.03	48		
5Cr (A182)	60	3.0	9.88	48		
5Cr (A182)	60	8.0	6.26	48		
13Cr (S41000)	60	3.0	0.48	48		
13Cr (S41000)	60	8.0	0.13	48		
CS (C110)	38	10.34	6.66	168	2 % NaCl	[91]
CS (C110)	38	15.51	6.40	168		

Material	Temperature (°C)	pCO_2 (MPa)	Corrosion rate (mm/y)	Exposure time (h)	Electrolyte	Ref.
CS (C110)	38	20.68	14.22	168		
CS (C110)	38	10.34	12.72	168		
CS (C110)	38	20.68	12.81	168		
CS (C110)	38	31.03	12.66	168		
CS (C110)	38	41.37	6.81	168		
CS (C110)	38	15.51	12.61	168		
CS (C110)	38	31.03	11.96	168		
CS (C110)	38	46.54	14.07	168		
CS (C110)	38	62.05	10.80	168		
CS (T95)	38	20.68	14.62	168		
CS (C110)	38	20.68	12.79	168	2 % NaCl	[110]
CS (Q125)	38	20.68	2.99	168		

Influence of H_2S presence on CO_2 corrosion

H_2S, known as "sour gas," is present in various stages of oil and gas processes, including extraction, transportation, and refining, typically at concentrations ranging from 0 to 10 % [2,19]. Driven by the activity of sulfate-reducing bacteria (SRB), the risks of H_2S corrosion and microbiologically induced corrosion in oil and gas systems are significantly amplified [118]. These bacteria contribute to the increased presence of H_2S gas in production lines, even in fields previously considered sweet. SRB activity is particularly pronounced at the interfaces where produced water, seawater, and steel surfaces meet, creating favorable conditions for the formation and growth of biofilms. The chemical environment at these interfaces, enriched with volatile fatty acids, further promotes SRB proliferation [119].

SRB are anaerobic microorganism that utilizes sulfate (SO_4^-) as an electron acceptor, reducing it to H_2S while metabolizing organic compounds or hydrogen. This biological process not only increases H_2S concentration in production systems but also promotes the formation of biofilms on metal surfaces, altering local electrochemical conditions and facilitating corrosion [120]. These bacterial biofilms create microenvironments with distinct pH and ion concentration gradients, leading to localized corrosion such as pitting and under-deposit corrosion. Different SRB strains exhibit varying levels of aggressiveness depending on their metabolic pathways and environmental conditions. A detailed review of the characteristics and habitats of thermophilic SRB can be found in [55]

Additionally, the formation of FeS layers due to SRB activity can have both protective and damaging effects on carbon steel. While dense FeS layers may reduce further corrosion under certain conditions, porous or loosely adherent FeS films can act as conductive pathways, facilitating electron transfer and accelerating localized attack [121]. The structural integrity and adhesion properties of FeS films depend on multiple factors, including H_2S concentration, bacterial activity, and alloy composition.

When H_2S dissolves into water and ionizes, it generates H^+ ions and creates a low pH environment, leading to the corrosion of metals. The H^+ ions readily capture electrons, accelerating both anodic iron dissolution and cathodic hydrogen evolution. Due to its corrosive nature, H_2S production often necessitates specialized production equipment, such as stainless-steel tubing, which can be costly. Similar to CO_2, H_2S is usually non-corrosive in the absence of water.

The corrosion products formed in downhole environments due to H_2S include polymorphous iron sulfides such as amorphous FeS, mackinawite FeS, cubic ferrous sulfide FeS, troilite FeS, pyrrhotite $Fe_{1-x}S$, pyrite FeS_2. The formation of these corrosion products is influenced by factors such as pH, temperature, and duration of exposure [122-124]. Bai *et al.* [125] characterized the crystal structure and morphology of

these corrosion products in an aqueous H_2S environment.

Different corrosion products have varying effects on steel corrosion in H_2S environments. Under specific conditions, Ma *et al.* [126] observed the formation of metastable mackinawite, which subsequently converted into troilite and pyrite, exhibiting an inhibiting effect on iron corrosion. Mackinawite, being porous, offers limited protection and can result in high corrosion rates [18]. Pehlke reported a maximum corrosion rate of 1.8 mm/y for 1018 CS in environments of SAGD wells containing H_2S, with the corrosion products identified as pyrrhotite [127]. Due to its very low solubility, FeS is easier to identify as the main corrosion product [128,129], and its formation can be described by Reactions (10) - (14). H_2S dissociates, as shown in Reaction (13), to form hydrogen (H^+) and hydrogen sulfide ions (HS^-. The HS^- ions dissociate further to sulfide ions (S^{2-}) and H^+, Reaction 11. The cathodic reactions involve the reduction of H^+ to form hydrogen gas, as well as the formation of FeS, as shown in Reactions (13) - (14).

$$H_2S \rightleftharpoons HS^- + H^+ \quad (10)$$

$$HS^- \rightleftharpoons S^{2-} + H^+ \quad (11)$$

Anodic reaction: $Fe \rightarrow Fe^{2+} + 2e^-$ (12)

Cathodic reaction: $2H^+ + 2e^- \rightarrow H_2$ (13)

$$Fe^{2+} + S^{2-} \rightarrow FeS \quad (14)$$

The main corrosion product, FeS, has very low solubility in water or water-based muds, where H_2S, HS^-, and S^{2-} ions are in dynamic equilibrium with water, H^+, and OH^- ions, depending on pH [42,69]. At low pH, H_2S is dominant, while the HS^- ion becomes dominant at mid-range pH, and S_2 ions dominate at high pH. This equilibrium dictates that sulfide ions revert to H_2S if pH decreases.

A comparative analysis of the impact of varying H_2S on CO_2 corrosion is discussed by Rida Elgaddafi *et al.*, where they provided valuable insights into the corrosion behavior of 3 carbon steels - T95, C110, and Q125 - in CO_2 and H_2S environments [110]. Their study highlights the significant influence of H_2S on both corrosion rates and the characteristics of corrosion scales formed on these materials. The corrosion tests were conducted at 38 °C and 41.37 MPa total pressure, with pCO_2 of approximately 50 % and varying H_2S concentrations of 0, 10, 50, and 150 ppm. Generally, the addition of H_2S to CO_2 environments in small quantities accelerates the corrosion, while higher concentrations can lead to the formation of protective scales that inhibit the corrosion.

For T95 carbon steel, the corrosion rate increased from 14.62 mm/y, in CO_2 only environment, to 19.67 mm/y when 10 ppm H_2S was introduced. Interestingly, as the H_2S concentration increased to 50 ppm H_2S, the corrosion rate decreased to 16.17 mm/y, likely due to the formation of a partially protective scale. However, at 150 ppm H_2S, the rate rose slightly to 17.16 mm/y, attributed to the breakdown of the protective layer. Similarly, for C110, an initial rise in the corrosion rate from 12.79 mm/y in CO_2 only environment to 13.97 mm/y when 10 ppm H_2S was introduced. This was followed by a significant reduction to 9.36 mm/y at 50 ppm H_2S, suggesting the formation of a more stable protective layer.

In contrast, the corrosion rate of Q125 in CO_2 only environment was initially 2.99 mm/y, and increased to 9.26 mm/y when 10 ppm H_2S was introduced. The alloy exhibited a steady increase in corrosion rates from 9.26 mm/y at 10 ppm H_2S to 9.94 at 50 and 10.05 mm/y at 150 ppm. This behavior was attributed to the nature of the corrosion scales: Denser and more effective at lower H_2S concentrations but becoming more porous and scattered at higher concentrations, reducing their protective effectiveness.

In addition to carbon steels, the corrosion performance of martensitic and low-alloy steels in downhole environments was studied by S. Trasatti *et al.* [111]. They investigated the corrosion behavior of 9Cr-1Mo steel grades and martensitic steels, including AISI 410 and Super 13Cr, at 2 temperatures of 100 and 150 °C, 2 CO_2 partial pressures of 1.0 and 1.4 MPa, and H_2S partial pressures of 10 kPa. The study reported moderate corrosion rates for 8.95Cr and 8.93Cr steels, ranging from 0.08 to 0.44 mm/y, depending on the temperature and partial pressures of CO_2 and H_2S. AISI 410 exhibited excellent corrosion resistance, with a corrosion rate as low as 0.001 mm/y at 100 °C, with

pCO_2 and pH_2S of 1.0 MPa and 10 kPa, respectively, and 0.07 mm/y at 150 °C, with pCO_2 and pH_2S of 1.4 MPa and 10 kPa, respectively. Similarly, Super 13Cr showed strong performance, with a corrosion rate of 0.02 mm/y at 150 °C, 1.0 MPa pCO_2, and 10 kPa pH_2S. A slight increase in corrosion rate to 0.04 mm/y was observed when pCO_2 was increased to 1.4 MPa.

Liu *et al.* [130] further contributed to the understanding of alloy performance in downhole environments by investigating the corrosion behavior of HS110S steel at temperatures ranging from 150 to 350 °C, 0.25 MPa pCO_2, and 0.17 kPa pH_2S. Their findings revealed pronounced effects of temperature on the corrosion rate. Under static conditions, the corrosion rate increased with increasing temperature. At 150 °C, the corrosion rate was 0.11 mm/y which increased to 0.97 mm/y at 350 °C. The tests were also conducted under dynamic conditions, at which corrosion rates were reported higher due to the enhanced mass transfer of corrosion species and the fluid shear stresses that could disturb the protective corrosion product layer.

Similarly, Kermani *et al.* [113] examined the corrosion performance of 3Cr steels and L80 steel in 10 % NaCl at 50 °C, 0.095 MPa pCO_2, and 5 kPa pH_2S. Their results showed that L80 steel exhibited a higher corrosion rate of 2.9 mm/y, whereas 3Cr steel demonstrated better corrosion resistance with a rate of 0.56 mm/y. A similar behavior was observed in their study for sweet corrosion, where the Cr-enriched protective layer acts as a diffusion barrier and inhibits the corrosion.

Ren *et al.* [116] studied the relationship between corrosion rates and pH_2S for N80, investigating the influence of H_2S partial pressure at 100 °C and 1.7 MPa pCO_2. For N80 steel, introducing H_2S at 2 kPa resulted in a high corrosion rate of 3.08 mm/y. However, as pH_2S increased to 10 kPa, the corrosion rate decreased sharply to 0.96 mm/y, and further increases to 14 and 20 kPa reduced the corrosion rate to 0.69 and 0.54 mm/y, respectively. This behavior was attributed to the formation of protective iron sulfide films at higher pH_2S.

Yan *et al.* [117] studied the pH_2S influence on 3Cr80 steel at 90 °C and 0.4 pCO_2, under dynamic conditions, by varying pH_2S from 0.2 to 400 kPa. Their study revealed that as pH_2S increased from 0.2 to 4 kPa, the corrosion rate steadily decreased, with the minimum corrosion rate of 0.72 and 0.71 mm/y occurring at 0.8 and 4 kPa. Beyond this range, a different trend was observed, as pH_2S increased to 80 kPa the corrosion rate rose to 1.52 mm/y, and at 400 kPa, it doubled to 2.1 mm/y compared to pure pCO_2 conditions. The findings highlighted a dual effect of H_2S, where at low levels, protective layers effectively reduced the corrosion rate, while at higher levels, these layers became unstable, leading to increased general and localized corrosion.

These findings collectively emphasize the complex interactions between environmental factors - such as temperature, fluid dynamics, presence of H_2S - and alloy composition. They also underscore the critical role of protective scale formation and stability in mitigating corrosion in CO_2-H_2S environments. **Table 3** summarizes the performance of various alloys under sour corrosion conditions across different conditions

Table 3 Performance summary of various alloys under sour corrosion conditions.

Material	Temperature (°C)	pCO_2 (MPa)	pH_2S (kPa)	Corrosion rate (mm/y)	Exposure time (h)	Electrolyte	Ref.
9B (8.95Cr)	100	1	10	0.09	720		
9C (8.93Cr)	100	1	10	0.08	720		
AISI 410	100	1	10	0.001	720		
9A (9.78Cr)	100	1.4	10	0.14	720		
9D (8.53Cr)	100	1.4	10	0.36	720	1.71 M NaCl	[111]
9A (9.78Cr)	150	1	10	0.28	720		
9B (8.95Cr)	150	1	10	0.34	720		
9C (8.93Cr)	150	1	10	0.31	720		
9D (8.53Cr)	150	1	10	0.36	720		

Material	Temperature (°C)	pCO_2 (MPa)	pH_2S (kPa)	Corrosion rate (mm/y)	Exposure time (h)	Electrolyte	Ref.
9A (9.78Cr)	150	1.4	10	0.18	720		
9B (8.95Cr)	150	1.4	10	0.27	720		
9C (8.93Cr)	150	1.4	10	0.44	720		
9D (8.53Cr)	150	1.4	10	0.22	720		
AISI 410	150	1.4	10	0.07	720		
Super 13	150	1.4	10	0.04	720		
CS (T95)	38	20.69	10	19.67	168	2 % NaCl	[110]
CS (T95)	38	20.69	50	16.17	168		
CS (T95)	38	20.69	150	17.16	168		
CS (C110)	38	20.69	10	13.97	168		
CS (C110)	38	20.69	50	9.36	168		
CS (Q125)	38	20.69	10	9.26	168		
CS (Q125)	38	20.69	50	9.94	168		
CS (Q125)	38	20.69	150	10.05	168		
L80	50	0.095	5	2.9	144	10 % NaCl	[113]
3Cr	50	0.095	5	0.56	144		
N80	100	1.7	2	3.08	72	0.35 M NaCl	[116]
N80	100	1.7	10	0.95804	72		
N80	100	1.7	14	0.6919	72		
N80	100	1.7	20	0.53815	72		
HS110S	150	0.25	170	0.2413	168	0.90 M NaCl	[130]
HS110S	200	0.25	170	0.6761	168		
HS110S	250	0.25	170	1.3153	168		
HS110S	350	0.25	170	1.9236	168		
3Cr80	90	0.4	0.2	0.76	168	0.48 M NaCl	[117]
3Cr80	90	0.4	0.4	0.77	168		
3Cr80	90	0.4	0.8	0.72	168		
3Cr80	90	0.4	4	0.71	168		
3Cr80	90	0.4	80	1.52	168		
3Cr80	90	0.4	400	2.1	168		

Influence of O_2 presence on CO_2 corrosion

In oilfield operations, oxygen-induced corrosion poses a significant challenge, particularly for the internal surfaces of production equipment. Oxygen is typically absent at depths below 100 m (330 feet); however, contamination can occur in facilities where processing and handling of produced fluids take place near atmospheric pressure. Common sources of oxygen ingress include leaking seals in pumps, venting through casing or process systems, open hatches, and exposure during operations such as drilling and mud pit handling [131].

Oxygen is a potent oxidizing agent with rapid reduction kinetics, shown by Reaction (15):

$$\frac{1}{2}O_2 + H_2O + 2e^- \rightarrow 2OH^- \quad (15)$$

Its solubility in water and brines is relatively low, making the rate of oxygen transport a limiting factor in the corrosion processes of carbon and low-alloy steels, especially in non-acidic conditions. This limited transport also contributes to localized corrosion, such as crevice corrosion and under-deposit attacks arising from restricted oxygen flow in certain areas [132,133].

The presence of O_2 in CO_2-dominated environments can significantly elevate the corrosion rate of steels. Zhang *et al.* [66] demonstrated that O_2 reacts with $FeCO_3$, promoting CO_2 hydration and increasing H^+ concentrations, as shown in Reaction (16):

$$4FeCO_3 + O_2 + 4H_2O \rightarrow 2Fe_2O_3 + 4H_2CO_3 \quad (16)$$

This reaction undermines the formation of compact and protective $FeCO_3$ scales on steel surfaces, increasing their susceptibility to corrosion. Lin *et al.* [134] studied 3Cr steel in O_2-CO_2 environments under HT/HP, observing the formation of porous iron hydroxides rather than protective $Cr(OH)_3$ scales. Similarly, Zhang *et al.* [135] reported that O_2 exacerbates N80 steel corrosion, varying its effects on temperature and O_2 concentration.

Oxygen contamination in downhole environments can result from processes such as the reinjection of produced water, CO_2, and inhibitors [136,137]. Air-assisted steam injection for secondary oil recovery, for instance, introduces O_2 concentrations of 5 to 20 % under HT/HP conditions [137]. Additionally, trace amounts of O_2 are introduced during thermal exploitation methods [138,139]. Even at low concentrations, O_2 strongly enhances corrosion at elevated temperatures due to its depolarizing nature [140].

In O_2-containing environments, the cathodic reaction shifts to O_2 reduction, as shown in Reaction (18). The ferrous ions produced in the anodic reaction (Reaction (17)) combine with hydroxide ions to form iron hydroxide (Reaction (19)), which further oxidizes and dehydrates at higher temperatures to form iron oxides (Reactions (20) and (21)) [66]:

Anodic reaction: $$Fe \rightarrow Fe^{2+} + 2e^- \quad (17)$$

Cathodic reaction: $$O_2 + 2H_2O + 4e^- \rightarrow 4OH^- \quad (18)$$

$$4Fe(OH)_2 + O_2 + 2H_2O \rightarrow 4Fe(OH)_3 \quad (19)$$

$$Fe(OH)_2 + 2Fe(OH)_3 \rightarrow Fe_3O_4 + 4H_2O \quad (20)$$

$$2Fe(OH)_3 \rightarrow Fe_2O_3 + 3H_2O \quad (21)$$

Xiang *et al.* [93] studied X70 steel in CO_2/SO_2/O_2/H_2O environments and found that the corrosion rate rises with temperature, peaks, and then declines. This behavior is attributed to reduced O_2 solubility at high temperatures and the protective nature of the corrosion product layer. The presence of SO_2 in CO_2 corrosive environments can influence the corrosion mechanism. SO_2 ionizes when dissolved in water to form hydrogen sulfite (HSO_3^-) and sulfite (SO_3^-) ions, Reactions (22) and (23). The sulfite ions then react with Fe^{2+} to precipitate $FeSO_3$, Reaction (24), which competes with $FeCO_3$ formation, affecting the protectiveness of the corrosion scale.

$$SO_2 + H_2O \rightarrow H^+ + HSO_3^- \quad (22)$$

$$HSO_3^- \rightarrow H^+ + SO_3^{2-} \quad (23)$$

$$Fe^{2+} + SO_3^{2-} \rightarrow FeSO_3 \quad (24)$$

The presence of O_2 further modifies the corrosion process by oxidizing sulfite ions to sulfate ions, leading to the formation of $FeSO_4$ instead, as per Reaction (25). However, Hua *et al.* [141] study did not report the formation of $FeSO_4$, when carbon steel was exposed to static water-saturated CO_2 in the presence of 20 ppm O_2 and (2, 50 and 100) ppm SO_2 at 35 °C and 8 MPa for 48 h exposure. In contrast, Xiang *et al.* [105]; Choi *et al.* [142] observed $FeSO_4$ on the steel surface under different test conditions. Xiang *et al.* [105] performed tests at 10 MPa and 50 °C, exposing the steel to water-saturated CO_2 with 0.02 - 0.2 MPa SO_2 and a significantly higher O_2 concentration of 1,000 ppm. Similarly, Choi *et al.* [142] conducted experiments with 0.08 MPa SO_2 and 0.33 MPa O_2 in water-saturated CO_2 conditions at 8 MPa and 50 °C. The formation of $FeSO_4$ in these studies indicates that both the SO_2 and O_2 concentrations influence its precipitation. A higher O_2 level enhances oxidation reactions, converting sulfite (SO_3^{2-}) to sulfate (SO_4^{2-}), which subsequently reacts

with Fe^{2+} to form $FeSO_4$, as shown in Reactions (25) and (26). The lack of $FeSO_4$ detection in Hua *et al.* [141]'s study was explained by the lower O_2 concentration (20 ppm), which might not have been sufficient to drive the oxidation of sulfite to sulfate, preventing $FeSO_4$ formation under their experimental conditions.

$$2\,SO_3^{2-} + O_2 \rightarrow 2\,SO_4^{2-} \quad (25)$$

$$Fe^{2+} + SO_4^{2-} \rightarrow FeSO_4 \quad (26)$$

Carbon steels are particularly vulnerable to O_2-induced corrosion at high temperatures. Zhang *et al.* [137] observed that in an O_2-Cl^--H_2O environment under HT/HP conditions, the corrosion rate of P110 steel reached 73 mm/y at 20 MPa air pressure. High Cl^- concentrations can mitigate O_2 corrosion by reducing dissolved O_2 levels in high-salinity fluids.

Water containing both dissolved O_2 and CO_2 is more corrosive than water with only 1 corrosive component. For instance, type 304 stainless steel showed significantly higher corrosion currents in CO_2-O_2 environments compared to CO_2 alone [143]. However, the combined effects of CO_2 and varying dissolved O_2 concentrations on erosion-corrosion under HT/HP conditions require further investigation. **Table 4** summarizes the performance of various alloys under CO_2- O_2 across different conditions.

Table 4 Performance Summary of various alloys under CO_2 – O_2 conditions.

Material	Temperature (°C)	pO_2 (MPa) or $[O_2]$	pCO_2 (MPa)	Corrosion rate (mm/y)	Exposure time (h)	Electrolyte	Ref.
3Cr	120	0.5	0	0.331	120	Simulated brine	[134]
3Cr	120	0.5	2.5	5.87	120		
N80	120	0.5	0	1.973	120		[135]
N80	120	0.5	2.5	4.47	120		
X70	25	0.02 mol *	10	1.09	120	Water injection - saturated CO_2	[93]
X70	50	0.02 mol *	10	2.52	120		
X70	75	0.02 mol *	10	3.06	120		
X70	93	0.02 mol *	10	1.25	120		
304	650	2.03 (kPa)	99.30 (kPa)	3.5	24	Molten mixed salt	[143]
316L	650	2.03 (kPa)	99.30 (kPa)	2.9	24		
310S	650	2.03 (kPa)	99.30 (kPa)	0.5	24		
P110	150	5 **		32.07	12	Simulated oil field injection water	[137]
P110	150	10 **		60.25	12		
P110	150	20 **		72.83	12		
3Cr	120	0.2	2.5	4.3	120	Formation water	[144]
3Cr	120	0.4	2.5	5.1	120		
3Cr	120	0.6	2.5	5.5	120		
X65	35	20 (ppm)	8	0.09	48		[145]

Material	Temperature (°C)	pO_2 (MPa) or [O_2]	pCO_2 (MPa)	Corrosion rate (mm/y)	Exposure time (h)	Electrolyte	Ref.
X65	35	500 (ppm)	8	0.07	48	Water-saturated supercritical CO_2	
X65	35	1,000 (ppm)	8	0.03	48		
5Cr	35	20 (ppm)	8	0.12	48		
5Cr	35	500 (ppm)	8	0.04	48		
5Cr	35	1,000 (ppm)	8	0.02	48		

Types of corrosion

The integrity and longevity of equipment and tools in the oil and gas industry depend heavily on understanding the various types of corrosion prevalent in downhole environments. Common types that frequently affect downhole structures include pitting corrosion, crevice corrosion, under-deposit corrosion (UDC), SCC, and erosion-corrosion. Extensive efforts, both in laboratory and industrial settings, have been devoted to comprehending these forms of corrosion. Research related to these corrosion types is summarized in **Table 5**. Notably, all these forms of corrosion are localized, indicating a high risk for metal structures in downhole environments.

Table 5 Summary of corrosion types in downhole environments.

Corrosion type	Temperature	Gas involved	Pressure	References
Pitting corrosion	85 - 232 °C	H_2S, CO_2	0.1 - 7 MPa	[24,128,129,146-150]
Crevice corrosion	25 - 130 °C	H_2S, CO_2	0.1 - 35 MPa	[125,132,133,151-158]
Under-deposit corrosion	25 - 170 °C	H_2S, CO_2	0.1 - 10 MPa	[17,19,159-168]
Stress corrosion cracking	25 - 220 °C	H_2S, CO_2	0.1 - 59 MPa	[7,148,149,169-178]
Erosion-corrosion	60 - 140 °C	O_2, CO_2	0.2 - 56 MPa	[20,21,134,176-189]

This section addresses these significant forms of corrosion encountered in downhole operations. Each type presents unique challenges that impact reliability and operational safety. Numerous studies have focused on understanding the general mechanisms of each type of corrosion in the oil and gas industry [190-196]. It aims to examine the impact of various downhole operational factors on different types of corrosion, including corrosive gases, temperature, stress, and flow conditions. It also reports the corrosion behavior of various oilfield construction materials.

Pitting corrosion

Among all types of corrosion attacks, pitting corrosion is one of the main causes of failures in oilfield production, posing a significant threat due to the harsh environments encountered during extraction [146]. Pitting corrosion compromises the integrity of downhole equipment, such as tubular and casing, which are essential for efficient and safe operations. Pits formed can act as stress concentrators, potentially leading to catastrophic failures and costly downtime [197]. Understanding the factors that predict pitting corrosion is crucial for developing sound mitigation strategies.

The characteristics of pits vary depending on the dissolved gas present, whether it is CO_2, H_2S, O_2, or a mixture of these gases. The shape of the corrosion pit sides and bottoms often provides crucial clues in diagnosing corrosion failures. Martin *et al.* [198] discussed the pits' characteristics under dissolved gas corrosion. In a dissolved CO_2 environment with H_2S content below 10 ppm, 3 to 6 mm straight-sided pits form at gas breakout areas of iron carbonate products, as illustrated in **Figure 7(a)** [199]. When the H_2S

concentration increases, the corrosion morphology changes due to the formation of FeS on the surface. In such cases, pits ranging from 3 to 10 mm in diameter are characterized by sloping edges with a nested pit at the bottom. A mixture of straight-sided and sloping-sided pits occurs in environments containing CO_2 and 10 to 20 ppm H_2S. **Figure 7(b)** shows the straight-sided and sloping-sided pits for a corroded X65 sample [200]. The presence of O_2 along with H_2S and CO_2, as is common in oil and gas production, intensifies the corrosion of steel. Pits formed in such an environment, with 20 ppm or greater H_2S, tend to have broad, smooth sides and bottoms that are usually found in crevices [198,201]. When small amounts of O_2 enter a sweet environment, the morphology of pits changes minimally, but with faster growth.

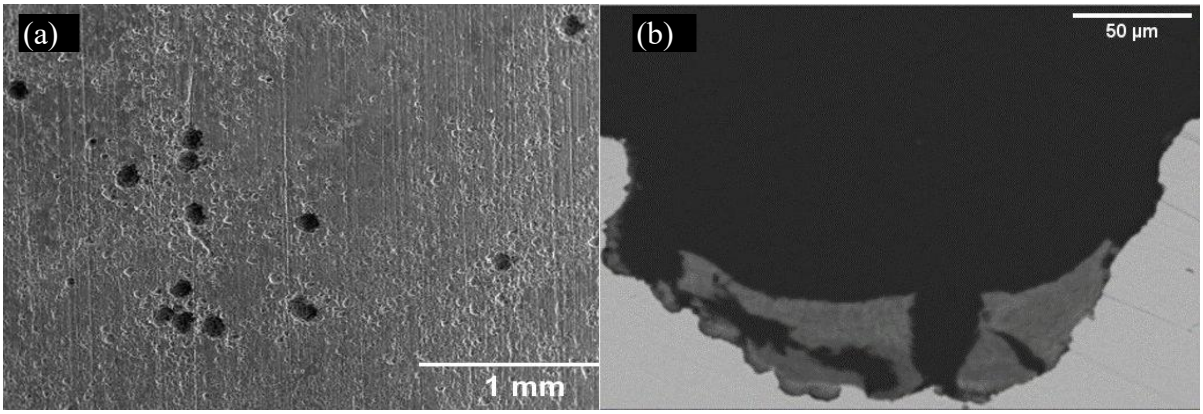

Figure 7 Morphology of corrosion pits under different corrosive gases: (a) corrosion of L415N in a CO_2 environment for 30 days at 25 °C and 5.8 MPa [199]; (b) Corrosion of X65 in an H_2S environment at 20 ppm H_2S, 0.097 MPa CO_2, 20 $ppb_{(w)}$ [O_2], 7 days exposure time at 30 °C [200]. Reprinted with permission from [199,200].

Pitting morphology influences the severity and progression of material degradation. Deep pitting compromises the mechanical integrity by reducing the thickness and creating stress concentration points. As pitting depth and/or its frequency increases, the fracture pressure of casing materials decreases markedly [202]. Pitting depth was also linked to a reduction in ultimate tensile strength [203,204]. The localized stress at the pit base could exceed the material's yield strength leading to crack formation. In H_2S environments, pits can be initiation sites for stress corrosion cracking [205]. Additionally, pitting alters the internal surface topology of casings and pipelines, leading to increased turbulence and flow resistance. These irregularities act as favorable factors for erosion-corrosion processes, where turbulence flow around pits leads to localized removal of protective films, accelerating material loss and deepening the pits [206].

The influence of various parameters on localized/pitting corrosion has been investigated by Zhang *et al.* [200]. **Figures 8(a) - 8(e)** highlights the complex interactions between environmental factors and corrosion behavior. The experimental findings indicate that pitting initiates only in the presence of H_2S and propagates when CO_2 is also present, highlighting the synergistic role of these gases in localized attacks. Specifically, pitting was observed within narrow ranges of H_2S (0.02 - 0.09 mbar) and CO_2 (0.53 - 0.97 bar) partial pressures, at pH levels 4 and 5, and at 30 °C but not higher temperatures. The presence of NaCl was not necessary for pit initiation, but increased chloride concentrations correlated with higher pitting density, suggesting a galvanic coupling effect. Pit formation is closely linked to the integrity of the thin FeS layer, where localized breakdown exposes steel surfaces to the aggressive buffering effect of H_2CO_3, driving further propagation. The pitting penetration rate represents the depth at which corrosion progresses into the metal over time and is typically derived from the deepest pit observed on the surface after a given exposure. The penetration ratio provides a comparative measure of localized versus general corrosion by relating the maximum pit depth to the average general corrosion. It is calculated as the ratio of the deepest pit depth to the uniform corrosion rate obtained from weight loss measurements. The findings clearly illustrate the

relationship between these parameters and localized corrosion behavior, emphasizing the importance of controlling operational conditions to mitigate pitting risks.

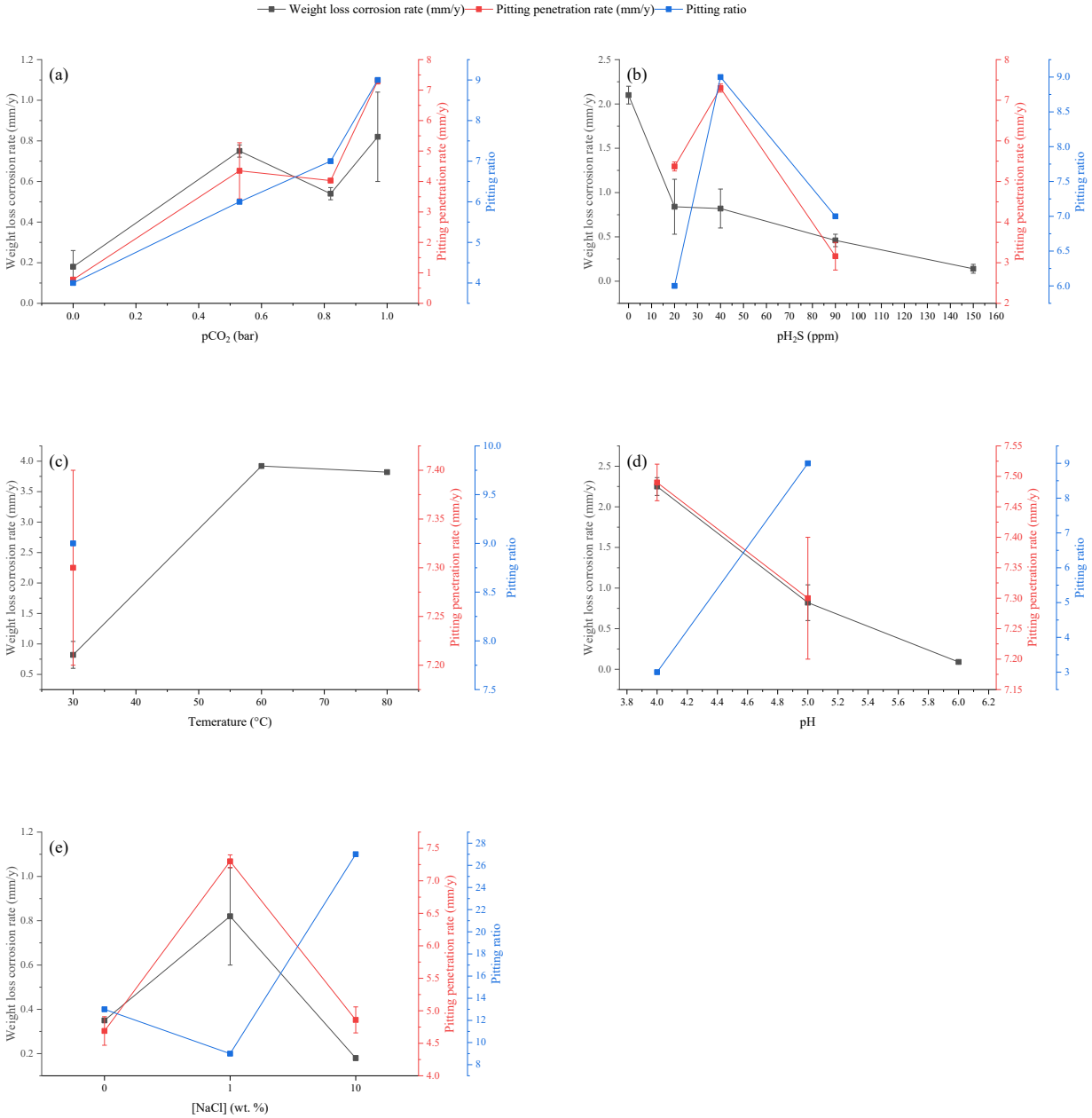

Figure 8 Influence of various environmental conditions on the pitting corrosion occurrence of X65 carbon steel for 168 h exposure [200]. (a) experimental conditions: 30 °C, pH 5, 0.04 mbar pH_2S, 1 wt.% NaCl, 300 rpm, 20 $ppb_w[O_2]$, (b) experimental conditions: 30 °C, pH 5, 0.97 bar pCO_2, 1 wt.% NaCl, 300 rpm, 20 $ppb_w[O_2]$, (c) experimental conditions: PH 5, 0.97/0.82/0.53 bar pCO_2, 0.04 mbar pH_2S, 1 wt.% NaCl, 300 rpm, 20 $ppb_w[O_2]$, (d) experimental conditions: 30 °C, 0.97 bar pCO_2, 0.04 mbar pH_2S, 1 wt.% NaCl, 300 rpm, 20 ppb_w[O2], (e) experimental conditions: 30 °C, pH 5, 0.97 bar pCO_2, 0.04 mbar pH_2S, 300 rpm, 20 $ppb_w[O_2]$.

To mitigate corrosion in downhole environments, CRAs are typically used for the construction of downhole structures [26]. CRA suffers less from corrosion due to the formation of protective passive films, which act as a physical barrier between the metal matrix and corrosive environments [147]. However, passive films are susceptible to the attack of halide ions, especially chloride ions, resulting in film breakdown

[148]. Specifically, pitting corrosion can initiate and develop at these defects in the film. Chlorides commonly exist in formation water and produce water [149,150] or are contained in the production annulus to provide hydrostatic pressure over the packer [150]. Moreover, the presence of H_2S also enhances the possibility of pitting corrosion in the downhole. Therefore, downhole tubing might be susceptible to pitting corrosion in the presence of chlorides or H_2S.

To date, the susceptibility of various steels to pitting corrosion in the downhole environment has been widely studied [146,149,193,197,198,207,208]. The relationship between the corrosion potential (E_{corr}) and the repassivation potential (E_{rp}) indicates the likelihood of localized corrosion, such as pitting and crevice corrosion. E_{rp} is the potential where localized corrosion does not occur [207]. Whenever E_{corr} exceeds E_{rp}, localized corrosion is predicted.

Cao *et al.* [149] investigated the pitting corrosion of 6 CRAs in chloride plus H_2S environments at temperatures ranging from 85 to 232 ℃. Results showed that the existence of H_2S reduced the repassivation potentials of most CRAs in most cases, increasing their susceptibility to pitting corrosion. The E_{rp} data are shown in **Table 6**. Notably, the presence of Cr, Mo, and Ni content increases the repassivation potentials in H_2S at high temperatures.

Table 6 provides a detailed summary of E_{rp} values under varying conditions of temperature, pressure, chloride concentration, and H_2S exposure. In environments containing H_2S and CO_2, the susceptibility of Ni-based alloy 718 to pitting corrosion increases with higher Cl^- concentrations, as the elevated chloride levels compromise the stability of the passive film [209,210]. Additionally, super duplex stainless steel 25Cr demonstrated susceptibility to pitting corrosion under stress in solutions containing ammonium bisulfite and chloride at 90 ℃ [150]. Pitting corrosion was observed on specimens subjected to axial load and internal pressure, indicating a similar corrosion behavior of this stainless steel in downhole environments. Alloys with higher Cr and Mo content, such as S32750, N08535, and N08029/28, generally exhibit higher repassivation potentials, indicating improved resistance to localized corrosion. Conversely, alloys exposed to higher H_2S concentrations tend to show significantly lower Erp values, reinforcing the role of H_2S in destabilizing passive films.

Table 6 Summary of experimental E_{rp} values for various steels [149].

Alloy	Temperature (℃)	Pressure (atm)	Chloride (NaCl)	H_2S (wt%)	E_{rp} (mV_{SHE})	E_{corr} (mV_{SCE})
S15Cr (S42625)	85	1	0.003 - 0.3 M	0 %	From −99 to 32	From −689 to −627[a]
				1 %	From −126 to 173	From −613 to −538[a]
			0.03 - 3.0 M	100 %	From −424 to −234	From −525 to −394[a]
2507 (S32750)	85	1	0.003 - 3.0 M	0 %	From −64 to 240	From −442 to −433
				1 %	From −200 to 191	From −531 to −348
				100 %	From −363 to −153	From −519 to −343
2535 (N08535)	85	1	2.5 - 25 %	0 %	From −46 to 60	From −671 to −538
				100 %	From −260 to −209	From −414 to −355
	232	60.9 - 63.6	2.5 - 25 %	0 %	From −356 to −158	From −542 to −538
		49.3 - 66.3	2.5 - 25 %	75 %	From −388 to −247	From −371 to −350
29 (N08029)	85	1	1.65 - 25 %	0 %	From −42 to 59	−589
				100 %	From −267 to −92	From −371 to −350
	150	28.2 - 28.9	1.65 - 25 %	0 %	From -256 to −59	From −572 to −525
		25.5 - 37.1		100 %	From −297 to −178	From −393 to −369
	200	47.3 - 50.0		0 %	From −253 to −176	-
		45.2 - 47.3		71 %	From −376 to −294	-
28	85	1	25 %	0 %	−136	-

Alloy	Temperature (°C)	Pressure (atm)	Chloride (NaCl)	H_2S (wt%)	E_{rp} (mV_{SHE})	E_{corr} (mV_{SCE})
(N08028)				100 %	−279	-
	150	28.2	25 %	0 %	−274	-
		27.2		100 %	−257	-
	200	45.9		0 %	−337	-
		45.2		71 %	−281	-

[a] E_{corr} values were reported for 13Cr

Crevice corrosion

Crevices are always present in any engineering structure. Crevice corrosion is a localized form of corrosion that often occurs in geometrically narrow locations, making it considerably more difficult to detect than general corrosion. This type of corrosion is attributed to the limited diffusion of corrosive species and the presence of stagnant electrolyte [132]. Specifically, crevice corrosion is primarily driven by the concentration difference of corrosive species between the internal and external crevice environments, which makes the solution within the crevice more aggressive and damages the passive film. Despite potentially long incubation periods before initiating an attack, crevice corrosion can rapidly accelerate material damage [152].

Researchers have proposed 2 mechanisms for crevice corrosion: Critical crevice solution (CCS) and potential drop [133,153-155]. In the CCS mechanism, the crevice solution becomes acidic due to oxygen depletion within the crevice, leading to passive film breakdown and rapid metal corrosion. In the potential drop mechanism, oxygen depletion causes a potential drop within the crevice, contributing to crevice corrosion. Both theories emphasize oxygen depletion as a critical factor. Yu *et al.* [156] found that increases in temperature and oxygen content could promote crevice corrosion occurrence and facilitate corrosion processes inside and outside the crevice. Chen *et al.* [157] studied the effects of crevice geometry on the corrosion behavior of 304 stainless steel during crevice corrosion at 290 °C, concluding that both crevice width and length affect oxidation behavior. However, the oxygen concentration is typically deficient in downhole environments due to high temperatures, eliminating the possibility of crevice corrosion caused by oxygen concentration differences.

Undoubtedly, temperature can affect the crevice corrosion resistance of alloys [158,159]. The critical temperature is often used to express crevice corrosion resistance; above this critical temperature, crevice corrosion may occur. Temperature changes mainly affect the critical breakdown potential of passive films. Both the repassivation potential and the breakthrough potential linearly decrease with increasing temperature [157]. Moreover, in the case of downhole crevice corrosion, the key factor is the diffusion of dissolved CO_2 and H_2S, which can further control the cathodic reaction in anaerobic downhole environments.

Haugan *et al.* [159] investigated the crevice corrosion of 25Cr super-duplex stainless steel in a deaerated 3.5 wt.% NaCl solution at elevated temperatures. At 60 °C, crevice corrosion was found close to the edge of crevice formers. Pehlke measured the crevice corrosion rates of several downhole materials, i.e., K-55, GLV-J55, and TN-55TH, in a simulated environment containing 6.9 % CO_2 and 6.5 % H_2S with a pressure of 3,000 kPa at 170 °C [127]. The metals were paired as follows: K-55/TN-55TH, K-55/GLV-J55, and K-55/K-55. When tested alone, the corrosion rate of K-55 was lower at 0.215 mm/y compared to its rate when coupled with the other metals. The corrosion rate of K-55 increased to 0.241 and 0.276 mm/y when coupled with TN-55TH and GLV-J55, respectively. This suggests galvanic corrosion effects on the corrosion susceptibility of K-55.

Other factors influencing crevice corrosion include crevice geometry, metal composition and microstructure, and environmental factors. The ideal gap for crevice corrosion is between 0.1 and 100 μm [192]. Rougher surfaces decrease the critical crevice temperature, thereby increasing susceptibility to corrosion. Metal composition and microstructure also play a role. For instance, stainless steels with higher Cr,

Mo, Ni, and W content exhibit better resistance due to the formation of a protective passive film. The microstructure's heterogeneity and the presence of precipitates during heat treatments significantly impact the passive film stability and the metal's overall corrosion resistance. Detailed descriptions of other factors are outlined in [190].

E_{rp} serves as a critical parameter in assessing the susceptibility of alloys to crevice corrosion. It provides insight into the alloys' ability to resist localized corrosion in downhole environments. Studies on alloys such as duplex stainless steel 2507, S13Cr stainless steel, alloy 2535, and alloy 29 reveal variations of E_{rp} under varying Cl^- and H_2S concentrations at elevated temperatures [208,211,211]. The E_{rp} data is provided in **Table 7**. At high H_2S concentrations, E_{rp} typically decreases with increasing Cl^- concentration due to enhanced anodic dissolution, intensifying the tendency for localized corrosion. Anderko *et al.* [211] reported a consistent behavior for E_{rp} potentials reduction by 0.15 - 0.2 V at 85 °C. However, increasing the temperature diminishes the H_2S effect on E_{rp}. Conversely, at lower H_2S concentrations, the formation of protective metal sulfide layers inhibits corrosion, increasing E_{rp} at low Cl^- concentrations [208,211]. Metal sulfide influence dominates at Cl^- concentrations below 0.3 and increases E_{rp} by almost 200 mV. These effects were also found to be pronounced for the least corrosion-resistant alloys [211].

Table 7 Summary of experimental E_{rp} measured for alloys 2507, S13Cr, 2535, and 29 in Cl^- and H_2S environments at different test conditions.

Alloy	Temperature (°C)	Pressure (atm)	Chloride (NaCl)	H_2S (wt%)	E_{rp} (mV)	Reference Electrode	Refs
2507 (S32750)	85	1	0.003 - 3.0 M	0 %	−199 to 205	SCE	[212]
				1 %	−299 to 254		
				100 %	−444 to −204		
S13Cr (S41425)	85	1	0.0003 - 0.3 M	0 %	−328 to −106	SCE	[208]
				1 %	−200 to 73		
			0.03 M	100 %	−368		
2535 (N08535)	85	1	0.44 - 5.7 M	0 %	−327 to −183	SCE	[211]
				10 %	−440 to −349		
				100 %	−432 to −371		
	232	59.6 - 62.6	0.44 - 5.7 M	0 %	−226 to −40	Ag/AgCl	
		55.8 - 62.6		10 %	−272 to −155		
		51 - 65.3		75.3 %	−292 to −130		
29 (N08029)	85	1	0.287 - 5.7 M	0 %	−270 to −190	SCE	
				10 %	−424 to −328		
				100 %	−419 to −296		
	150	27.2 - 27.9	0.287 - 5.7 M	0 %	−267 to −123	Ag/AgCl	
		26.5 - 27.9		10 %	−376 to −296		
		24.5 - 36.1		100 %	−332 to −318		

Under-deposit corrosion

UDC poses a significant threat to oil and gas production and transportation [168]. One prominent characteristic of UDC is the formation of tiny, occluded spots under deposits, creating occluded-cell blockages on substrates [160,161]. UDC often occurs when deposits or scales, resulting from high ion concentrations in formation or produced water, are present in oil and gas production wells. When dissolved mineral contents become oversaturated, minerals

precipitate, leading to scale formation [162]. The presence of scale can introduce various issues to production wells, such as fluid flow restrictions, downhole tubing blockages, and corrosion [163,164]. FeS is a common scale formation, potentially related to steel tubing corrosion in downhole environments. During well production, acidization stimulation may be used by injecting acid, like HCl (~26 %), to enhance oil recovery [165]. The dissolution of metal in acid generates Fe^{2+} ions, which combine with sulfide ions (S^{2-}) from ionized H_2S to form FeS scale as a corrosion product [19]. However, FeS scale, being loose and porous, fails to act as a protective film against corrosion.

The primary factors affecting UDC due to deposits are their composition, porosity, and coverage, which are often interrelated. Deposits found in pipelines can be categorized into inorganic, organic, and mixed types [168]. Inorganic deposits, such as iron oxides, sulfides, and carbonates, are well-studied in UDC investigations. Common iron oxides i.e., Fe_2O_3, Fe_3O_4, and various forms of FeOOH, which are generally porous, tend to cause localized corrosion [213-216]. FeS such as mackinawite and pyrrhotite also influence UDC, with mackinawite being more porous and less protective [217]. Iron carbonate can either inhibit or promote UDC depending on its compactness and coverage [218,219]. Organic deposits, primarily composed of wax and bitumen, along with mixed deposits, contribute to localized corrosion, though they are less frequently studied [220].

In most cases, both pitting and crevice corrosion are observed beneath FeS scale. A crude oil pipeline often experiences severe under-deposit pitting corrosion at the bottom where significant deposits accumulate [166]. Standlee *et al.* [21] examined the corrosion of X65 steel under FeS deposits in an H_2S-containing solution. After several days of exposure, they observed corrosion pits on steel coupons, with a measured corrosion rate under FeS deposits of 2.1 mm/y, which is 10 times higher than those without FeS deposits. Wang *et al.* [19] analyzed the inorganic scale of a tubular pulled out of the hole during a workover. They visually observed a 2-layer scale structure with different colors, with the pipe side having an orange/red layer and the fluid side having a black/gray layer. This indicates that FeS does not protect against corrosion, thus allowing corrosion to occur under the scale. Kvarekval *et al.* [169] investigated localized corrosion of X65 steel under high pH_2S and FeS deposits at elevated temperatures. At 120 °C, a maximum localized corrosion rate of 28 mm/y was recorded under FeS deposits, significantly increasing steel corrosion. **Figure 9** shows a cross-section of a FeS-deposit sample with corrosion film. The corrosion layer consists of the native corrosion layer, fused FeS powder with corrosion products, and the remnant of applied FeS powder. Zhang *et al.* [170] explored the mechanism of enhanced corrosion rates under deposits, finding that galvanic corrosion between bare steel and deposit-covered steel is the primary cause of increased corrosion rates.

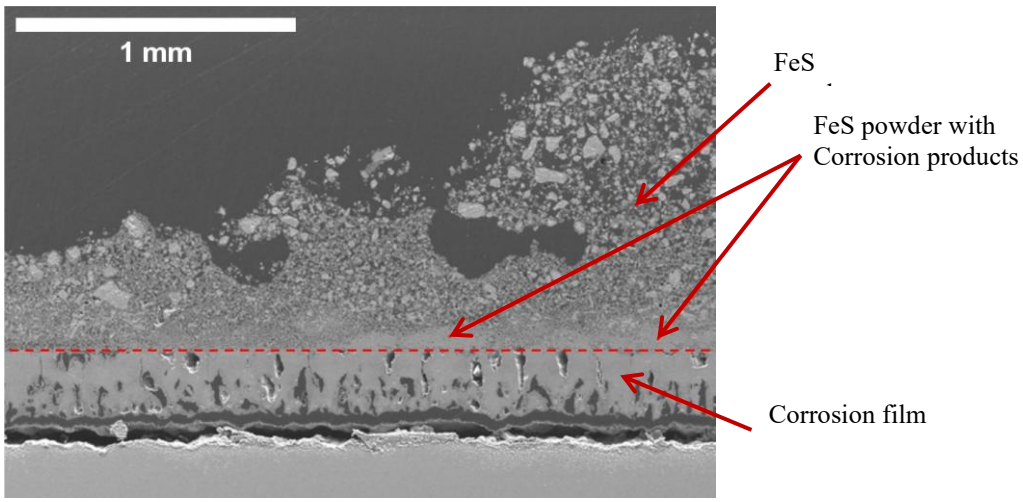

Figure 9 SEM image of a cross-section of FeS deposited sample, showing corrosion film at 25 °C, 0.5 MPa H_2S, and 2 MPa CO_2 [169]. Reprinted with permission from [169].

Stress corrosion cracking

SCC is a critical service failure mechanism in engineering materials, characterized by the slow growth of cracks due to the simultaneous presence of a corrosive environment and stress. These stresses can originate from various sources such as hoop stress from internal pressure, residual stresses from pipe manufacturing and construction (e.g., field bends), and operational stresses from in-service damage [221]. In the downhole environment, although SCC failures are not common, they can have catastrophic consequences due to their sudden and unexpected nature. Specifically, in oil wells, the presence of H_2S gas creates acidic aqueous solutions that induce sulfide stress cracking (SSC) at room temperature and SCC at high temperature [171]. This phenomenon is recognized as a primary cause of pipeline failure in sulfide environments [172], driven by the formation and uptake of atomic hydrogen produced during the cathodic reaction in H_2S environments mentioned in Reaction 13 [173]. The hydrogen atoms then penetrate the metal matrix through both adsorption and absorption, leading to a loss of ductility in steel structures [174].

It has been widely acknowledged that localized corrosion, such as pitting corrosion, is often a precursor to SCC. Metals and alloys susceptible to pitting corrosion are also prone to SCC in downhole environments [175]. Various CRAs have been found susceptible to SCC in chloride and H_2S-containing environments at elevated temperatures. For instance, Lasebiken *et al.* [150] reported that cracks can initiate from corrosion pits on super-duplex stainless steel 25Cr pipes under internal pressure of 48.3 MPa in a 3.5 % NaCl solution containing ammonium bisulfite at 90 ℃. Similarly, Zhang *et al.* [210] observed the depth development of corrosion pits on stress-loaded Ni-based alloy 718 C-ring specimens in a CO_2 and H_2S - containing solution with 200 g/L NaCl at 205 ℃, indicating potential SCC failure during long-term service in downhole conditions.

Ziaei *et al.* [176] documented rapid chloride SCC failure of 316 stainless steel gauge covers in downhole conditions after long-term service. The produced water contained 15 g/L chloride, 2.4 % H_2S, and 2.4 % CO_2 at 130 °C and 35 MPa pressure. Rihan *et al.* [15] investigated the SCC of P110 downhole tubular steel using circumferential notch tensile specimens in an H_2S and NaCl environment. They observed intergranular crack propagation and secondary cracking patterns on the fracture surface, which confirmed the susceptibility of P110 steel to SCC under such conditions. Lei *et al.* [177] built a full-scale tubular goods corrosion test system to simulate the safety performance of super 13Cr in downhole conditions at 120 °C coupled with spent acid. Their findings indicated that super 13Cr is sensitive to SCC during and after the acidizing process in spent acid, necessitating precise control during well operations.

While SCC in downhole environments may not be prevalent, the potential for severe and unexpected failures necessitates thorough understanding and monitoring. Research and case studies emphasize the importance of considering environmental factors, material selection, and operational controls to mitigate the risks associated with SCC in oilfield production.

Erosion-corrosion

Erosion-corrosion is a significant degradation mechanism in downhole environments, where oil and gas products within the tubing typically contain multi-phase fluids [178]. The phenomenon results from the combined effects of erosion, caused by the impingement of hard solid particles, and corrosion, induced by the fluid carrying these particles [179]. The synergy between erosion and corrosion can lead to severe damage to the downhole structures [180]. For example, screens used for sand control in downhole equipment are often damaged by the continuous impact of sand-containing fluids, resulting in high repair costs and operational downtime [23]. Moreover, downhole environments frequently contain corrosive gases, such as CO_2 and H_2S, which can exacerbate metal loss, especially at high temperatures. Therefore, understanding the erosion-corrosion of metallic structures in downhole is crucial for ensuring safety and economic efficiency.

Erosion-corrosion involves 2 pathways of metal loss: Mechanical erosion from solid particle impact and electrochemical corrosion. These pathways can interact, significantly increasing the total metal loss [181]. Studies have shown that the erosion process typically has a greater effect than corrosion, with fluid velocity

and impact angle being critical parameters [182]. For instance, Tang *et al.* [222] studied the erosion-corrosion of X65 steel in simulated oil sand slurry through an impingement jet system. Their experimental setup of the impingement jet system is illustrated in **Figure 10**. The study concluded that steel passivity, established in static oil-water emulsion, was disrupted when introduced to a flowing fluid. This was explained by the increased steel activity, which was further increased in oil-water-sand slurry, resulting in a substantial rise in anodic current density. Tian and Cheng investigated the hydrodynamic conditions' influence on the electrochemical corrosion behavior of X65 steel pipe in simulated oil sand slurry [223]. They found that electrode rotating speed enhances oxygen diffusion and reduction, raising cathodic polarization current while improving steel oxidation. Additionally, higher temperatures increase anodic current due to enhanced steel reactivity, and the presence of oil and sand in the solution affects steel corrosion by influencing oxygen solubility and mechanical abrasion.

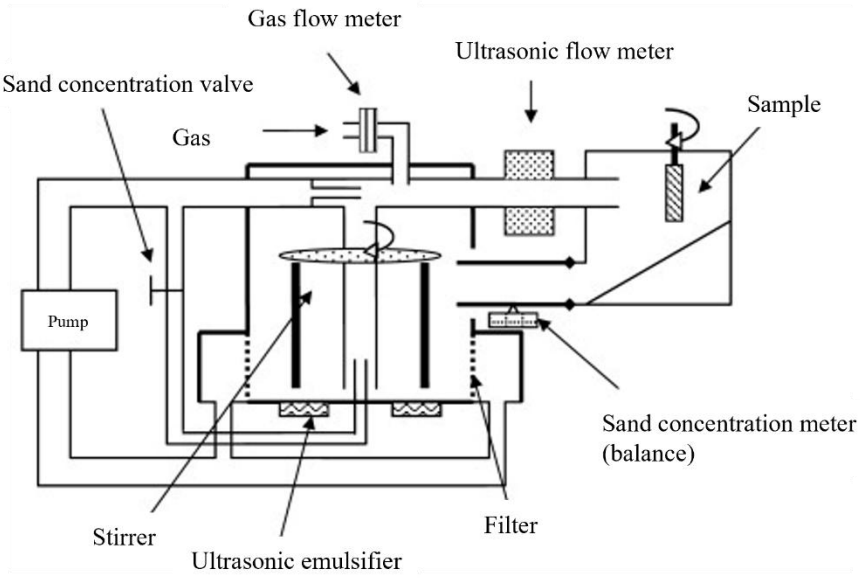

Figure 10 Experimental setup for the impingement jet system [222].

Yu *et al.* [136] found that the overall metal loss of the specimens more than doubles when the fluid velocity doubles. Lu *et al.* [22] reported a 68 % increase in erosion-corrosion rate as fluid velocity increased from 0.1 to 1.0 m/s. In their failure analysis of downhole tubing under a temperature range from 75 to 140 ℃, they observed that tubing failed after approximately 3 years of service at the premium connection with a fluid velocity of only 0.1 m/s, due to the sudden change in tube geometry at the connection.

For passive materials, the critical flow velocity (CFV) could be used to efficiently evaluate the erosion-corrosion property. Zheng *et al.* [184] systematically studied the CFV behavior for 304 stainless steel with coating and found that higher CFV values corresponded to higher erosion-corrosion resistance, closely associated with the passive film formed on the material surface [183-187]. Yi *et al.* [183] reached similar conclusions, reinforcing the importance of passive films in mitigating erosion-corrosion [183,188]. The synergistic relationship between erosion and corrosion results in damage greater than the sum of the 2 processes individually. Factors, such as temperature and the presence of various gases, not only increase the corrosion rate but also amplify the effect on erosion-corrosion rate due to this synergy. Yu's work demonstrated that the presence of O_2 and CO_2 in aqueous solutions significantly enhances the erosion-corrosion rate [136]. Aguirre *et al.* [189] found that increased dissolved oxygen promoted localized corrosion, different from pitting, with dissolved oxygen content and flow velocity being the most relevant factors by statistical analysis [224].

Andrews *et al.* [225] investigated the erosion-corrosion of L80, 13Cr steel, and C90 carbon steel using liquid jet impingement tests at different temperatures. They found that C90 experienced severe erosion-corrosion damage, and the rate increased with fluid temperature. In contrast, L80 and 13Cr steel showed no significant erosion-corrosion even with 4.14 MPa CO_2 at 100 ℃, highlighting the role of material corrosion resistance.

Summary

Corrosion mechanisms in downhole environments often do not occur in isolation; rather, they interact, leading to accelerated material degradation and complex failure modes. The previously discussed corrosion types can influence each other, amplifying their detrimental effects. Understanding these interactions leads to accurate risk assessments and the selection of effective mitigation strategies. **Table 8** summarizes the key synergistic effects between different corrosion mechanisms.

Table 8 Synergistic effects of different corrosion types.

Corrosion types	Interactions and impact	References
Pitting and Erosion-Corrosion	Erosion-corrosion accelerates pitting by removing protective oxide layers and increasing surface roughness, creating localized areas for pitting initiation.	[226-228]
SCC and Pitting	Pitting corrosion creates localized degradation points, acting as stress concentrators, which increase the likelihood of SCC initiation, especially under tensile stress.	[221,229-231]
SCC and UDC	Under-deposit corrosion creates localized regions with reduced oxygen, promoting SCC in susceptible alloys. Stress from external loads or internal pressure can amplify this effect, causing cracking at these localized corrosion sites.	[232-235]

Pitting corrosion, as previously discussed, is a highly localized form of attack that can serve as a precursor to SCC. Once a pit forms, it acts as a stress concentrator, increasing susceptibility to crack initiation under applied stress. Similarly, erosion-corrosion can exacerbate pitting by mechanically stripping away protective oxide layers, reducing repassivation potential, and exposing fresh metal surfaces to corrosive environments.

Crevice and under-deposit corrosion (UDC) create localized environments with oxygen depletion and increased acidity, which can further destabilize passive films, facilitating SCC initiation. The presence of aggressive species, such as chlorides and sulfides, can further intensify these effects, particularly in high-temperature, high-pressure (HPHT) downhole conditions.

Given these interactions, effective corrosion mitigation strategies must account for the combined effects of multiple mechanisms. Additionally, environmental modifications - such as flow control, chemical inhibition, and proper solids management - can help reduce the impact of synergistic corrosion effects in oilfield applications.

Corrosion control techniques

The cause-and-effect diagram in **Figure 11** summarizes the factors contributing to various types of corrosion encountered in downhole environments. The major aspects are: (a) Chemical Environment: This includes the chemical composition and conditions of the downhole environment. (b) Mechanical Factors: This considers the stresses and flow conditions experienced by downhole equipment during installation, operation, and production. (c) Galvanic Effects: This contributes to corrosion at metal interfaces. (d) Microbial Activity: This includes the presence of SRB and acid-producing bacteria (APB), which produce corrosive byproducts. (e) Additional Factors: These include salinity, material properties, and induced chemicals that alter overall corrosion susceptibility.

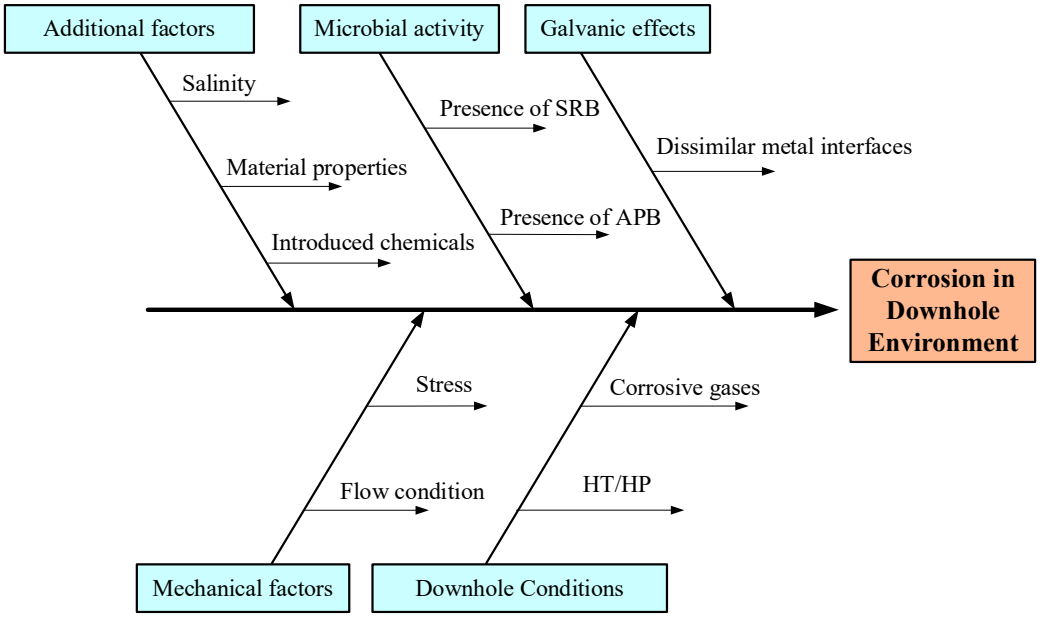

Figure 11 Common root causes of corrosion in downhole environments.

Effective corrosion control extends the life of wells and production equipment, accounting for 35 % in savings related to corrosion losses [236]. The unique challenges of downhole environments require specialized corrosion control strategies. As previously discussed, these environments can vary significantly in terms of chemical composition, temperature, pressure, and flow condition, all of which influence the type and rate of corrosion. Corrosion prevention measures are generally considered from 3 key aspects: Finding corrosion-resistant materials, altering the corrosion environment, and controlling the chemical or electrochemical interactions between materials and the environment. In practice, 3 techniques are used to mitigate corrosion: Corrosion inhibition techniques, coatings, and CRA selection. Understanding the specific conditions and corrosion mechanisms for selecting appropriate materials, protective measures, and monitoring techniques is essential.

Corrosion inhibition techniques

Corrosion of metals is a major global economic problem, especially in oil and gas gathering and transportation systems [237]. Corrosion inhibition techniques are widely used in such areas to extend the life of equipment and pipelines, especially for carbon steel components [34]. These techniques can both prevent metal dissolution and improve economic viability [238-240]. Specifically, inhibitors increase the dispersion of crude oil in water, reduce the interfacial tension between oil and water, and change the wettability of metal surfaces to form a hydrophobic film. This film hinders the diffusion of water molecules into the cathode region and inhibits the cathode reaction [241].

Various methods of applying corrosion inhibitors are employed in oil fields to protect tubing lining from corrosion. A successful corrosion control program should include effective inhibitor selection, optimal design and maintenance of the inhibitor injection system, continual monitoring, and regular planned analysis and reporting of system expectations [34,242]. Inhibitors can be applied using either batch-wise or continuous injection programs. Continuous corrosion inhibitors are injected by different methods, depending on the well's configuration. Inhibitors can be injected through the annular space if the annulus is open without packers or a polished bore receptacle (PBR) or through the injection mandrels in the tubing string, capillary tubing, or gas-lift systems, for a dual string completion process. Batch applications involve periodically coating the tubing walls. Inhibitor slugs are displaced down the well using dead crude, diesel, or nitrogen, with retreatment periods ranging from a few weeks to several months. All inhibitor systems must be evaluated for

their properties and performance under downhole conditions.

Corrosion inhibitors can be classified into 2 main categories: Organic and inorganic. Inorganic corrosion inhibitors are utilized in boiler and cooling waters, while organic inhibitors are used in oilfield production [29]. Thus, organic inhibitors will be the focus of this review. Organic inhibitors in oil and gas fields are surface-active compounds containing a nitrogen group, such as amines, quaternary ammonium compounds, imidazolines, and oxyalkylated amines, but they can also contain sulfur-, phosphorous-, and oxygen-containing organic molecules [242,243]. Their solubility, whether oil-soluble, oil-soluble-water dispersible, or water-soluble, determines their effectiveness, application, and the testing methods used for evaluation [242]. Currently used inhibitors in the industry meet the requirements related to pour point, solubility, performance, and emulsion tendency [34]. Papavinasam *et al.* [197] reviewed the laboratory methodologies to evaluate corrosion inhibitors for oil and gas pipelines. Laboratory tests included wheel test [244-246], static test, bubble test [247,248], rotating cylinder/disc electrode tests [249-252], jet impingement test [89,247,253-255], and rotating cage test [256]. Details of those tests can be found in ASTM G170 - 06 and NACE 1D182, 5A195 and 1D196 [244,245,249,254].

Table 9 exhibits the various applications of corrosion inhibitors in different media and conditions. Aromatic amines, aminoalcohols, amino acids, and nitrogen or oxygen-containing 5-membered and 6-membered heterocycles all show good inhibition performance [257-261]. Moreover, it was observed that the same inhibitor could behave differently depending on the solution. For instance, polarization measurements reveal that N-(5,6-diphenyl-4,5-dihydro-[1,2,4] triazin-3-yl)-guanidine (NTG) acts as a cathodic inhibitor in HCl and as a zwitterionic inhibitor in H_2SO_4 [262]. Ahamad studied the inhibition performance of mebendazole on mild steel in a molar hydrochloric acid solution through weight loss and electrochemical methods [263]. The maximum inhibition efficiency of 96.2 % was observed in the presence of a 2.54×10^{-4} M inhibitor. Hosseini *et al.* [264] investigated the influence of sodium dodecylbenzenesulphonate (SDBS) and hexamethylenetetramine (HA) on the corrosion of mild steel in H_2SO4 solution using weight loss, electrochemical impedance, and Tafel polarization measurements. It was observed that the inhibition efficiency increased as a function of concentration for HA, while an optimum efficiency was obtained at a concentration close to 250 ppm for SDBS. Concentration regions of mixing HA and SDBS showed synergistic and antagonistic inhibition behaviors, likely due to electrostatic interactions between adsorbed ions. Additionally, inhibitors not only adsorb onto the substrate surface but can also enhance corrosion resistance by modifying solution resistivity [265]. However, the compatibility of inhibitors with the materials of injecting systems, downhole treatment chemicals, emulsion tendency, water disposal requirements, and fire and safety requirements should be accounted for [242,266].

Table 9 The application of corrosion inhibitors in various conditions.

Corrosion inhibitors	Type	Alloys	Solution	Refs
Polyoxyethylene sorbitan trioleate	Non-ionic	ST3 steel	$CaCl_2$ and $MgCl_2$ / NaCl and $NaHCO_3$	[224]
Three type of oleic acid monoamide	Non-ionic	API X65 steel	HCl	[267]
2-((alkylimino)methyl)phenylbis(53-hydroxy-3,6,9,12,15,18,21,24,27,30,33,36,39,42,45,48,51-heptadecaoxatripentacontyl) phosphate	Non-ionic	Carbon steel	H_2SO_4	[268]
Schiff base nonionic surfactants	Zwitterionic	X-65 tubing steel	Formation water	[257]

Corrosion inhibitors	Type	Alloys	Solution	Refs
1-benzyl-4-phenyl-1H-1,2,3-triazole	/	Mild steel	HCl	[259]
2-mercaptobenzothiazole (MBT)	Zwitterionic	Brass	NaCl	[260]
Polyoxyethylene sorbitan monooleate (Tween-80)	Anionic			
N-(5,6-diphenyl-4,5-dihydro-[1,2,4]triazin-3-yl)-guanidine (NTG)	Cationic	Mild steel	HCl	[258]
	Zwitterionic		H_2SO_4	
Mebendazole	Zwitterionic	Mild steel	HCl	[261]
Sodium dodecylbenzenesulphonate (SDBS)	Anionic	Mild steel	H_2SO_4	[262]
Hexamethylenetetramine (HA)	Cationic			
Imidazoline-based inhibitors	/	Carbon steel	NaCl	[263]

The current trends in corrosion inhibitors cover the development of eco-friendly alternatives derived from natural biodegradable sources. This is driven by the increasing environmental concerns and regulatory restrictions on traditional corrosion inhibitors. Bio-based inhibitors, extracted from plant-derived compounds such as tannins, alkaloids, flavonoids, and organic acids, have demonstrated excellent anticorrosion properties by adsorbing onto metal surfaces and forming protective layers that prevent oxidation and degradation [269]. These inhibitors are non-toxic and sustainable, making them ideal for applications in oil and gas production where conventional inhibitors may pose ecological risks. Additionally, polymers derived from vegetable oils, such as linseed oil and caster oil, have been incorporated into inhibitor formulations to enhance adhesion and hydrophobicity, improving corrosion resistance under harsh conditions [269,270].

Another significant advancement is the use of nanomaterials in green inhibitors, where cellulose nanocrystals and graphene-based additives enhance the film-forming capabilities and improve inhibitor retention on metal surfaces [270,271]. Waterborne inhibitors, combined with self-healing smart coatings, have also been developed to provide long-term protection in dynamic environments, reducing the need for frequent reapplication and minimizing environmental impact [270,272]. Despite their advantage, challenges such as limited long-term stability and effectiveness under extreme conditions, such as the high temperature, pressure, and salinity in downhole environments, require further research to optimize formulation and deployment strategies. The ongoing development of hybrid organic-inorganic inhibitors and synergistic blends of bio-based inhibitors with nanomaterials hold promise for achieving high-performance, sustainable corrosion protection in oilfield applications.

Surface coatings

Surface coatings are widely used in oilfield production to control corrosion and ensure the longevity and integrity of downhole tubing and equipment. These protective coatings are applied both externally and internally to provide a barrier against harsh downhole environments. This method outweighs other control measures by its ease of application, storage, handling, restoration, and cost [29]. There are 3 mechanisms, or their combination, of surface coatings by which corrosion can be controlled:

(a) Barrier Protection: Preventing contact between the corrosive medium and the metal substrate, as well as inhibiting ion migration through the coatings. (b) Sacrificial Anode: Acting as a sacrificial anode for cathodic protection. (c) Passivation/Inhibition: Utilizing passivation or inhibition species to protect against external corrosive agents [273].

To better understand the effectiveness of coatings in oilfield applications, **Table 10** summarizes the key characteristics.

Table 10 Summary of key characteristics and selection criteria for surface coatings used in downhole environments.

Characteristic	Description
Electrical Insulation	Prevents electrochemical corrosion by blocking current flow, isolating the substrate from its environment, and providing high dielectric strength.
Moisture Barrier	Reduces water absorption to enhance cathodic protection (CP) and minimize moisture-driven degradation.
Good Adhesion to Surface	Ensures strong adhesion to the substrate and internal cohesion within the coating for lasting protection.
Resistance to Disbanding	Maintains integrity and adhesion under cathodic protection (CP), enhancing reliability and long-term performance.
Temperature Resistance	Performs reliably under varying temperatures, including ambient conditions during application and high operating temperatures in service.
Mechanical Strength	Provides durability against mechanical stresses, including pressure, wear, and environmental factors like UV radiation.
Chemical Resistance	Resists degradation from exposure to chemicals, such as hydrocarbons, acids, or bases, commonly encountered in oilfield environments.
Corrosion Inhibition	Contains corrosion inhibitors or sacrificial components to enhance protection against specific corrosive agents.
Applicability	Allows application through methods that do not compromise the properties of the coated material or equipment.
Ability to Withstand Handling/Installation	Resistant to damage caused by impact, abrasion, or flexing during transportation, handling, or installation.
Surface Preparation Requirements	Compatible with the required level of surface preparation, ensuring adhesion and effectiveness without excessive pre-treatment costs.
Accessibility	Suitable for pipelines or equipment that may be difficult to access, enabling easy application or maintenance.
Ease of Repair	Allows for quick and effective field repairs with minimal effort or specialized equipment.
Cost Effectiveness	Balances performance with affordability, considering overheads, maintenance, and lifecycle costs.
Nontoxic Interaction with the Environment	Complies with environmental and health standards, ensuring that the coating is non-toxic and eco-friendly.

Various coatings are employed in downhole environments, categorized as metallic such as zinc and nickel, and non-metallic comprising organic [274,275], inorganic [276,277] coatings, and hybrid coatings [273,278,279]. Among these, organic coatings are widely used and have been confirmed as effective in protecting metals against harsh corrosive environments [280].

Organic coatings such as epoxies, polyurethanes, and polytetrafluoroethylene (PTFE), are popular due to their excellent adhesion, chemical resistance, and flexibility. They are composed of a complex mixture of binders, pigments, fillers, solvents, and additives, with the binder being the primary component [281]. Binders hold pigment particles together and provide adhesion to the substrate. Common binders include epoxies,

phenolics, polyolefins, polyurethanes, polyamides, or their combination. Pigments provide color and opacity and can impart specific functional properties such as corrosion inhibition [282-284]. Examples include titanium dioxide for opacity and brightness [285], zinc-rich pigment for sacrificial agents [286], and chromate and phosphates for corrosion inhibition [287], and iron oxide for color and UV protection [288]. Fillers enhance properties like mechanical strength, durability, and anticorrosive action [289,290], with examples including calcium carbonate for durability and cost-effectiveness, silica for thickening, and mechanical properties enhancement [291], mica for mechanical stability and barrier properties enhancement [292], and zinc phosphate for corrosion inhibition properties [293]. Solvents, such as xylene, toluene, and acetone, dissolve or disperse other components and evaporate after application, leaving a solid coating film [294]. Additives provide specific properties, such as surfactants for wetting and dispersion of pigments, curing agents to control the curing process, and antifoaming agents to prevent bubble formation during application [295].

Epoxy resins are widely used as organic coatings due to their superior chemical inertness, electrical insulating properties, and strong adhesion to heterogeneous substrates. These qualities make them highly effective against corrosive agents such as oxygen, water, and chloride ions [296,297]. However, their use comes with 2 notable disadvantages. Firstly, the epoxy resins commonly employed for corrosion protection are typically solvent-borne systems containing volatile compounds that harm the environment and human health [280]. Secondly, solvent evaporation can create micro-pores in the epoxy coating during the curing process, allowing electrolyte permeation and compromising corrosion resistance [279].

Traditional coatings pose environmental concerns, including contamination of heavy metal and toxic additives, microplastic and nanoparticles, chemical leaching into soil and water, and complex disposal requirements. Some coatings contain hazardous components like chromates and lead, which can leach into the environment, affecting ecosystems. To address environmental concerns, there has been a shift towards eco-friendly waterborne systems to reduce volatile organic compounds (VOC) emissions, which contribute to air pollution and health risks. For example, waterborne polyaniline (PANI) - containing coatings with epoxy resins as the matrix has demonstrated higher corrosion protection [298]. Additionally, Cui *et al.* [299] found that incorporating well-dispersed h-BN nanosheets into a waterborne epoxy system significantly improved corrosion protection performance. To tackle the issue of micro-pores formed during the curing process, incorporating anticorrosive fillers such as pigments into organic coatings can enhance barrier performance and corrosion resistance [300,301]. Using micro-sized anticorrosive pigments is one approach to achieving a coating with reliable corrosion protection properties [302,303]. However, nano-sized pigments have shown superior barrier properties compared to micro-sized additives, even at low concentrations [304], and have become a focal point of research in recent decades. Nanofillers block the micro-pores in the coating matrix and reduce electrolyte diffusion to the coating/metal interface. Their high specific surface area can increase the coating's cross-linking density, further enhancing barrier properties [305,306].

Materials selection and process optimization

Selecting materials capable of withstanding harsh downhole environmental conditions while providing mechanical strength and cost-effective performance throughout the well's life is critical. Corrosion issues in oilfield production vary based on the materials used, including general and pitting corrosion due to corrosive gases and chlorides in formation water, localized corrosion due to protective film breakdown, and hydrogen damage [307]. **Table 11** summarizes a rule of thumb guideline for assessing corrosion susceptibility based on the partial pressures of CO_2 and H_2S.

Table 11 Rule of thumb guidelines for assessing corrosion susceptibility and severity factors in the oilfield environment [308].

Corrosion type	Condition	Severity
Sweet corrosion	$pCO_2/pH_2S > 500$ $pH_2S < 0.01$ psi	$pCO_2 < 7$ psi: Noncorrosive [a] pCO_2 7 - 15 psi: Likely Corrosive pCO_2 15 - 30 psi: Corrosive $pCO_2 > 30$ psi: Severely corrosive
Sour corrosion	$pH_2S \geq 0.05$ psi	$pCO_2/pH_2S < 20$: Sever sour mechanism pCO_2/pH_2S 20 - 500: Transition severity
Solid sulfur deposition	$pH_2S \geq 10$ psi	Likelihood of solid sulphur separation with drastic pressure loss. [b]
pH influence on sour corrosion	pH > 5: Protective sulphide formation	pH 4.0 - 5.0: Transition effect, localized deformation of sulphide pH 3.5 - 4.0: Higher corrosion rates expected

[a] Except if acetic acid is present at a concentration over 300 ppm.

[b] In HPHT wells, there is a likelihood of deposition if T < 110 °C and H_2S mol.% > 5 and if the pressure-volume-temperature (PVT) study indicated sulphur deposition at the well's temperature and pressure or if oxygen influx into the formation and reacts with H_2S to form S.

Casing materials vary by depth, with higher-strength materials required at greater depths [309]. These materials often include carbon and low alloy steels such as API H40, K55, C75-1, Q125, and H140. For production tubing, different materials are selected based on specific conditions: Carbon steel is used for low water cut and absence of CO_2; carbon steel with inhibitors is employed when corrosion rates can be reduced to 0.1 - 0.15 mm/y; and corrosion-resistant alloys are used for higher corrosion rates [307]. **Table 12** summarizes the conditions under which corrosion rates are influenced by H_2S, CO_2, and their combination, along with guidelines for using carbon steel in well tubular. More details on various corrosion allowance recommendations for different oilfield components are provided in Appendix, **Table A3**.

Table 12 Guidelines for carbon steel use under various corrosive conditions and recommended corrosion allowance [308,310].

Condition	Guidelines for carbon steel use	Corrosion allowance (CA)
CO_2 only system	Corrosion rates are generally low.	No specific CA
H_2S only system	Corrosion rate increases with pCO_2.	No specific CA
CO_2 and H_2S system	Formation of iron sulphide can be protective, reducing corrosion rates.	CA of 3 mm if conditions are met.
Microbiologically influenced corrosion (MIC)	Potential for increased corrosion; use biocides or control measures.	Specific assessment required.
Hydrogen induced cracking (HIC)	Prone to HIC in high hydrogen environments; use suitable material.	Increase CA and specific material considerations.
Applicability rules for carbon steel in well-tubular		
$pCO_2 < 3$ psi, $pH_2S < 0.05$ psi, T: 60 - 120 °C		Adequate CA
$pCO_2 > 3$ psi, $pH_2S < 0.05$ psi, T: 60 - 120 °C, Corrosion rate < 6 mm/y		Use of CA + Corrosion inhibitor
$pCO_2 > 3$ psi, $pH_2S > 0.05$ psi, T > 60 °C, $[Cl^-] < 5{,}000$ ppm, Corrosion rate < 6 mm/y		NACE carbon steel + CA + Corrosion inhibitor
$pH_2S > 0.05$ psi, $pCO_2/pH_2S > 500$, Corrosion rate < 6 mm/y		NACE carbon steel + CA + Corrosion inhibitor

In sour service environments, carbon and low alloy steels are susceptible to SCC. **Figure 12** presents the SSC regions of environmental severity according to ISO 15156-1 [311]. This figure categorizes the environmental severity based on pH_2S and the *in-situ* pH. The figure is divided into 4 regions. Conditions indicated in region 0, with pH_2S less than 0.05 psi, do not require special precautions on material selection; however, cracking could still occur on highly susceptible steels.

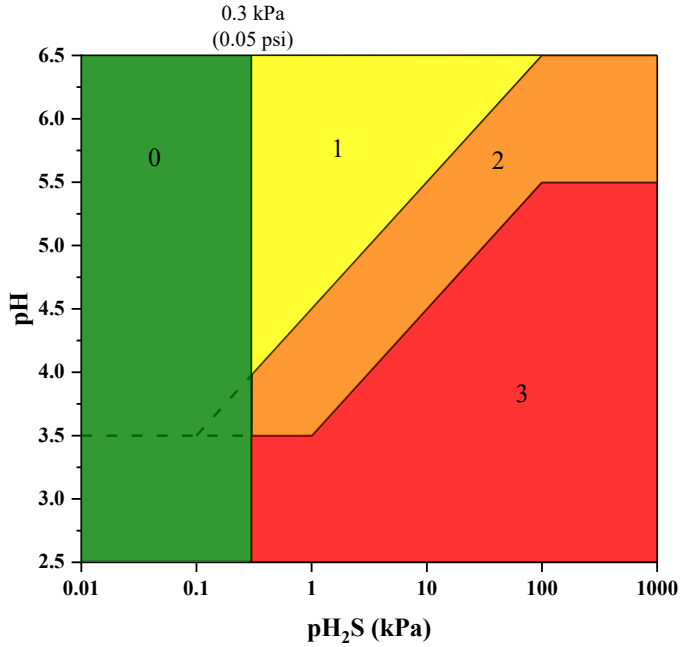

Figure 12 NACE MR0175/ISO 15156-1 SSC classification of environmental severity for carbon and low alloy steels [311].

Several additional factors affect steel performance and selection, including the physical and metallurgical properties of steel affecting its resistance to SSC and hydrogen induced-cracking (HIC), stress concentrations potentially increasing cracking risks, and high-strength steels, with yields above 965 MPa, may suffer HIC in aqueous environments without H_2S. ISO 3183 grades - L245 through L450 could be selected in regions 1, 2, and 3. Cr-Mo low alloy steels (UNS G41XX0) can be used in Region 2 for downhole casing, tubing, and tubular components. Additionally, ISO 11960 grades can be selected for sour services throughout Region 1. For temperatures above 65 °C, N80 type Q, R95, and C110 are suitable. For temperatures exceeding 80 °C, N80 and P110 can be used. For temperatures over 107 °C, Q125 is appropriate. For all temperature ranges, materials such as H40, J55, K55, M65, L80 type 1, C90 type 1, and T95 type 1 are included in the selection. Materials that do not conform to ISO 15156-1 A.2 and A.3 should undergo qualification tests according to the standard.

For pipeline steels, restricted chemistries are set to ensure weldability. Significant efforts have been made to develop CRAs by modifying material manufacturing and surface processes to maintain desirable properties that meet practical engineering demands [312]. The formation of an oxide layer on the surface, which acts as a protective barrier, significantly enhances the material's corrosion resistance [313]. Alloy composition and processing are critical in influencing passive film growth and microstructure transformation.

A common approach in CRA design is to alter 1 alloying element or add additional alloying elements [314]. CRA design has focused on several specified metals, including stainless steels, Ni-based alloys, Co-Cr-Mo alloys, and Ti alloys [315-318]. Notably, Ni-based alloys exhibit high corrosion resistance at elevated temperatures due to the presence of elements like Ti and Cr [319,320]. The alloying elements, along with their respective composition, can significantly improve corrosion resistance. Still, the vast compositional space makes it challenging to identify

optimal composition through experiments alone, highlighting the need for computational tools to enhance efficiency [321].

Thermochemical processing [318,322,323] and surface finishing [324,325] are effective methods for improving corrosion resistance by altering the microstructure or enhancing surface quality, respectively. These processing techniques have been certified as excellent approaches for improving corrosion resistance.

Guidelines were developed for the use of CRAs that are summarized in Appendix, **Table A4**. The guidelines detail the recommended materials based on specific environmental factors such as temperatures, chloride concentration, and H_2S partial pressure, ensuring optimal corrosion resistance and cost-effectiveness.

Compared to CRAs, chemical inhibitors and coatings offer cost-effective corrosion protection in environments where full CRA deployment may not be economically feasible. However, continuous monitoring and replenishment is required for inhibitors, as their efficiency can be compromised under high-shear stress or aggressive chemical conditions. The long-term effectiveness of inhibitors is highly dependent on factors such as fluid composition, temperature, pressure, and flow conditions. While some inhibitors maintain effectiveness over extended periods, others degrade due to thermal breakdown or chemical interactions, requiring frequent re-application to sustain performance [326-328]. Coatings, while providing excellent initial protection, are susceptible to degradation over time due to mechanical damage, permeability issues, and adhesion loss in extreme environments. The durability of these coatings is influenced by downhole conditions such as pressure fluctuations, mechanical wear, and temperature variations. On the other hand, CRAs provide long-term durability and reliability, particularly in downhole and subsea applications where maintenance is challenging. Nickel-based alloys, duplex stainless steels, and super-austenitic stainless steels exhibit high corrosion resistance, but their long-term performance depends on factors such as exposure to aggressive environments, mechanical stresses, and potential galvanic interactions. While each mitigation strategy has advantages and limitations, the selection depends on operational conditions, cost considerations, and maintenance/application feasibility.

Favorable corrosion in downhole settings - advanced dissolvable tools

Evolution of dissolvable frac plug technology

Multi-stage plug-and-perf hydraulic fracturing is a key method for oil and gas extraction in unconventional reservoirs [329]. This technique involves injecting a pressurized liquid, typically water mixed with proppants and thickening agents, to fracture bedrock formations [330]. The process requires frac plugs to isolate lower wellbore zones, enabling sequential fracturing. Since commercialization of hydraulic fracturing in 1949 [331], frac plug technology has evolved significantly. Walton *et al.* [332] categorized this evolution into 3 phases: The cast iron age (1950s - 1990s), the composite age with the birth of horizontal completions (1990s - present), and the dissolvable age (2010s - present). The industry is currently transitioning between composite and dissolvable frac plugs.

Traditional frac plugs, made from cast iron, composite materials, and non-dissolving elastomers, require milling or removal post-fracturing with a coiled tubing unit to maximize production, an operation that can be costly, time-consuming, and pose risks such as tool sticking and wellbore damage from milling debris [333].

Driven by efficiency needs and advances in available materials, dissolvable frac plugs (DFPs) have become a valuable innovation in oil and gas well completions. These plugs eliminate or simplify the milling process with coiled tubing, significantly improving operational efficiency and safety while reducing overall risk and cost. DFPs are engineered to degrade completely, ensuring an unobstructed wellbore for production. Material selection is critical, with high-strength dissolvable metals designed to dissolve in water-based wellbore fluids, formation fluids, or production fluids [334]. The adaptation of DFPs enables longer laterals to be produced more reliably, increasing well production by over 20 % [335].

Dissolution behavior and related influencing factors

The dissolution behavior of DFPs is primarily controlled by downhole chemistry and temperature. The

interaction of alloying elements with wellbore fluids and temperature variations dictates the dissolution rate [334]. Most alloys used in modern dissolvable plugs are magnesium- or aluminum-based, requiring operators to analyze well fluid chemistry for predictable dissolution. However, downhole chemistry varies significantly-horizontally, vertically, and across different wells. Variations arise from water sources, pumped fluids, and reservoir conditions.

The operating conditions of oil and gas wells further impact dissolution. For example, Alberta's wells are categorized based on bottom-hole temperature: Power generation (> 120 °C), industrial heat (> 90 °C), and direct heat (> 60 °C) [336]. The Elmworth gas field in Alberta has a reservoir pressure of 2,200 psi and a temperature of 77.22 °C [337]. Additionally, brine concentration influences dissolution rates, with Alberta brines containing sodium, calcium chlorides, magnesium, bicarbonates, and sulfates [338]. Salinity ranges from 200,000 to 420,000 mg/L (3.41 - 7.19 M NaCl or 1.80 - 3.78 M $CaCl_2$). Given these variations, selecting appropriate dissolvable materials requires assessing downhole conditions (temperature, fluid chemistry) and operational requirements (design parameters, differential pressure, dissolution timeframe).

Advances in aluminum-based dissolvable alloys

The development of dissolvable materials, particularly aluminum-based alloys, has attracted significant interest due to their potential applications in various fields, including hydrogen generation and advanced manufacturing processes. Recent studies have explored the effects of various alloying elements such as Ga, In, Sn, Mg, Cu, and Fe on the microstructure and reactivity of aluminum alloys [28,339-345]. He *et al.* [344] investigated Al alloys containing 3 wt.% of Ga, In, and Sn, prepared by the arc melting technique. It was revealed that different low melting point phases at Al grain boundaries have melting points depending on the alloy compositions. The reactivity of these alloys with water was examined at various temperatures, showing that reaction temperatures above 40 °C exceed the ternary Ga-In-Sn eutectic point. The study found that the alloys mainly consist of Al (Ga) solid solution, β In_3Sn, and γ $InSn_4$ phases. The presence of β and γ phases depends on the Sn content, and the Al-water reaction is governed by the GIS mixture rather than the ternary eutectic. It was concluded that hydrogen generation rates were influenced by grain boundary phases and the water temperature.

In a subsequent study, He *et al.* [339] prepared Al-Mg-Ga-In-Sn alloys using arc melting and melt-spinning techniques. The study assessed the impact of Mg on Al-water reactions, highlighting the segregation of In and Sn and the formation of intermetallic compounds on the Al surface. It was observed that rapid solidification significantly enhanced the reaction rate and hydrogen yield due to the refinement of Al grains. Compared with the as-cast alloys, the rapidly solidified alloys exhibited refined Al grains (2 - 4 μm) and decreased precipitation phases. Enhanced reaction rate and hydrogen yield in rapidly solidified alloys were attributed to grain refinement. In another study, He *et al.* [340] focused on varying Cu contents in Al-Cu-Ga-In-Sn alloys, to examine Cu influence on Al-water reactions. It was concluded that the presence of Al_2Cu phases hindered the Al-water reaction by affecting the formation and distribution of the low melting point Ga-In-Sn phase and cutting off direct contact with Al matrix. In a similar study, Wei *et al.* [341] prepared Cu-containing Al-Ga-$InSn_4$ alloys and investigated their microstructure and hydrogen evolution. They found that adding Cu increased hydrogen yield and stabilized the Al-water reaction. Cu prevented the growth of Al grains and induced pulverization of the Al(Ga) solid solution, increasing the specific surface area and reaction rate. It was concluded that the presence of Al(Cu) solid solution and elemental Cu enhanced the reaction rate. SEM images of the low melting phases and Al_2Cu are illustrated in **Figure 13** [341,344]. In **Figure 13(a)**, the In_3Sn (bright particles) can be seen dispersed in the Al_2Cu phases (grey sheets) preventing the direct contact of the low melting point phases with the Al matrix. This results in Al being not depleted. **Figure 13(b)** shows the formation of low melting point intermetallic phases, In_3Sn as particles and $InSn_4$ as sheets, in Al-Ga-In-Sn alloy.

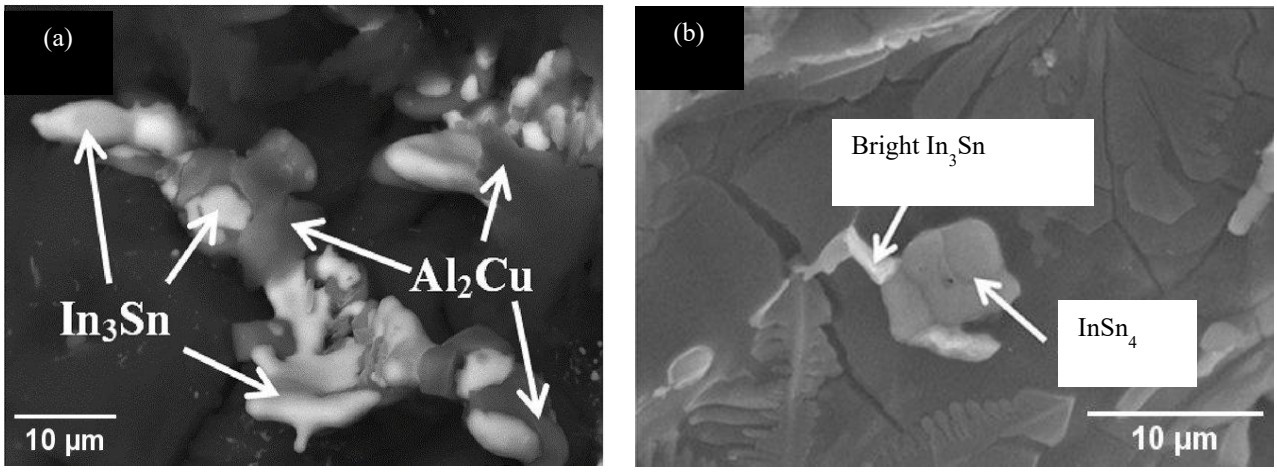

Figure 13 SEM images showing low melting point phases for (a) Al-Cu-Ga-In-Sn with 3 % Cu, showing reaction by-products [340], and (b) Al-1.75wt.% Ga-0.625wt.% In-0.625wt.% Sn [344]. Reprinted with permission from [340,344].

Wang *et al.* [342] prepared Fe-bearing Al-Ga-In-Sn alloys and studied their microstructure and Al-water reactivity. The study revealed that Fe formed dendrites on Al grain surfaces without affecting the reactivity. The Al-water reaction was confirmed to depend on the eutectic reaction of Al with Ga, In, and Sn. It was also observed that besides Al(Ga) and In_3Sn, $InSn_4$ -phases were found in an alloy with extra Sn addition, enhancing the reactivity of Al with water. In another study, Wang *et al.* [343] prepared an Al alloy ribbon with finer Al grains using a rapid spinning technique and then annealed it at various temperatures. The study found that Al grain size and the size and number of Ga-In-Sn particles are critical factors for hydrogen evolution rates. Annealing at moderate temperatures (350 °C) maximized hydrogen generation. The Al-water reaction was attributed to the formation of the quaternary eutectic, as some Al atoms from the Al grain entered into Ga-In-Sn through the eutectic reaction.

The mechanical properties and corrosion behavior of Al-based dissolvable alloys are presented in **Figure 14** [28,345]. Ezz *et al.* [28] study explored Al-Zn-Cu-Mg-based dissolvable alloys with alloying elements like Ag, Ga, In, Sn, Zr, Ti, V, and Cr. The alloys were prepared using melting and casting techniques. Their study highlighted a trade-off between dissolvability and mechanical properties, where low melting point intermetallic phases enhanced dissolvability but compromised mechanical strength. Alloys with the highest Ga-In-Sn content exhibited intense corrosion but poor mechanical properties. This trend is illustrated in **Figure 14(a)**, where alloy DA18 demonstrated superior dissolution but limited mechanical strength. The study identified In-containing phases as the primary factor driving Al degradation, while course phases further reduced strength.

Similarly, Wang *et al.* [345] study examined Al-6Cu-6Mg-5Sn-3Ga-xIn (x=0, 0.5, 1, 3, and 5 wt.%) alloys, prepared via melting and casting techniques. Their findings revealed that the primary phases in the alloys are α-Al, Al_2MgCu, Mg_2Sn, and Al-In eutectic phases, with Ga in solid solution and In segregating at α-Al grain boundaries. **Figure 14(b)** presents the correlation between mechanical and corrosion properties as a function of In content, showing that the highest mechanical and corrosion rates were observed in Alloy 3, containing 1 wt.% In.

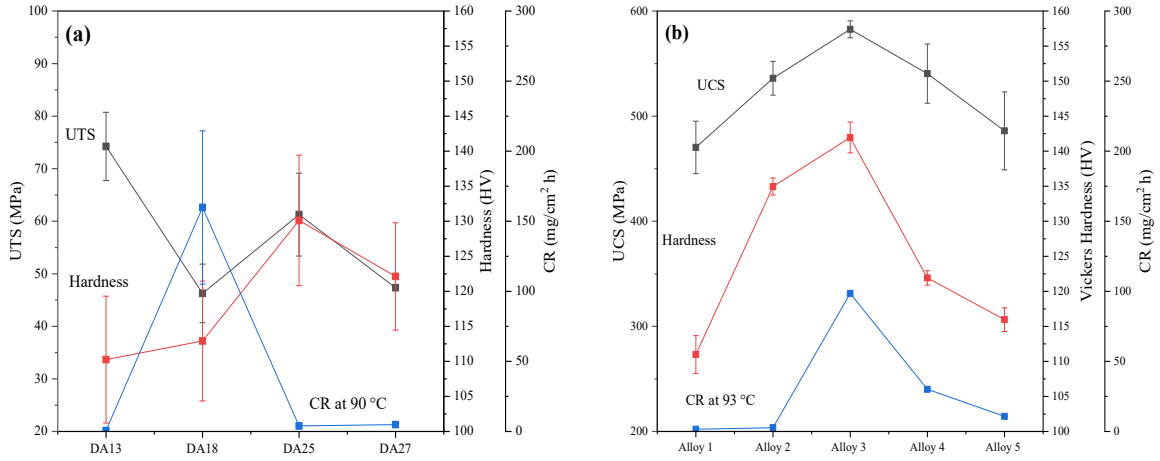

Figure 14 Mechanical properties at room temperature and immersion corrosion rates for: (a) Al-Zn-Mg-Cu-based dissolvable alloys [28], and (b) Al-6Cu-6Mg-5Sn-3Ga-xIn dissolvable alloy [345]. Immersion corrosion rates at 90 °C for (a) and 93 °C for (b). The alloy composition is provided in Appendix A, **Table A2**.

Environmental considerations

The adoption of DFPs in hydraulic fracturing operations offers environmental advantages over traditional composite or cast-iron plugs, particularly in reducing waste, lowering carbon emissions, reducing operational risks, and improving overall sustainability. Unlike traditional composite or cast-iron plugs, DFPs eliminate the generation of plug debris. This not only reduces the amount of waste that must be transported and disposed of but also minimizes the risk of formation damage and fluid migration, which are critical concerns in well integrity and groundwater protection [346].

A major environmental benefit of dissolvable plugs is their contribution to lowering greenhouse gas emissions. Traditional milling operations rely heavily on coiled tubing interventions, which consume large amounts of diesel fuel and extend wellsite activities. According to an environmental impact assessment by Environmental Resources Management (ERM), DFPs can lower carbon footprints by up to 91 %, preventing approximately 67.3 metric tons of CO_2 equivalent (CO_2e) per well. On a 6-well pad, this reduction is equivalent to taking 84 cars off the road, highlighting the scalability of their environmental benefits [347]. Additionally, Vista Energy has reported in a case study significant reductions in diesel consumption, minimizing the daily consumption of 6,000 L during cleanout operations given that each liter of diesel burned contributes approximately 2.7 kg of CO_2. The estimated CO_2e emissions eliminated were reported to be 424 metric tons per 1,000 plugs. The widespread use of dissolvable plugs translates into substantial emissions reductions across multiple well pads [348].

Beyond carbon footprint reduction, the use of DFPs enhances overall sustainability by streamlining well completion processes. The elimination of plug milling reduces rig time, leading to faster well turnovers and improved operational efficiency. Vista Energy, for example, successfully completed 143 frac stages in 4 wells within 19 days using dissolvable plugs, a record completion time in their region. The efficiency gains from reduced intervention not only lower operational costs but also minimize surface disturbances, contributing to a smaller environmental footprint [348]. Additionally, because dissolvable plugs do not require retrieval, the risk of wellbore fluid exposure to surface ecosystems is significantly reduced, further protecting sensitive environmental areas [346].

Commercial applications and case studies

The successful application of dissolvable frac plugs (DFPs) has revolutionized oil and gas well completion practices, eliminating the need for plug retrieval and reducing operational complexity. Several field applications have demonstrated the reliability and efficiency of these plugs, highlighting their advantages in reducing operational costs, minimizing downtime, and improving environmental sustainability.

One notable case study demonstrating the effectiveness of DFPs was reported in Weiyuan Gasfield, China [349]. The well had a downhole temperature of 133 °C and a depth of 5,328 m, with a

horizontal length of 1,533 m and a casing diameter of 114.3 mm. In this well, casing deformation and irregular wellbore conditions posed significant challenges for conventional composite plugs. The wellbore environment led to blocking and sticking issues during tool string delivery, preventing smooth plug deployment. In previous operations, milling out traditional plugs in deformed casing introduced operational risks, and coiled tubing intervention was difficult due to complex downhole conditions.

A mixed design of dissolvable metal and rubber sealing was used to isolate 2 fracturing stages, with an effective sealing time of 30 - 36 h. Compared to conventional composite plugs, which require milling operations post-fracturing, the use of dissolvable plugs in this case eliminated the need for intervention, reduced wellsite activity, and accelerated time to production.

Another successful application of DFPs was documented in Texas, USA, where SLB's third-generation ReacXion dissolvable frac plugs were deployed [350]. These plugs streamlined well clean-up and reduced time to production by more than 6 days. In comparison, traditional plug-and-perf methods would have required multiple coiled tubing trips for milling, increasing operational costs, emissions, and downtime. By removing the need for mechanical intervention, the dissolvable plugs significantly improved operational efficiency and reduced carbon footprint.

Further demonstrating the commercial viability of dissolvable plugs, SLB reported the deployment of 2,000 ReacXion frac plugs across 4 wells in the Vaca Muerta Basin, Argentina [348]. The elimination of milling operations resulted in an estimated reduction of 424 metric tons of CO_2 emissions per 1,000 plugs deployed. Conventional composite plugs would have required extensive diesel-powered milling, contributing to increased emissions and prolonged wellsite operations. The successful performance of dissolvable plugs in this case validated their reliability and environmental benefits over traditional methods.

These case studies illustrate the growing adoption of dissolvable frac plugs as a preferred alternative to traditional composite plugs. By reducing intervention time, enhancing wellsite efficiency, and minimizing environmental impact, DFPs offer a compelling solution for modern hydraulic fracturing operations. **Table 13** lists commercial dissolvable frac plugs available from major suppliers in the market.

Table 13 Summary of some DFP products and their performance in various case studies.

Company	Material	Product	Specifications	Case Study
Nine [351]	-	Stringer™	Pressure rating: 10,000 psi Temperature rating: Up to 230 °F	*Charter Oak Production Company* • 114 plugs in 2 wells • $200,000 on savings
NOV [352]	Magnesium base	VapR	Pressure rating: 10,000 psi Temperature rating: Up to 250 °F	*Utica shale play of the Appalachian basin* • 160 °F and 11,400 psi, • extended duration testing up to 11 h
Halliburton [353]	Aluminum base	Illusion	Pressure rating: 10,000 psi Temperature rating: Up to 250 °F	*Wolfcamp Formation, Delaware basin* • 117 plugs in 16 wellbores, • $51 million in production value. *Austin Chalk formation* • 270 °F, and 10,000 psi, • reliable and consistent operation
SLB [348]	Aluminum base	ReacXion	Pressure rating: 10,000 psi Temperature rating: Up to 250 °F	*Vaca Muerta, Argentina* • Nearly 2,000 plugs deployed • 100 % reliability. • 143 frac stages in 4 wells

Company	Material	Product	Specifications	Case Study
				• less than 19 days on the first well pad • estimated 424 metric tons of CO_2 emissions avoided per 1,000 plugs deployed
EXPRO [354]	-	BLACK GOLD™	Pressure rating: 10,000 psi Temperature rating: Up to 300 °F	*South Texas* • 23 plugs • reliable in harsh environments, • running speed of up to 650 ft/min
INNOVEX [355]	-	RzrCAT	Pressure rating: 10,000 psi Temperature rating: Up to 350 °F	-
VerTechs [356]	-	WIZARD	Pressure rating: 10,000 - 15,000 psi Temperature rating: Up to 330 °F	*Southwestern shale of China* • casing deformity challenges • 10 - 23 % in estimated losses • 30+ stages were addressed in 6 wells • saving 120 h

A potential direction for future developments in dissolvable tools is enhancing material performance through advanced modeling for alloy design. The integration of artificial intelligence and machine learning will enable more accurate predictions of dissolution behavior, optimizing tool reliability under varying downhole conditions. Additionally, research into alloys with customized corrosion properties will allow precise control over dissolution rates. These advancements will improve operational efficiency and reduce environmental impact.

Conclusions

Corrosion in downhole environments presents significant challenges for the integrity and performance of oil and gas equipment. This study has explored the impact of corrosive gases such as CO_2, H_2S, and O_2, as well as the various forms of corrosion that occur under these extreme conditions. Furthermore, analysis of corrosion control techniques, including corrosion inhibition, surface coatings and material selections have been provided. Additionally, the review also highlights advances in favorable corrosion in downhole settings through advanced dissolvable alloys. While these approaches have demonstrated substantial effectiveness, continued advancements are necessary to enhance their reliability and adaptability to increasingly demanding operational environments. Future directions in downhole corrosion and mitigation should focus on the following key areas:

1) Future work in corrosion inhibition should focus on developing environmentally friendly and biodegradable inhibitors to minimize environmental impact while maintaining high efficiency. Additionally, smart inhibitors that respond dynamically to changes in downhole conditions, such as pH, temperature, and chloride concentration, present a promising direction for enhancing corrosion protection.

2) In the area of surface coatings, next-generation nanostructured and multifunctional coatings with self-healing properties offer potential for improved durability and corrosion resistance. Hybrid coatings that integrate metallic, ceramic, and polymeric layers could further enhance protection against sour environments. Additionally, the development of real-time monitoring coatings with embedded sensors could enable proactive maintenance and early detection of failure.

3) Material selection remains a cornerstone of corrosion mitigation, and future research should explore novel high-performance alloys, such as high-entropy alloys and high-nitrogen stainless steel, designed for downhole applications. The optimization of nickel-based and super duplex stainless steels should also be investigated for improving resistance to localized

corrosion in aggressive environments. Moreover, additive manufacturing techniques provide an opportunity to engineer alloys with controlled microstructures for superior corrosion resistance.

4) The development of DFPs, with controllable dissolution rates, represents a significant advancement in reducing post-fracture clean-up and enhancing operations safety. Research is needed to better understand the performance and reliability of DFPs under varying environmental conditions. Additionally, further investigation into how corrosive gases interact with new alloy compositions is essential to assess their effectiveness in extreme environments. A comprehensive economic evaluation comparing advanced corrosion control technologies with traditional methods is also necessary to ensure cost-effective implementation.

5) Process optimization is another key area for future research, particularly in the integration of machine learning (ML) and artificial intelligence (AI) for predictive corrosion modeling. AI-driven models could enhance corrosion rate estimation and material performance evaluation, leading to more effective maintenance strategies. Additionally, advancements in real-time monitoring systems will enable more accurate corrosion assessment and early intervention.

Addressing these future research directions will help advancing downhole corrosion technologies and mitigation strategies. A focused effort on integrating these advancements into practical applications will be essential to ensuring long-term reliability and cost-effectiveness in extreme operating conditions.

Acknowledgements

The authors gratefully acknowledge the financial support of Discovery Grant from the Natural Sciences and Engineering Research Council (NSERC) of Canada. Jianguo Liu would like to acknowledge the financial support from the China Scholarship Council.

References

[1] PR Roberge. *Handbook of corrosion engineering.* 3rd ed. McGraw-Hill Education, New York, 2019.

[2] JI Al-Tammar, M Bonis, HJ Choi and Y Al-Salim. Saudi Aramco downhole corrosion/scaling operational experience and challenges in HP/HT gas condensate producers. *In*: Proceedings of the SPE International Oilfield Corrosion Conference and Exhibition, Aberdeen, Scotland. 2014.

[3] GH Koch, MPH Brongers, NG Thompson, YP Virmani and JH Payer. *Corrosion cost and preventive strategies in the United States.* National Technical Reports Library, United States, 2002.

[4] MB Kermani and D Harrop. The impact of corrosion on the oil and gas industry. *SPE Production & Facilities* 1996; **11(03)**, 186-190.

[5] PHMSA. Pipeline incident 20 year trends, Available at: https://www.phmsa.dot.gov/data-and-statistics/pipeline/pipeline-incident-20-year-trends, accessed February 2025.

[6] Government of Canada. Pipeline incident data, Available at: https://open.canada.ca/data/en/dataset/7dffedc4-23fa-440c-a36d-adf5a6cc09f1/resource/cce956c1-556d-4fbb-bb24-20f46e1b39d0, accessed February 2025.

[7] A Al-Saeed, R Chandra, N Ai-Mai, M Al-Awadi and Q Dashti. Corrosion monitoring, root cause analysis and selection criteria for future well completion design in deep HPHT sour wells. *In*: Proceedings of the Society of Petroleum Engineers - SPE International Conference and Exhibition on Oilfield Corrosion, Aberdeen, United Kingdom. 2012, p. 113-123.

[8] R Case, S Mahajanam, J Dunn, M Joosten, M Achour, H Marchebois and M Bonis. High temperature corrosion studies in simulated SAGD produced fluids. *Corrosion* 2015; **71(4)**, 536-545.

[9] RH Davis. The versatility of internal thermoplastic tubular liners in mitigating downhole corrosion and wear. *In*: Proceedings of the CORROSION 2003, NACE International, San Diego, California. 2003.

[10] M Koteeswaran. 2010, CO_2 and H_2S corrosion in oil pipelines. Master's Thesis, University of Stavanger, Norway, 2010.

[11] LT Popoola, AS Grema, GK Latinwo, B Gutti and AS Balogun. Corrosion problems during oil and gas production and its mitigation. *International Journal of Industrial Chemistry* 2013; **4(1)**, 35.

[12] S Howard and M Chrenowski. Corrosion in formate brines - 20 years of laboratory testing and field experience. *In*: Proceedings of the Offshore Technology Conference, Kuala Lumpur, Malaysia. 2014, p. 2572-2586.

[13] MA Migahed and IF Nassar. Corrosion inhibition of tubing steel during acidization of oil and gas wells. *Electrochim Acta* 2008; **53(6)**, 2877-2882.

[14] Y Wang, L Zhang, J Deng, Y Wang, S Ren and C Hu. An innovative air assisted cyclic steam stimulation technique for enhanced heavy oil recovery. *Journal of Petroleum Science and Engineering* 2017; **151**, 254-263.

[15] R Rihan, B Al-Wakaa, N Tanoli and H Shalaby. The susceptibility of P110 downhole tubular steel to sulfide stress cracking in H_2S and NaCl. *Journal of Petroleum Science and Engineering* 2019; **174**, 1034-1041.

[16] U Lotz, LV Bodegom and C Ouwehand. The effect of type of oil or gas condensate on carbonic acid corrosion. *Corrosion* 1991; **47(8)**, 635-645.

[17] S Ramachandran, A Gupta, G Al-Muntasheri, J Leal and I Syafil. Analysis of high temperature sour gas wells to mitigate corrosion and scale formation. *In*: Proceedings of the SPE Saudi Arabia Section Annual Technical Symposium and Exhibition, Al-Khobar, Saudi Arabia. 2015.

[18] P Bai, H Zhao, S Zheng and C Chen. Initiation and developmental stages of steel corrosion in wet H_2S environments. *Corrosion Science* 2015; **93**, 109-119.

[19] Q Wang, H Al-Ajwad, S Shen, Y Al-Salim, T Chen and J Leal. Sour corrosion products formed in high H_2S gas wells. *In*: Proceedings of the CORROSION 2019, NACE International, Nashville, Tennessee, United States. 2019.

[20] T Chen, Q Wang, F Chang, J Leal and M Espinosa. Root cause analysis for iron sulfide deposition in sour gas wells. *In*: Proceedings of the Society of Petroleum Engineers - SPE Kuwait Oil and Gas Show and Conference, Mishref, Kuwait. 2019.

[21] S Standlee, KD Efird and D Spiller. Under deposit corrosion from iron sulfide. *In*: Proceedings of the Corrosion 2011, NACE International, Houston, Texas, United States. 2011.

[22] LU Shuanlu, X Jianmin, Y Kang, C Zeliang and D Xunchang. Premium connection downhole tubing corrosion. *Materials Performance* 2008; **47(5)**, 66-69.

[23] SR Jackson, B Gundemoni and P Barth. Sand control in corrosive and erosive downhole conditions at high temperatures. *In*: Proceedings of the Society of Petroleum Engineers - SPE Asia Pacific Oil and Gas Conference and Exhibition, Perth, Australia. 2016.

[24] DC His and RC Woollam. Field evaluation of downhole corrosion mitigation methods at Prudhoe Bay Field, Alaska. *In*: Proceedings of the SPE International Oilfield Chemistry Symposium Proceedings, Houston, Texas, United States. 2001.

[25] T Chen, F Chang, F Liang and Q Wang. Evaluation of a newly developed coating material for corrosion protection using downhole corrosion and scale monitoring tool in sour gas wells. *In*: Proceedings of the CORROSION 1997, NACE International, Nashville, Tennessee, United States. 2019.

[26] D Raghu and JBC Wu. Recent developments in wear and corrosion resistant alloys for oil industry. *In*: Proceedings of the CORROSION 1997, NACE International, New Orleans, Louisiana, United States. 1997.

[27] W Badeghaish, M Noui-Mehidi and O Salazar. The future of nonmetallic composite materials in upstream applications. *In*: Proceedings of the Society of Petroleum Engineers - SPE Gas and Oil Technology Showcase and Conference 2019, Dubai, UAE. 2019.

[28] E Ahmed, H Henein, A Qureshi and J Liu. The microstructure, mechanical behaviour, and dissolvability of novel Al-Cu-Zn-Mg-based alloys. *Canadian Metallurgical Quarterly* 2024; **63(2)**, 440-459.

[29] VA Solovyeva, KH Almuhammadi and WO Badeghaish. Current downhole corrosion control solutions and trends in the oil and gas industry: A review. *Materials* 2023; **16(5)**, 1795.

[30] DS Chauhan, MA Quraishi, AA Sorour and C Verma. A review on corrosion inhibitors for high-pressure supercritical CO_2 environment: Challenges and opportunities. *Journal of Petroleum Science and Engineering* 2022; **215**, 110695.

[31] KK Selvan and RC Panda. Mathematical modeling, parametric estimation, and operational control for natural gas sweetening processes. *ChemBioEng Reviews* 2018; **5(1)**, 57-74.

[32] S Cao, F He and J Gao. Corrosion problems in the oil country tubular goods and their mitigation - A

review. *Anti-Corrosion Methods and Materials* 2017; **64(5)**, 465-478.

[33] R Kiran, C Teodoriu, Y Dadmohammadi, R Nygaard, D Wood, M Mokhtari and S Salehi. Identification and evaluation of well integrity and causes of failure of well integrity barriers (a review). *Journal of Natural Gas Science and Engineering* 2017; **45**, 511-526.

[34] M Askari, M Aliofkhazraei, R Jafari, P Hamghalam and A Hajizadeh. Downhole corrosion inhibitors for oil and gas production - A review. *Applied Surface Science Advances* 2021; **6**, 100128.

[35] K Xhanari, Y Wang, Z Yang and M Finšgar. A review of recent advances in the inhibition of sweet corrosion. *Chemical Record* 2021; **21(7)**, 1845-1875.

[36] MJ Goodwin, OM Musa and JW Steed. Problems associated with sour gas in the oilfield industry and their solutions. *Energy and Fuels* 2015; **29(8)**, 4667-4682.

[37] RJ Johnson, BD Folwell, A Wirekoh, M Frenzel and L Skovhus. Reservoir souring - latest developments for application and mitigation. *Journal of Biotechnology* 2017; **256**, 57-67.

[38] M Elkhodbia, A Negi, G Mubarak, I Barsoum and A AlFantazi. Review on sulfide stress cracking in sour service for OCTG and recent advances in modeling of hydrogen-assisted fracture. *Geoenergy Science and Engineering* 2023; **230**, 212174.

[39] IB Obot, MM Solomon, SA Umoren, R Suleiman, M Elanany, NM Alanazi and AA Sorour. Progress in the development of sour corrosion inhibitors: Past, present, and future perspectives. *Journal of Industrial and Engineering Chemistry* 2019; **79**, 1-18.

[40] SB Paul. Investigation of sweet and sour corrosion of mild steel in oilfield environment by polarization, impedance, XRD and SEM studies. *Corrosion Science and Technology* 2018; **17(5)**, 249-256.

[41] A Pfennig, M Wolf and A Kranzmann. Corrosion and corrosion fatigue of steels in downhole ccs environment - a summary. *Processes* 2021; **9(4)**, 594.

[42] AM Nejad. A review of contributing parameters in corrosion of oil and gas wells. *Anti-Corrosion Methods and Materials* 2018; **65(1)**, 73-78.

[43] IA Fioravante, RS Nunes, HA Acciari and EN Codaro. Films formed on carbon steel in sweet environments - a review. *Journal of the Brazilian Chemical Society* 2019; **30(7)**, 1341-1349.

[44] IB Obot, IB Onyeachu, SA Umoren, MA Quraishi, AA Sorour, T Chen, N Aljeaban and Q Wang. High temperature sweet corrosion and inhibition in the oil and gas industry: Progress, challenges and future perspectives. *Journal of Petroleum Science and Engineering* 2020; **185**, 106469.

[45] G Mubarak, C Verma, I Barsoum, A Alfantazi and KY Rhee. Internal corrosion in oil and gas wells during casings and tubing: Challenges and opportunities of corrosion inhibitors. *Journal of the Taiwan Institute of Chemical Engineers* 2023; **150**, 105027.

[46] M Askari, M Aliofkhazraei and S Afroukhteh. A comprehensive review on internal corrosion and cracking of oil and gas pipelines. *Journal of Natural Gas Science and Engineering* 2019; **71**, 102971.

[47] P Gao and K Fan. Sulfur-oxidizing bacteria (SOB) and sulfate-reducing bacteria (SRB) in oil reservoir and biological control of SRB: A review. *Archives of Microbiology* 2023; **205(5)**, 162.

[48] N Dopffel, S Jansen and J Gerritse. Microbial side effects of underground hydrogen storage - knowledge gaps, risks and opportunities for successful implementation. *International Journal of Hydrogen Energy* 2021; **46(12)**, 8594-8606.

[49] XX Li, SM Mbadinga, JF Liu, L Zhou, SZ Yang, JD Gu and BZ Mu. Microbiota and their affiliation with physiochemical characteristics of different subsurface petroleum reservoirs. *International Biodeterioration & Biodegradation* 2017; **120**, 170-185.

[50] R Rabus, SS Venceslau, L Wöhlbrand, G Voordouw, JD Wall and IAC Pereira. A post-genomic view of the ecophysiology, catabolism and biotechnological relevance of sulphate-reducing prokaryotes. *Advances in Microbial Physiology* 2015; **66**, 55-321.

[51] BJ Little, DJ Blackwood, J Hinks, FM Lauro, E Marsili, A Okamoto, SA Rice, SA Wade and HC

Flemming. Microbially influenced corrosion - any progress? *Corrosion Science* 2020; **170**, 108641.

[52] AK Tripathi, P Thakur, P Saxena, S Rauniyar, V Gopalakrishnan, RN Singh, V Gadhamshetty, EZ Gnimpieba, BK Jasthi and RK Sani. Gene sets and mechanisms of sulfate-reducing bacteria biofilm formation and quorum sensing with impact on corrosion. *Frontiers in Microbiology* 2021; **12**, 754140.

[53] MAA Khan, M Hussain and F Djavanroodi. Microbiologically influenced corrosion in oil and gas industries: A review. *International Journal of Corrosion and Scale Inhibition* 2021; **10(1)**, 80-106.

[54] J Gaspar, J Mathieu, Y Yang, R Tomson, JD Leyris, KB Gregory and PJJ Alvarez. Microbial dynamics and control in shale gas production. *Environmental Science & Technology Letters* 2014; **1(12)**, 465-473.

[55] B Anandkumar, RP George, S Maruthamuthu, N Parvathavarthini and UK Mudali. Corrosion characteristics of sulfate-reducing bacteria (SRB) and the role of molecular biology in SRB studies: An overview. *Corrosion Reviews* 2016; **34** (**1-2**), 41-63.

[56] YS Choi, D Young, S Nešić and LGS Gray. Wellbore integrity and corrosion of carbon steel in CO_2 geologic storage environments: A literature review. *International Journal of Greenhouse Gas Control* 2013; **16**, S70-S77.

[57] E Olorundaisi, T Jamiru and AT Adegbola. Mitigating the effect of corrosion and wear in the application of high strength low alloy steels (HSLA) in the petrochemical transportation industry - A review. *Materials Research Express* 2020; **6(12)**, 1265k9.

[58] A Khan, A Qurashi, W Badeghaish, MN Noui-Mehidi and MA Aziz. Frontiers and challenges in electrochemical corrosion monitoring; surface and downhole applications. *Sensors* 2020; **20(22)**, 1-35.

[59] M Shamlooh, S Abdelrady, M Buasali and K Farouque. Well integrity protection using corrosion inhibitor treatment system for sour gas producers in Bahrain field. *In*: Proceedings of the SPE Middle East Oil and Gas Show and Conference, Manama, Bahrain. 2019.

[60] P Kalita, V Sharma, L Pandey and P Tiwari. *Secondary and tertiary oil recovery processes. In*: L Pandey and P Tiwari (Eds.). Green energy and technology. Springer, Singapore, 2022 p. 23-50.

[61] National Petroleum Council. CO_2 enhanced oil recovery, Available at: https://webstore.iea.org/insights-series-2015-storing-co2-, accessed February 2025.

[62] S Anderson and R Newell. Prospects for carbon capture and storage technologies. *Annual Review of Environment and Resources* 2004; **29(1)**, 109-142.

[63] RS Haszeldine. Carbon capture and storage: how green can black be? *Science* 2009; **325(5948)**, 1647-1652.

[64] LS Melzer. *Carbon dioxide enhanced oil recovery (CO_2 EOR): Factors involved in adding carbon capture, utilization and storage (CCUS) to enhanced oil recovery.* Center for Climate and Energy Solutions, Midland, Texas, United States, 2012.

[65] FM Song. A comprehensive model for predicting CO_2 corrosion rate in oil and gas production and transportation systems. *Electrochimica Acta* 2010; **55(3)**, 689-700.

[66] Y Zhang, G Zhao and YF Cheng. Effect of O_2 on down-hole corrosion during air-assisted steam injection for heavy oil recovery. *Corrosion Engineering Science and Technology* 2019; **54(4)**, 310-316.

[67] JK Heuer and JF Stubbins. An XPS characterization of $FeCO_3$ films from CO_2 corrosion. *Corrosion Science* 1999; **41(7)**, 1231-1243.

[68] PL Fosbøl, K Thomsen and EH Stenby. Review and recommended thermodynamic properties of $FeCO_3$. *Corrosion Engineering, Science and Technology* 2010; **45(2)**, 115-135.

[69] L Zheng, J Landon, NS Matin and K Liu. $FeCO_3$ coating process toward the corrosion protection of carbon steel in a postcombustion CO_2 capture system. *Industrial & Engineering Chemistry Research* 2016; **55(14)**, 3939-3948.

[70] QY Li, LJ Mao and SW Zhou. Effects of chloride content on CO_2 corrosion of carbon steel in simulated oil and gas well environments. *Corrosion Science* 2014; **84**, 165-171.

[71] R Elgaddafi, R Ahmed and S Osisanya. Modeling and experimental study on the effects of temperature on the corrosion of API carbon steel in CO_2-saturated environment. *Journal of Petroleum Science and Engineering* 2021; **196**, 107816.

[72] R Barker, D Burkle, T Charpentier, H Thompson and A Neville. A review of iron carbonate ($FeCO_3$) formation in the oil and gas industry. *Corrosion Science* 2018; **142**, 312-341.

[73] G Schmitt and M Horstemeier. Fundamental aspects of CO_2 metal loss corrosion - part II: Influence of different parameters on CO_2 corrosion mechanisms. *In*: Proceedings of the CORROSION 2006, NACE International, San Diego, California, United States, 2006.

[74] K Patchigolla, JE Oakey and EJ Anthony. Understanding dense phase CO_2 corrosion problems. *Energy Procedia* 2014; **63**, 2493-2499.

[75] M Ueda and H Takabe. Effect of environmental factor and microstructure on morphology of corrosion products in CO_2 environments. *In*: Proceedings of the Corrosion 1999, NACE International, Houston, Texas, United States. 1999.

[76] C Waard and DE Milliams. Carbonic acid corrosion of steel. *Corrosion* 1975; **31(5)**, 177-181.

[77] K Videm and A Dugstad. Corrosion of carbon steel in an aqueous carbon dioxide environment. *Materials Performance* 1989; **28(4)**, 5890061.

[78] YS Choi, S Nesic and HG Jung. Effect of alloying elements on the corrosion behavior of carbon steel in CO_2 environments. *In*: Proceedings of the Corrosion 2018, NACE International, Phoenix, Arizona, United State. 2018.

[79] E Gulbrandsen, J Kvarekval and H Miland. Effect of oxygen contamination on the inhibition of CO_2 corrosion. *In*: Proceedings of the Corrosion 2001, Houston, Texas, United States. 2001.

[80] S Dong, W Liu, J Zhang, X Lin, J He and M Lu. Effect of oxygen on CO_2 corrosion and erosion-corrosion behavior of N80 steel under high temperature and high pressure. *In*: Proceedings of the Corrosion 2014, NACE International, San Antonio, Texas, United States. 2014.

[81] S Wang. 2009, Effect of oxygen on CO_2 corrosion of mild steel. Master's Thesis. Ohio University, United States.

[82] C de Waard, U Lotz and DE Milliams. Predictive model for CO_2 corrosion engineering in wet natural gas pipelines. *Corrosion* 1991; **47(12)**, 976-985.

[83] A Dugstad. Mechanism of protective film formation during CO_2 corrosion of carbon steel. *In*: Proceedings of the CORROSION 98, NACE International, San Diego, California, United States.1998.

[84] A Dugstad, B Morland and S Clausen. Corrosion of transport pipelines for CO_2-effect of water ingress. *Energy Procedia* 2011; **4**, 3063-3070.

[85] CA Palacios and JR Shadley. CO_2 corrosion of N-80 steel at 71 °C in a 2-phase flow system. *Corrosion* 1993; **49(8)**, 686-693.

[86] S Nesic. Effects of multiphase flow on internal CO_2 corrosion of mild steel pipelines. *Energy and Fuels* 2012; **26(7)**, 4098-4111.

[87] AM Nor, MF Suhor, MF Mohamed, M Singer and S Nesic. Corrosion of carbon steel in high CO_2 environment: Flow effect. *In*: Proceedings of the CORROSION 2011, NACE International, Houston, Texas, United States. 2011.

[88] B Mishra, S Al-Hassan, DL Olson and MM Salama. Development of a predictive model for activation-controlled corrosion of steel in solutions containing carbon dioxide. *Corrosion* 1997; **53**(**11**), 852-859.

[89] ME Orazem and J Filho. Application of a submerged impinging jet to investigate the influence of temperature, dissolved CO_2, and fluid velocity on corrosion of pipeline grade steel in brine. *In*: Proceedings of the CORROSION 2001, NACE International, Houston, Texas, United States. 2001.

[90] U Lotz and T Sydberger. CO_2 corrosion of carbon steel and 13Cr steel in particle-laden fluid. *Corrosion* 1988; **44(11)**, 800-809.

[91] R Elgaddafi, R Ahmed, S Hassani, S Shah and SO Osisanya. Corrosion of C110 carbon steel in high-pressure aqueous environment with mixed hydrocarbon and CO_2 gas. *Journal of Petroleum Science and Engineering* 2016; **146**, 777-787.

[92] ZR Ye, ZC Qiu, R Yi, PF Sui, XQ Lin and K Li. Effect of temperature on corrosion behaviour of N80 steel in CO_2-saturated formation water. *IOP Conference Series: Materials Science and Engineering* 2019; **504(1)**, 012040.

[93] Y Xiang, Z Wang, Z Li and WD Ni. Effect of temperature on corrosion behaviour of X70 steel in high pressure $CO_2/SO_2/O_2/H_2O$ environments. *Corrosion Engineering Science and Technology* 2013; **48(2)**, 121-129.

[94] HS Klapper, J Stevens and G Wiese. Pitting corrosion resistance of CrMn austenitic stainless steel in simulated drilling conditions-role of pH, temperature, and chloride concentration. *Corrosion* 2013; **69(11)**, 1095-1102.

[95] M Xu, Q Zhang, XX Yang, Z Wang, J Liu and Z Li. Impact of surface roughness and humidity on X70 steel corrosion in supercritical CO_2 mixture with SO_2, H_2O, and O_2. *The Journal of Supercritical Fluids* 2016; **107**, 286-297.

[96] M Al-Khateeb, R Barker, A Neville and H Thompson. An experimental and theoretical investigation of the influence of surface roughness on corrosion in CO_2 environments. *Journal of Corrosion Science and Engineering* 2018; **20**, 1-29.

[97] YS Choi and S Nešic. Effect of water content on the corrosion behavior of carbon steel in supercritical CO_2 phase with impurities. *In*: Proceedings of the Corrosion 2011, NACE International, Houston, Texas, United States, 2011.

[98] MF Mohamed, AM Nor, MF Suhor, M Singer, YS Choi and S Nešic. Water chemistry for corrosion prediction in high pressure CO_2 environments. *In*: Proceedings of the Corrosion 2011, NACE International, Houston, Texas, United States. 2011.

[99] Y Zhang, K Gao and G Schmitt. Effect of water on steel corrosion under supercritical CO_2 conditions. *Materials Performance* 2011; **50(6)**, 62-68.

[100] Y Zhang, K Gao and G Schmitt. Water effect on steel under supercritical CO_2 condition. *In*: Proceedings of the Corrosion 2011, NACE International, Houston, Texas, United States. 2011.

[101] YS Choi and S Nešić. Determining the corrosive potential of CO_2 transport pipeline in high pCO_2-water environments. *International Journal of Greenhouse Gas Control* 2011; **5(4)**, 788-797.

[102] Y Xiang, Z Wang, X Yang, W Ni and Z Li. Corrosion behavior of X70 steel in the supercritical CO_2 mixed with SO_2 and saturated water. *In*: Proceedings of the 21st International Offshore and Polar Engineering Conference, Maui, Hawaii, United States. 2011.

[103] J Wang, D Ryan, EJ Anthony, N Wildgust and T Aiken. Effects of impurities on CO_2 transport, injection and storage. *Energy Procedia* 2011; **4**, 3071-3078.

[104] N Kladkaew, R Idem, P Tontiwachwuthikul and C Saiwan. Studies on corrosion and corrosion inhibitors for amine-based solvents for CO_2 absorption from power plant flue gases containing CO_2, O_2 and SO_2. *Energy Procedia* 2011; **4**, 1761-1768.

[105] Y Xiang, Z Wang, C Xu, C Zhou, Z Li and W Ni. Impact of SO_2 concentration on the corrosion rate of X70 steel and iron in water-saturated supercritical CO_2 mixed with SO_2. *The Journal of Supercritical Fluids* 2011; **58(2)**, 286-294.

[106] P Ahmadi and A Chapoy. CO_2 solubility in formation water under sequestration conditions. *Fluid Phase Equilibria* 2018; **463** 80-90.

[107] EM Russick, GA Poulter, CLJ Adkins and NR Sorensen. Corrosive effects of supercritical carbon dioxide and cosolvents on metals. *The Journal of Supercritical Fluids* 1996; **9(1)**, 43-50.

[108] A Al-Hashem and JA Carew. CO_2 corrosion of L-80 steel in simulated oil well conditions. *In*: Proceedings of the CORROSION 2002, NACE International, Denver, Colorado, United States. 2002.

[109] J Whittaker, Q Liu, DJ Brown and R Marsden. Corrosion management and mechanism study on SAGD Brackish water system. *In*: Proceedings of the Corrosion 2014, NACE International, San Antonio, Texas, United States. 2014.

[110] R Elgaddafi, R Ahmed and S Shah. Modeling and experimental studies on CO_2-H_2S corrosion of API carbon steels under high-pressure. *Journal of Petroleum Science and Engineering* 2017; **156**, 682-696.

[111] S Trasatti, L Scoppio and T Cheldi. H_2S and CO_2 corrosion of some 9Cr1Mo alloys for downhole applications. *In*: Proceedings of the Corrosion 2001, NACE International, Houston, Texas, United States. 2001.

[112] S Hassani, TN Vu, NR Rosli, SN Esmaeely, YS Choi, D Young and S Nesic. Wellbore integrity and corrosion of low alloy and stainless steels in high pressure CO_2 geologic storage environments: An experimental study. *International Journal of Greenhouse Gas Control* 2014; **23**, 30-43.

[113] B Kermani, JC Gonzales, GL Turconi, TE Perez and C Morales. In-field corrosion performance of 3 %Cr steels in sweet and sour downhole production and water injection. *In*: Proceedings of the Corrosion 2004, NACE International, New Orleans, Louisiana, United States. 2004.

[114] CF Chen, GX Zhao and ML Yan. Characteristics of CO_2 corrosion product film in Cr oil casing steel. *Journal of the Chinese Society of Corrosion and Protection* 2002; **22**, 335-338.

[115] Z Yuling, T Qingchao, D Xuyan, X Xu and W Guofu. The CO_2 corrosion behaviour of 25Mn2 and 2Cr steels under certain downhole condition. *Corrosion Engineering, Science and Technology* 2024; **59(1)**, 3-12.

[116] C Ren, D Liu, Z Bai and T Li. Corrosion behavior of oil tube steel in simulant solution with hydrogen sulfide and carbon dioxide. *Materials Chemistry and Physics* 2005; **93(2-3)**, 305-309.

[117] W Yan, J Deng, P Zhu and X Xing. Investigation of pH_2S influence on 3 % Cr tubing steel corrosion behaviours in CO_2-H_2S-Cl- environment. *Corrosion Engineering Science and Technology* 2015; **50(7)**, 525-532.

[118] M de Romero. The mechanism of SRB action in MIC, based on sulfide corrosion and iron sulfide corrosion products. *In*: Proceedings of the Corrosion 2005, NACE International, Houston, Texas, United States. 2005.

[119] S Maxwell. Implications of re-injection of produced water on microbially influenced corrosion (MIC) in offshore water injection systems. *In*: Proceedings of the Corrosion 2005, NACE International, Houston, Texas, 2005.

[120] M Nemati, GE Jenneman and G Voordouw. Mechanistic study of microbial control of hydrogen sulfide production in oil reservoirs. *Biotechnology and Bioengineering* 2001; **74(5)**, 424-434.

[121] HA Videla and LK Herrera. Microbiologically influenced corrosion: Looking to the future. *International Microbiology* 2005; **8(3)**, 169-180.

[122] Y Li, RA van Santen and T Weber. High-temperature FeS-FeS_2 solid-state transitions: Reactions of solid mackinawite with gaseous H_2S. *Journal of Solid State Chemistry* 2008; **181(11)**, 3151-3162.

[123] J Tang, Y Shao, J Guo, T Zhang, G Meng and F Wang. The effect of H_2S concentration on the corrosion behavior of carbon steel at 90 C. *Corrosion Science* 2010; **52(6)**, 2050-2058.

[124] C Zhou, S Zheng, C Chen and G Lu. The effect of the partial pressure of H_2S on the permeation of hydrogen in low carbon pipeline steel. *Corrosion Science* 2013; **67**, 184-192.

[125] P Bai, S Zheng, H Zhao, Y Ding, J Wu and C Chen. Investigations of the diverse corrosion products on steel in a hydrogen sulfide environment. *Corrosion Science* 2014; **87**, 397-406.

[126] H Ma, X Cheng, G Li, S Chen, Z Quan, S Zhao and L Niu. The influence of hydrogen sulfide on corrosion of iron under different conditions. *Corrosion Science* 2000; **42(10)**, 1669-1683.

[127] T Pehlke. Studies of aqueous hydrogen sulfide corrosion in producing SAGD wells. *In*: Proceedings of the Society of Petroleum Engineers - SPE Thermal Well Integrity and Design Symposium, Alberta, Canada. 2017.

[128] D Rickard. The solubility of FeS. *Geochimica et Cosmochimica Acta* 2006; **70(23)**, 5779-5789.

[129] F Shi, L Zhang, J Yang, M Lu, J Ding and H Li. Polymorphous FeS corrosion products of pipeline steel under highly sour conditions. *Corrosion Science* 2016; **102**, 103-113.

[130] W Liu, Z Zhou, Z Li, M Li, Q Li, Z Ye, J Yao and X Zhong. The high-temperature mechanical properties of HS110S steel and its corrosion behaviors in harsh downhole environment. *Anti-Corrosion Methods and Materials* 2022; **69(5)**, 550-560.

[131] YT Al-Janabi. *An overview of corrosion in oil and gas industry. In*: VS Saji and SA Umoren (Eds.).

Corrosion inhibitors in the oil and gas industry. John Wiley & Sons, New Jersey, United States, 2020, p. 1-39.

[132] AJ Betts and LH Boulton. Crevice corrosion: Review of mechanisms, modelling, and mitigation. *British Corrosion Journal* 1993; **28(4)**, 279-295.

[133] SM Sharland. A review of the theoretical modelling of crevice and pitting corrosion. *Corrosion Science* 1987; **27(3)**, 289-323.

[134] XQ Lin, W Liu, J Zhang, S Dong, HL Zhang, XB Li, CC Xu and MX Lu. Characteristics of corrosion scale of 3Cr steel at high temperature and pressure in an O_2 and CO_2 environment. *Wuli Huaxue Xuebao/ Acta Physico - Chimica Sinica* 2013; **29(11)**, 2405-2414.

[135] J Zhang, X Lin, S Lu, T Wang, W Liu, S Dong, C Yang and M Lu. Corrosion behavior and mechanism of N80 steel under high temperature and high pressure CO_2-O_2 coexisting condition. *In*: Proceedings of the CORROSION 2013, NACE International, Orlando, Florida, United States. 2013.

[136] B Yu, DY Li and A Grondin. Effects of the dissolved oxygen and slurry velocity on erosion-corrosion of carbon steel in aqueous slurries with carbon dioxide and silica sand. *Wear* 2013; **302(1-2)**, 1609-1614.

[137] Y Zhang, G Zhao and YF Cheng. Downhole O_2 corrosion during air-assisted steam injection for secondary or tertiary oil recovery. *Corrosion Engineering Science and Technology* 2020; **55(3)**, 189-195.

[138] X Lin, W Liu, F Wu, C Xu, J Dou and M Lu. Effect of O_2 on corrosion of 3Cr steel in high temperature and high pressure CO_2-O_2 environment. *Applied Surface Science* 2015; **329**, 104-115.

[139] M Zenghua, S Yongtao and L Haitao. Corrosion and protection of oil pipe steel P110 in multicomponent thermal fluid. *Chemical Engineering of Oil & Gas* 2012; **41(6)**, 583-585.

[140] KV Rybalka, LA Beketaeva and AD Davydov. Determination of corrosion current density on bulk nickel and nickel powder by the rate of cathodic depolarizer consumption. *Russian Journal of Electrochemistry* 2016; **52(10)**, 921-924.

[141] Y Hua, R Barker and A Neville. Understanding the influence of SO_2 and O_2 on the corrosion of carbon steel in water-saturated supercritical CO_2. *In*: Proceedings of the CORROSION 2015, NACE International, Dallas, Texas, United States. 2015.

[142] YS Choi, S Nesic and D Young. Effect of impurities on the corrosion behavior of CO_2 transmission pipeline steel in supercritical CO_2-water environments. *Environmental Science & Technology* 2010; **44(23)**, 9233-9238.

[143] SP Sah, E Tada and A Nishikata. Corrosion behaviour of austenitic stainless steels in carbonate melt at 923 K under controlled CO_2-O_2 environment. *Corrosion Science* 2018; **133**, 310-317.

[144] L Xia, Y Li, L Ma, H Zhang, N Li and Z Jiang. Influence of O_2 on the erosion-corrosion performance of 3Cr steels in CO_2 containing environment. *Materials* 2020; **13(3)**, 791.

[145] Y Hua, R Barker and A Neville. The effect of O_2 content on the corrosion behaviour of X65 and 5Cr in water-containing supercritical CO_2 environments. *Applied Surface Science* 2015; **356**, 499-511.

[146] H Mansoori, R Mirzaee, F Esmaeilzadeh, A Vojood and AS Dowrani. Pitting corrosion failure analysis of a wet gas pipeline. *Engineering Failure Analysis* 2017; **82**, 16-25.

[147] S Fajardo, DM Bastidas, M Criado and JM Bastidas. Electrochemical study on the corrosion behaviour of a new low-nickel stainless steel in carbonated alkaline solution in the presence of chlorides. *Electrochimica Acta* 2014; **129**, 160-170.

[148] L Freire, MJ Carmezim, MGS Ferreira and MF Montemor. The electrochemical behaviour of stainless steel AISI 304 in alkaline solutions with different pH in the presence of chlorides. *Electrochimica Acta* 2011; **56(14)**, 5280-5289.

[149] L Cao, A Anderko, F Gui and N Sridhar. Localized corrosion of corrosion resistant alloys in H_2S-containing environments. *Corrosion* 2016; **72(5)**, 636-654.

[150] D Lasebikan, A Akisanya and B Deans. Effect of ammonium bisulphite and chloride on the pitting and stress corrosion cracking resistance of super duplex stainless steel pipes under combined

internal pressure and axial tension. *Materials and Corrosion* 2019; **70(4)**, 661-675.

[151] S Zheng, C Li, Y Qi, L Chen and C Chen. Mechanism of (Mg, Al, Ca)-oxide inclusion-induced pitting corrosion in 316L stainless steel exposed to sulphur environments containing chloride ion. *Corrosion Science* 2013; **67**, 20-31.

[152] MI Abdulsalam. Behaviour of crevice corrosion in iron. *Corrosion Science* 2005; **47(6)**, 1336-1351.

[153] B Cai, Y Liu, X Tian, F Wang, H Li and R Ji. An experimental study of crevice corrosion behaviour of 316L stainless steel in artificial seawater. *Corrosion Science* 2010; **52(10)**, 3235-3242.

[154] S Nagarajan and N Rajendran. Crevice corrosion behaviour of superaustenitic stainless steels: Dynamic electrochemical impedance spectroscopy and atomic force microscopy studies. *Corrosion Science* 2009; **51(2)**, 217-224.

[155] JW Oldfield and WH Sutton. Crevice corrosion of stainless steels: II. experimental studies. *British Corrosion Journal* 1978; **13(3)**, 104-111.

[156] Q Yu, C Liu, X Pang, Q Liu and K Gao. CREVICE corrosion behaviors of Q235 weld joint. *Acta Metallurgica Sinica* 2014; **50(11)**, 1319-1326.

[157] D Chen, EH Han and X Wu. Effects of crevice geometry on corrosion behavior of 304 stainless steel during crevice corrosion in high temperature pure water. *Corrosion Science* 2016; **111**, 518-530.

[158] EC Hornus and MA Rodr'guez. Effect of temperature on the crevice corrosion resistance of Ni-Cr-Mo alloys as engineered barriers of nuclear repositories. *Procedia Materials Science* 2012; **1**, 251-258.

[159] EB Haugan, M Næss, CT Rodriguez, R Johnsen and M Iannuzzi. Effect of tungsten on the pitting and crevice corrosion resistance of type 25Cr super duplex stainless steels. *Corrosion* 2017; **73(1)**, 53-67.

[160] K Pourabdollah. Fouling formation and under deposit corrosion of boiler firetubes. *Journal of Environmental Chemical Engineering* 2021; **9(1)**, 104552.

[161] G Yang, L Ying and L Haichao. Experimental studies on the local corrosion of low alloy steels in 3.5 % NaCl. *Corrosion Science* 2001; **43(3)**, 397-411.

[162] AD Saad, MA Alghazal and MA Alkhowaildi. Prediction and management of scale and corrosion in a harsh operating environment: Challenges and innovative solutions. *In*: Proceedings of the Society of Petroleum Engineers - SPE Kingdom of Saudi Arabia Annual Technical Symposium and Exhibition, Dammam, Saudi Arabia. 2016.

[163] A Daminov, V Ragulin and A Voloshin. Mechanism formations of corrosion damage of inter equipment in wells by continuous scale-inhibitor dosing utilizing surface dosing systems: Testing scale and corrosion inhibitors. *In*: Proceedings of the SPE International Oilfield Corrosion Symposium, Aberdeen, United Kingdom. 2006.

[164] RH Hausler, RM Krishnamurthy and BWA Sherar. Observation of productivity loss in large oil wells due to scale formation without apparent production of formation brine. *In*: Proceedings of the CORROSION 2015, Dallas, Texas, United States. 2015.

[165] T Chen, Q Wang, F Chang and A Mukhles. Iron sulfide deposition in sour gas wells: A corrosion induced scale problem. *In*: Proceedings of the Society of Petroleum Engineers - SPE International Oilfield Corrosion Conference and Exhibition 2018, Aberdeen, Scotland, United Kingdom. 2018.

[166] Y Tan, Y Fwu and K Bhardwaj. Electrochemical evaluation of under-deposit corrosion and its inhibition using the wire beam electrode method. *Corrosion Science* 2011; **53(4)**, 1254-1261.

[167] PT Jakobsen and E Maahn. Temperature and potential dependence of crevice corrosion of AISI 316 stainless steel. *Corrosion Science* 2001; **43(9)**, 1693-1709.

[168] JR Vera, D Daniels and MH Achour. Under deposit corrosion (UDC) in the oil and gas industry: A review of mechanisms, testing and mitigation. *In*: Proceedings of the Corrosion 2012, NACE International, Utah, United States. 2012.

[169] J Kvarekvål and G Svenningsen. Effect of iron sulfide deposits on sour corrosion of carbon steel. *In*: Proceedings of the Corrosion 2016, NACE International, Vancouver, Canada. 2016.

[170] GA Zhang, N Yu, LY Yang and XP Guo. Galvanic corrosion behavior of deposit-covered and

uncovered carbon steel. *Corrosion Science* 2014; **86**, 202-212.

[171] M Monnot, RP Nogueira, V Roche, G Berthomé, E Chauveau, R Estevez and M Mantel. Sulfide stress corrosion study of a super martensitic stainless steel in H_2S sour environments: Metallic sulfides formation and hydrogen embrittlement. *Applied Surface Science* 2017; **394**, 132-141.

[172] M Al-Mansour, AM Alfantazi and M El-boujdaini. Sulfide stress cracking resistance of API-X100 high strength low alloy steel. *Materials & Design* 2009; **30(10)**, 4088-4094.

[173] B Kermani, JW Martin and DF Waite. Hydrogen sulfide cracking of downhole tubulars. *In*: Proceedings of the Middle East Oil Show, Bahrain. 1991.

[174] AA Fragiel, S Serna, J Malo-Tamayo, P Silva, B Campillo, E Martínez-Martínez, L Cota, MH Staia, ES Puchi-Cabrera and R Perez. Effect of microstructure and temperature on the stress corrosion cracking of 2 microalloyed pipeline steels in H_2S environment for gas transport. *Engineering Failure Analysis* 2019; **105**, 1055-1068.

[175] PR Rhodes. Environment-assisted cracking of corrosion-resistant alloys in oil and gas production environments: A review. *Corrosion* 2001; **57(11)**, 923-966.

[176] SMR Ziaei, J Mostowfi, MG Pour and SAR Ziaei. Failure analysis: Chloride stress corrosion cracking of AISI 316 stainless steel downhole pressure memory gauge cover. *Engineering Failure Analysis* 2013; **33**, 465-472.

[177] XW Lei, YR Feng, AQ Fu, JX Zhang, ZQ Bai, CX Yin and CH Lu. Investigation of stress corrosion cracking behavior of super 13Cr tubing by full-scale tubular goods corrosion test system. *Engineering Failure Analysis* 2015; **50**, 62-70.

[178] LH Blanche and RJK Wood. Erosion-corrosion synergism for multi-phase flowline materials. *La Houille Blanche* 1992; **47(7-8)**, 605-610.

[179] EAM Hussain and MJ Robinson. Erosion-corrosion of 2205 duplex stainless steel in flowing seawater containing sand particles. *Corrosion Science* 2007; **49(4)**, 1737-1754.

[180] Y Liu, A Alfantazi, RF Schaller and E Asselin. Localised instability of titanium during its erosion-corrosion in simulated acidic hydrometallurgical slurries. *Corrosion Science* 2020; **174**, 108816.

[181] BT Lu, JF Lu and JL Luo. Erosion-corrosion of carbon steel in simulated tailing slurries. *Corrosion Science* 2011; **53(3)**, 1000-1008.

[182] M Rameshk, M Soltanieh and SM Masoudpanah. Effects of flow velocity and impact angle on erosion-corrosion of an API-5 L X65 steel coated by plasma nitriding of hard chromium underlayer. *Journal of Materials Research and Technology* 2020; **9(5)**, 10054-10061.

[183] JZ Yi, HX Hu, ZB Wang and YG Zheng. On the critical flow velocity for erosion-corrosion in local eroded regions under liquid-solid jet impingement. *Wear* 2019; **422**, 94-99.

[184] ZB Zheng, YG Zheng, WH Sun and JQ Wang. Erosion-corrosion of HVOF-sprayed Fe-based amorphous metallic coating under impingement by a sand-containing NaCl solution. *Corrosion Science* 2013; **76**, 337-347.

[185] ZB Zheng, YG Zheng, WH Sun and JQ Wang. Effect of applied potential on passivation and erosion-corrosion of a Fe-based amorphous metallic coating under slurry impingement. *Corrosion Science* 2014; **82**, 115-124.

[186] ZB Zheng, YG Zheng, X Zhou, SY He, WH Sun and JQ Wang. Determination of the critical flow velocities for erosion-corrosion of passive materials under impingement by NaCl solution containing sand. *Corrosion Science* 2014; **88**, 187-196.

[187] ZB Zheng and YG Zheng. Erosion-enhanced corrosion of stainless steel and carbon steel measured electrochemically under liquid and slurry impingement. *Corrosion Science* 2016; **102**, 259-268.

[188] JZ Yi, HX Hu, ZB Wang and YG Zheng. Comparison of critical flow velocity for erosion-corrosion of 6 stainless steels in 3.5 wt% NaCl solution containing 2 wt% silica sand particles. *Wear* 2018; **416**, 62-71.

[189] J Aguirre, M Walczak and M Rohwerder. The mechanism of erosion-corrosion of API X65 steel under turbulent slurry flow: Effect of nominal flow velocity and oxygen content. *Wear* 2019; **438**, 203053.

[190] EM Costa, BA Dedavid, CA Santos, NF Lopes, C Fraccaro, T Pagartanidis and LP Lovatto. Crevice corrosion on stainless steels in oil and gas industry: A review of techniques for evaluation, critical environmental factors and dissolved oxygen. *Engineering Failure Analysis* 2023; **144**, 106955.

[191] ZB Wang, L Pang and YG Zheng. A review on under-deposit corrosion of pipelines in oil and gas fields: Testing methods, corrosion mechanisms and mitigation strategies. *Corrosion Communications* 2022; **7**, 70-81.

[192] R Baboian, J Schully, N Sridhar, D Dunn, C Brossia, G Cragnolino and J Kearns. *Chapter 19-crevice corrosion. In*: R Baboian (Ed.). Corrosion tests and standards: Application and interpretation. ASTM International, West Conshohocken, United States, 2005, p. 221.

[193] FO Pessu. 2015, Investigation of pitting corrosion of carbon steel in sweet and sour oilfield corrosion conditions: A parametric study. Ph. D. Dissertation. University of Leeds, United Kingdom.

[194] NU Obeyesekere. *Pitting corrosion. In*: AM El-Sherik (Ed.). Trends in oil and gas corrosion research and technologies: Production and transmission. Woodhead Publishing, Sawston, United Kingdom, 2017, p. 215-248.

[195] SA Shirazi, BS Mclaury, JR Shadley, KP Roberts, EF Rybicki, HE Rincon, S Hassani, FM Al-Mutahar and GH Al-Aithan. *Erosion-corrosion in oil and gas pipelines. In*: RW Revie (Ed.). Oil and gas pipelines: Integrity and safety handbook. Wiley, New Jersey, United States, 2015, p. 399-422.

[196] VS Raja and T Shoji. *Stress corrosion cracking: Theory and practice*. Elsevier, Amsterdam, The Netherlands, 2011.

[197] S Papavinasam, A Doiron and RW Revie. Model to predict internal pitting corrosion of oil and gas pipelines. *Corrosion* 2010; **66(3)**, 035006.

[198] RL Martin, DW Stegmann and PA Sookprasong. Oilfield corrosion failures analysis: Lessons learned from pitting morphologies. *In*: Proceedings of the International Petroleum Technology Conference, Bangkok, Thailand. 2016.

[199] X Jiang, Q Zhang, D Qu, K Xu and X Song. Corrosion behavior of L360 N and L415 N mild steel in a shale gas gathering environment - laboratory and on-site studies. *Journal of Natural Gas Science and Engineering* 2020; **82**, 103492.

[200] W Zhang, B Brown, D Young, G Bota, S Nesic and M Singer. Pitting mechanism of mild steel in marginally sour environments-part I: A parametric study based on formation of protective layers. *Corrosion Science* 2021; **183**, 109305.

[201] H Wang and J Wylde. Corrosion inhibitor development for slight sour environment with oxygen intrusion issue. *In*: Proceedings of the CORROSION 2010, NACE International, San Antonio, Texas, United States. 2010.

[202] JJ Wan, W Ji, Y He, J Li and Y Gao. Pitting and strip corrosion influence on casing strength of salt cavern compressed air energy storage. *Energies* 2023; **16(14)**, 5362.

[203] A Rahbar-Ranji, N Niamir and A Zarookian. Ultimate strength of stiffened plates with pitting corrosion. *International Journal of Naval Architecture and Ocean Engineering* 2015; **7(3)**, 509-525.

[204] A Sidharth. Effect of pitting corrosion on ultimate strength and buckling strength of plates - a review. *Digest Journal of Nanomaterials & Biostructures* 2009; **4(4)**, 783-788.

[205] Z Wang, P Wang, D Zeng, T Shi and W Deng. A study on the influential factors of stress corrosion cracking in C110 casing pipe. *Materials* 2022; **15(3)**, 801.

[206] YN Zhang, SG Zhang, JH Luo, Y Long, N Ji, B Fan and SM Wang. Effect of flow rate on the corrosion behavior of P110 steel in high-Ca^{2+} and high-Cl^{-} environment. *Metals* 2022, **12(7)**, 1183.

[207] A Anderko and D Miller. Calculating pitting corrosion, Available at: https://wiki.olisystems.com/wiki/Calculating_Pitting_Corrosion, accessed June 2024.

[208] A Anderko, F Gui, L Cao and N Sridhar. Modeling localized corrosion of corrosion-resistant alloys in oil and gas production environments. *In*: Proceedings of the CORROSION 2014, NACE International, San Antonio, Texas, United States. 2014.

[209] HS Klapper and J Stevens. Susceptibility to pitting corrosion of nickel-based alloy 718 exposed to simulated drilling environments. *Corrosion* 2014; **70(9)**, 899-906.

[210] R Zhang, C Ruan, H Yin, D Li, H Liao and M Lu. Effect of chloride ion concentration on corrosion resistance of nickel-based alloy 718 in H_2S and CO_2 containing environment. *Corrosion Science and Protection Technology* 2018; **30(3)**, 285-290.

[211] A Anderko, GR Engelhardt, F Gui, L Cao and N Sridhar. Localized corrosion of corrosion-resistant alloys in environments containing hydrogen sulfide. *In*: Proceedings of the CORROSION 2015, NACE International, Dallas, Texas, United States. 2015.

[212] F Gui, L Cao, R Thodla and N Sridhar. Localized corrosion and stress corrosion cracking of UNS S32750 in H_2S containing environment. *In*: Proceedings of the CORROSION 2016, NACE International, Vancouver, Canada, 2016.

[213] L Pang, Z Wang, Y Zheng, X Lai and X Han. On the localised corrosion of carbon steel induced by the in-situ local damage of porous corrosion products. *Journal of Materials Science & Technology* 2020; **54**, 95-104.

[214] P Guo, EC La Plante, B Wang, X Chen, M Balonis, M Bauchy and G Sant. Direct observation of pitting corrosion evolutions on carbon steel surfaces at the nano-to-micro- scales. *Scientific Reports* 2018; **8(1)**, 1-12.

[215] DA López, WH Schreiner, SR De Sánchez and SN Simison. The influence of carbon steel microstructure on corrosion layers: An XPS and SEM characterization. *Applied Surface Science* 2003; **207**(**1-4**), 69-85.

[216] F Xue, X Wei, J Dong, C Wang and W Ke. Effect of chloride ion on corrosion behavior of low carbon steel in 0.1 m $NaHCO_3$ solution with different dissolved oxygen concentrations. *Journal of Materials Science & Technology* 2019; **35(4)**, 596-603.

[217] M Liu, J Wang, W Ke and EH Han. Corrosion behavior of X52 anti-H_2S pipeline steel exposed to high H_2S concentration solutions at 90 °C. *Journal of Materials Science & Technology* 2014; **30(5)**, 504-510.

[218] R Barker, D Burkle, T Charpentier, H Thompson and A Neville. A review of iron carbonate ($FeCO_3$) formation in the oil and gas industry. *Corrosion Science* 2018; **142**, 312-341.

[219] A Shamsa, R Barker, Y Hua, E Barmatov, TL Hughes and A Neville. The role of Ca^{2+} ions on Ca/Fe carbonate products on X65 carbon steel in CO_2 corrosion environments at 80 and 150 °C. *Corrosion Science* 2019; **156**, 58-70.

[220] KT Ly, DJ Blumer, WM Bohon and A Chan. Novel chemical dispersant for removal of organic/inorganic Schmoo scale in produced water injection systems. *In*: Proceedings of the CORROSION 1998, NACE International, San Diego, California, 1998.

[221] J Beavers and TA Bubenik. Stress corrosion cracking. *In*: AM El-Sherik (Ed.). Woodhead publishing series in energy, trends in oil and gas corrosion research and technologies: Production and transmission. Woodhead Publishing, Sawston, United Kingdom, 2017, p. 295-314.

[222] X Tang, LY Xu and YF Cheng. Electrochemical corrosion behavior of X-65 steel in the simulated oil-sand slurry. II: Synergism of erosion and corrosion. *Corrosion Science* 2008; **50(5)**, 1469-1474.

[223] BR Tian and YF Cheng. Electrochemical corrosion behavior of X-65 steel in the simulated oil sand slurry. I: Effects of hydrodynamic condition. *Corrosion Science* 2008; **50(3)**, 773-779.

[224] J Aguirre and M Walczak. Multifactorial study of erosion-corrosion wear of a X65 steel by slurry of simulated copper tailing. *Tribology International* 2018; **126**, 177-185.

[225] P Andrews, TF Illson and SJ Matthews. Erosion-corrosion studies on 13 Cr steel in gas well environments by liquid jet impingement. *Wear* 1999; **233**, 568-574.

[226] QY Wang, SL Bai and Z Liu. Surface characterization and erosion-corrosion behavior of Q235 steel in dynamic flow. *Tribology Letters* 2013, **53(1)**, 271-279.

[227] MA Islam and Z Farhat. Erosion-corrosion mechanism and comparison of erosion-corrosion performance of API steels. *Wear* 2017; **376**, 533-541.

[228] RJK Wood. Erosion-corrosion mechanism and comparison effect on marine and offshore materials. *Wear* 2006; **261(9)**, 1012-1023.

[229] RH Jones. *Mechanisms of stress-corrosion cracking*. *In*: RH Jones (Ed.). Stress-corrosion cracking. 2nd ed. ASM International, Almere, The Netherlands, 2017, p. 1-41.

[230] LK Zhu, Y Yan, LJ Qiao and AA Volinsky. Stainless steel pitting and early-stage stress corrosion cracking under ultra-low elastic load. *Corrosion Science* 2013; **77**, 360-368.

[231] G van Boven, W Chen and R Rogge. The role of residual stress in neutral pH stress corrosion cracking of pipeline steels. part I: Pitting and cracking occurrence. *Acta Materialia* 2007; **55(1)**, 29-42.

[232] AB Cook, SB Lyon, NPC Stevens, M Gunther, G McFiggans, RC Newman and DL Engelberg. Assessing the risk of under-deposit chloride-induced stress corrosion cracking in austenitic stainless steel nuclear waste containers. *ECS Transactions* 2014; **49(6)**, 529-534.

[233] D Kuang and YF Cheng. Study of cathodic protection shielding under coating disbondment on pipelines. *Corrosion Science* 2015; **99**, 249-257.

[234] OE Albores-Silva, EA Charles and C Padovani. Effect of chloride deposition on stress corrosion cracking of 316L stainless steel used for intermediate level radioactive waste containers. *Corrosion Engineering, Science and Technology* 2011; **46(2)**, 124-128.

[235] C Örnek and DL Engelberg. Toward understanding the effects of strain and chloride deposition density on atmospheric chloride-induced stress corrosion cracking of type 304 austenitic stainless steel under $MgCl_2$ and $FeCl_3$: $MgCl_2$ droplets. *Corrosion* 2019; **75(2)**, 167-182.

[236] AMPP. Oil and gas production, Available at: https://www.ampp.org/technical-research/what-is-corrosion/corrosion n-reference-library/oil-gas, accessed July 2024.

[237] VN Ayukayeva, GI Boiko, NP Lyubchenko, RG Sarmurzina, RF Mukhamedova, US Karabalin and SA Dergunov. Polyoxyethylene sorbitan trioleate surfactant as an effective corrosion inhibitor for carbon steel protection. *Colloids and Surfaces A: Physicochemical and Engineering Aspects* 2019; **579**, 123636.

[238] Z Panossian, NL de Almeida, RMF de Sousa, G de Souza Pimenta and LBS Marques. Corrosion of carbon steel pipes and tanks by concentrated sulfuric acid: A review. *Corrosion Science* 2012; **58**, 1-11.

[239] D Wang, Y Li, B Chen and L Zhang. Novel surfactants as green corrosion inhibitors for mild steel in 15 % HCl: experimental and theoretical studies. *Chemical Engineering Journal* 2020; **402**, 126219.

[240] X Wang, H Yang and F Wang. A cationic gemini-surfactant as effective inhibitor for mild steel in HCl solutions. *Corrosion Science* 2010; **52(4)**, 1268-1276.

[241] NAF Al-Rawashdeh and AK Maayta. Cationic surfactant as corrosion inhibitor for aluminum in acidic and basic solutions. *Anti-Corrosion Methods and Materials* 2005; **52(3)**, 160-166.

[242] RD Tems. *Downhole corrosion. In*: AM El-Sherik (Ed.). Woodhead publishing series in energy, trends in oil and gas corrosion research and technologies: Production and transmission. Woodhead Publishing, New Jersey, United States, 2017, p. 79-94.

[243] M Finšgar and J Jackson. Application of corrosion inhibitors for steels in acidic media for the oil and gas industry: A review. *Corrosion Science* 2014; **86**, 17-41.

[244] NACE Task Group T-1D-34 Technical Committee Report. *Laboratory test methods for evaluating oilfield corrosion inhibitors*. NACE, Houston, Texas, United States, 1996.

[245] NACE Task Group T-1D-8 Technical Committee Report. *Wheel test method used for evaluation of film persistent inhibitors for oilfield applications*. NACE, Houston, Texas, United States, 1982.

[246] RR Hausler, DW Stegmann and RF Stevens. The methodology of corrosion inhibitor development for CO_2 systems. *Materials and Corrosion* 1989; **40(2)**, 98-113.

[247] BM Watson and J David. Oilfield corrosion inhibition under extremely high shear conditions. *In*: Proceedings of the CORROSION 2000, NACE International, Orlando, Florida, United States. 2000.

[248] G Chesnut and HJ Choi. Laboratory testing and selection of corrosion inhibitors for continuous application in multiphase pipelines. *In*: Proceedings of the Corrosion 1994, NACE International, Houston, Texas, United States. 1994.

[249] NACE Task Group T-5A-31 Technical Committee Report. *State-of-the-art report on controlled-flow laboratory corrosion tests*. NACE, Houston, Texas, United States, 1995.

[250] CG Law and J Newman. Corrosion of a rotating iron disk in laminar, transition, and fully developed turbulent flow. *Journal of the Electrochemical Society* 1986; **133(1)**, 37-42.

[251] G Liu, DA Tree and MS High. Relationships between rotating disk corrosion measurements and corrosion in pipe flow. *Corrosion* 1994; **50(8)**, 584-593.

[252] K Denpo and H Ogawa. Fluid flow effects on CO_2 corrosion resistance of oil well materials 8. *Corrosion* 1993; **49**, 442-449.

[253] JL Dawson and CC Shih. Inhibitor evaluations under controlled hydrodynamic shear. *In*: Proceedings of the Corrosion 2000, NACE International, Orlando, Florida, United States, 1991.

[254] ASTM G170-06(2020)e1. *Standard guide for evaluating qualifying oilfield and refinery corrosion inhibitors in the laboratory*. ASTM International, West Conshohocken, United States, 2020.

[255] JM Esteban, GS Hickey and ME Orazem. The impinging jet electrode: Measurement of the hydrodynamic constant and its use for evaluating film persistency. *Corrosion* 1990; **46(11)**, 896-901.

[256] GA Schmitt and W Bruckhoff. Flow loop versus rotating probes - experimental results and service applications. *Materials Performance* 1991; **30(2)**, 85.

[257] AA Farag and MR Noor El-Din. The adsorption and corrosion inhibition of some nonionic surfactants on API X65 steel surface in hydrochloric acid. *Corrosion Science* 2012; **64**, 174-183.

[258] CM Fernandes, LX Alvarez, NE dos Santos, ACM Barrios and EA Ponzio. Green synthesis of 1-benzyl-4-phenyl-1h-1,2,3-triazole, its application as corrosion inhibitor for mild steel in acidic medium and new approach of classical electrochemical analyses. *Corrosion Science* 2019; **149**, 185-194.

[259] MA Hegazy, AS El-Tabei, AH Bedair and MA Sadeq. An investigation of 3 novel nonionic surfactants as corrosion inhibitor for carbon steel in 0.5 m H_2SO_4. *Corrosion Science* 2012; **54(1)**, 219-230.

[260] MA Migahed, AA Farag, SM Elsaed, R Kamal, M Mostfa and H Abd El-Bary. Synthesis of a new family of Schiff base nonionic surfactants and evaluation of their corrosion inhibition effect on X-65 type tubing steel in deep oil wells formation water. *Materials Chemistry and Physics* 2011; **125(1-2)**, 125-135.

[261] K Ramji, DR Cairns and S Rajeswari. Synergistic inhibition effect of 2-mercaptobenzothiazole and tween-80 on the corrosion of brass in NaCl solution. *Applied Surface Science* 2008; **254(15)**, 4483-4493.

[262] KF Khaled. New synthesized guanidine derivative as a green corrosion inhibitor for mild steel in acidic solutions. *International Journal of Electrochemical Science* 2008; **3(4)**, 462-475.

[263] I Ahamad and MA Quraishi. Mebendazole: New and efficient corrosion inhibitor for mild steel in acid medium. *Corrosion Science* 2010; **52(2)**, 651-656.

[264] M Hosseini, SFL Mertens and MR Arshadi. Synergism and antagonism in mild steel corrosion inhibition by sodium dodecylbenzenesulphonate and hexamethylenetetramine. *Corrosion Science* 2003; **45(7)**, 1473-1489.

[265] LM Rivera-Grau, M Casales, I Regla, DM Ortega-Toledo, JA Ascencio-Gutierrez, J Porcayo-Calderon and L Martinez-Gomez. Effect of organic corrosion inhibitors on the corrosion performance of 1018 carbon steel in 3 % NaCl solution. *International Journal of Electrochemical Science* 2013; **8(2)**, 2491-2503.

[266] JR Perumareddi, VS Sastri and PR Roberge. *Selection of corrosion inhibitors based on structural features. In*: RW Revie, VS Sastri, DL Piron and P Mayer (Eds.). Materials performance

maintenance. Pergamon, İzmir, Turkey, 1991, p. 195-206.

[267] T Zhou, J Yuan, Z Zhang, X Xin and G Xu. The comparison of imidazolium Gemini surfactant [C14-4-C14im]Br2 and its corresponding monomer as corrosion inhibitors for A3 carbon steel in hydrochloric acid solutions: Experimental and quantum chemical studies. *Colloids and Surfaces A: Physicochemical and Engineering Aspects* 2019; **575**, 57-65.

[268] EF Moura, AOW Neto, TN de Castro Dantas, HS Júnior and A Gurgel. Applications of micelle and microemulsion systems containing aminated surfactants synthesized from ricinoleic acid as carbon-steel corrosion inhibitors. *Colloids and Surfaces A: Physicochemical and Engineering Aspects* 2009; **340(1-3)**, 199-207.

[269] M Faccini, L Bautista, L Soldi, AM Escobar, M Altavilla, M Calvet, A Domènech and E Domínguez. Environmentally friendly anticorrosive polymeric coatings. *Applied Sciences* 2021; **11(8)**, 3446.

[270] S Yadav, APS Raman, MB Singh, I Massey, P Singh, C Verma and A AlFantazi. Green nanoparticles for advanced corrosion protection: Current perspectives and future prospects. *Applied Surface Science Advances* 2024; **21**, 100605.

[271] J Panchal, D Shah, R Patel, S Shah, M Prajapati and M Shah. Comprehensive review and critical data analysis on corrosion and emphasizing on green eco-friendly corrosion inhibitors for oil and gas industries. *Journal of Bio-and Tribo-Corrosion* 2021; **7(3)**, 1-29.

[272] AA Nazeer and M Madkour. Potential use of smart coatings for corrosion protection of metals and alloys: A review. *Journal of Molecular Liquids* 2018; **253**, 11-22.

[273] RB Figueira, CJR Silva and EV Pereira. Organic-inorganic hybrid sol-gel coatings for metal corrosion protection: A review of recent progress. *Journal of Coatings Technology and Research* 2015; **12(1)**, 1-35.

[274] H Lu, S Zhang, W Li, Y Cui and T Yang. Synthesis of graphene oxide-based sulfonated oligoanilines coatings for syneristically enhanced corrosion protection in 3.5 % NaCl solution. *ACS Appl Mater Interfaces* 2017; **9(4)**, 4034-4043.

[275] B Ramezanzadeh, A Ahmadi and M Mahdavian. Enhancement of the corrosion protection performance and cathodic delamination resistance of epoxy coating through treatment of steel substrate by a novel nanometric sol-gel based silane composite film filled with functionalized graphene oxide nanosheets. *Corrosion Science* 2016; **109**, 182-205.

[276] M Cui, J Pu, J Liang, L Wang, G Zhang and Q Xue. Corrosion and tribocorrosion performance of multilayer diamond-like carbon film in NaCl solution. *RSC Advances* 2015; **5(127)**, 104829-104840.

[277] M Cui, J Pu, G Zhang, L Wang and Q Xue. The corrosion behaviors of multilayer diamond-like carbon coatings: Influence of deposition periods and corrosive medium. *RSC Advances* 2016; **6(34)**, 28570-28578.

[278] A Ahmadi, B Ramezanzadeh and M Mahdavian. Hybrid silane coating reinforced with silanized graphene oxide nanosheets with improved corrosion protective performance. *RSC Advances* 2016; **6(59)**, 54102-54112.

[279] B Ramezanzadeh, Z Haeri and M Ramezanzadeh. A facile route of making silica nanoparticles-covered graphene oxide nanohybrids (SiO_2-GO); fabrication of SiO_2-GO/epoxy composite coating with superior barrier and corrosion protection performance. *Chemical Engineering Journal* 2016; **303**, 511-528.

[280] M Cui, S Ren, H Zhao, Q Xue and L Wang. Polydopamine coated graphene oxide for anticorrosive reinforcement of water-borne epoxy coating. *Chemical Engineering Journal* 2018; **335**, 255-266.

[281] NS Sangaj and VC Malshe. Permeability of polymers in protective organic coatings. *Progress in Organic Coatings* 2004; **50(1)**, 28-39.

[282] Q Meng, T Ramgopal and GS Frankel. The influence of inhibitor ions on dissolution kinetics of Al and Mg using the artificial crevice technique. *Electrochemical and Solid-State Letters* 2002; **5(2)**, B1.

[283] P Schmuki, S Virtanen, HS Isaacs, MP Ryan, AJ Davenport, H Böhm and T Stenberg. Electrochemical behavior of Cr_2O_3/Fe_2O_3 artificial passive films studied by in situ XANES. *Journal*

of the Electrochemical Society 1998; **145(3)**, 791-801.

[284] M Sakashita and N Sato. The effect of molybdate anion on the ion-selectivity of hydrous ferric oxide films in chloride solutions. *Corrosion Science* 1977; **17(6)**, 473-486.

[285] N Jadhav and V Gelling. Titanium dioxide/conducting polymers composite pigments for corrosion protection of cold rolled steel. *Journal of Coatings Technology and Research* 2015; **12(1)**, 137-152.

[286] L Veleva. *Protective coatings and inorganic anti-corrosion pigments. In*: JV Koleske (Ed.). Paint and coating testing manual: 15th edition of the Gardner-Sward handbook. ASTM International, West Conshohocken, United States, 2012, p. 282.

[287] AC Bastos, MG Ferreira and AM Simões. Corrosion inhibition by chromate and phosphate extracts for iron substrates studied by EIS and SVET. *Corrosion Science* 2006; **48(6)**, 1500-1512.

[288] AM Atta, AM El-Saeed, HI Al-Shafey and GA El-Mahdy. Self-healing passivation of antimicrobial iron oxide nanoparticles for epoxy nanocomposite coatings on carbon steel. *International Journal of Electrochemical Science* 2016; **11(7)**, 5735-5752.

[289] J Mu, F Gao, G Cui, S Wang, S Tang and Z Li. A comprehensive review of anticorrosive graphene-composite coatings. *Progress in Organic Coatings* 2021; **157**, 106321.

[290] JM Yeh, CL Chen, YC Chen, CY Ma, KR Lee, Y Wei and S Li. Enhancement of corrosion protection effect of poly(o-ethoxyaniline) via the formation of poly(o-ethoxyaniline)-clay nanocomposite materials. *Polymer* 2002; **43(9)**, 2729-2736.

[291] T Wang, H Ge and K Zhang. A novel core-shell silica@graphene straticulate structured antistatic anticorrosion composite coating. *Journal of Alloys and Compounds* 2018; **745**, 705-715.

[292] N Jadhav, T Matsuda and V Gelling. Mica/polypyrrole (doped) composite containing coatings for the corrosion protection of cold rolled steel. *Journal of Coatings Technology and Research* 2018; **15(2)**, 363-374.

[293] S Yang, J Huang, J Chen, JJ Noël, I Barker, JD Henderson, P He, H Zhang, H Zhang and J Zhu. A comparative study on the anti-corrosive performance of zinc phosphate in powder coatings. *Coatings* 2022; **12(2)**, 217.

[294] RL Stout. *Solvents in today's coatings. In*: C Craver and C Carraher (Eds.). Applied polymer science: 21st century. Elsevier Science, Oxford, United Kingdom, 2000, p. 527-543.

[295] S Swarup and CK Schoff. A survey of surfactants in coatings technology. *Progress in Organic Coatings* 1993; **23(1)**, 1-22.

[296] B Ramezanzadeh, E Raeisi and M Mahdavian. Studying various mixtures of 3-aminopropyltriethoxysilane (APS) and tetraethylorthosilicate (TEOS) silanes on the corrosion resistance of mild steel and adhesion properties of epoxy coating. *International Journal of Adhesion and Adhesives* 2015; **63**, 166-176.

[297] SS Golru, MM Attar and B Ramezanzadeh. Effects of surface treatment of aluminium alloy 1050 on the adhesion and anticorrosion properties of the epoxy coating. *Applied Surface Science* 2015; **345**, 360-368.

[298] F Chen and P Liu. Conducting polyaniline nanoparticles and their dispersion for waterborne corrosion protection coatings. *ACS Applied Materials & Interfaces* 2011; **3(7)**, 2694-2702.

[299] M Cui, S Ren, J Chen, S Liu, G Zhang, H Zhao, L Wang and Q Xue. Anticorrosive performance of waterborne epoxy coatings containing water-dispersible hexagonal boron nitride (h-BN) nanosheets. *Applied Surface Science* 2017; **397**, 77-86.

[300] L Ma, F Chen, Z Li, M Gan, J Yan, S Wei, Y Bai and J Zeng. Preparation and anticorrosion property of poly(2,3-dimethylaniline) modified by nano-SiO_2. *Composites Part B: Engineering* 2014; **58**, 54-58.

[301] R Naderi and MM Attar. The role of zinc aluminum phosphate anticorrosive pigment in protective performance and cathodic disbondment of epoxy coating. *Corrosion Science* 2010; **52(4)**, 1291-1296.

[302] AC Bastos, MGS Ferreira and AM Simões. Comparative electrochemical studies of zinc chromate and zinc phosphate as corrosion inhibitors for zinc. *Progress in Organic Coatings* 2005; **52(4)**, 339-350.

[303] A Kalendová. Effects of particle sizes and shapes of zinc metal on the properties of anticorrosive coatings. *Progress in Organic Coatings* 2003; **46(4)**, 324-332.

[304] M Alexandre and P Dubois. Polymer-layered silicate nanocomposites: Preparation, properties and uses of a new class of materials. *Materials Science and Engineering: R: Reports* 2000; **28(1-2)**, 1-63.

[305] M Behzadnasab, SM Mirabedini, K Kabiri and S Jamali. Corrosion performance of epoxy coatings containing silane treated ZrO_2 nanoparticles on mild steel in 3.5 % NaCl solution. *Corrosion Science* 2011; **53(1)**, 89-98.

[306] M Nematollahi, M Heidarian, M Peikari, SM Kassiriha, N Arianpouya and M Esmaeilpour. Comparison between the effect of nanoglass flake and montmorillonite organoclay on corrosion performance of epoxy coating. *Corrosion Science* 2010; **52(5)**, 1809-1817.

[307] AK Lahiri. *Material selection and performance in oil and gas industry. In*: AK Lahiri (Ed.). Applied metallurgy and corrosion control. Springer, Singapore, 2017, p. 269-347.

[308] S Bhat. Material selection for oilfield development - narration of practical experience. *Corrosion* 2017; **73**, 1-11.

[309] BE Urband and SMorey. High strength sour service C110 casing. *In*: Proceedings of the SPE/IADC Drilling Conference, Amsterdam, Netherlands. 1999.

[310] IJ Rippon. Carbon steel pipeline corrosion engineering: Life cycle approach. *In*: Proceedings of the CORROSION 2001, NACE International, Houston, Texas, United States. 2001.

[311] International Organization for Standardization (ISO). *ISO 15156-1:2015. Petroleum and natural gas industries - materials for use in H_2S-containing environments in oil and gas production - part 1: General principles for selection of cracking-resistant materials*. ISO, Geneva, Switzerland, 2015.

[312] LR Krishna, Y Madhavi, PS Babu, DS Rao and G Padmanabham. Strategies for corrosion protection of non-ferrous metals and alloys through surface engineering. *Materials Today: Proceedings* 2019; **15**, 145-154.

[313] JM Cordeiro, BE Nagay, MT Mathew and VAR Barão. *Designing corrosion-resistant alloys. In*: Inamuddin, R Boddula, MI Ahamed and AM Asiri (Eds.). Alloy materials and their allied applications. Scrivener Publishing, Texas, United States, 2020, p. 27-38.

[314] AM Manzoni and U Glatzel. New multiphase compositionally complex alloys driven by the high entropy alloy approach. *Materials Characterization* 2019; **147**, 512-532.

[315] CW Chan, S Lee, G Smith, G Sarri, CH Ng, A Sharba and HC Man. Enhancement of wear and corrosion resistance of beta titanium alloy by laser gas alloying with nitrogen. *Applied Surface Science* 2016; **367**, 80-90.

[316] VV Firouzdor, K Sridharan, G Cao, M Anderson and TR Allen. Corrosion of a stainless steel and nickel-based alloys in high temperature supercritical carbon dioxide environment. *Corrosion Science* 2013; **69**, 281-291.

[317] T Akimoto, T Ueno, Y Tsutsumi, H Doi, T Hanawa and N Wakabayashi. Evaluation of corrosion resistance of implant-use Ti-Zr binary alloys with a range of compositions. *Journal of Biomedical Materials Research Part B: Applied Biomaterials* 2018; **106(1)**, 73-79.

[318] Y Qiu, S Thomas, MA Gibson, HL Fraser and N Birbilis. Corrosion of high entropy alloys. *npj Materials Degradation* 2017; **1**, 15.

[319] JJ Marattukalam, AK Singh, S Datta, M Das, VK Balla, S Bontha and SK Kalpathy. Microstructure and corrosion behavior of laser processed NiTi alloy. *Materials Science and Engineering: C* 2015; **57**, 309-313.

[320] Y Xie, TD Nguyen, J Zhang and DJ Young. Corrosion behaviour of Ni-Cr alloys in wet CO_2 atmosphere at 700 and 800 °C. *Corrosion Science* 2019; **146**, 28-43.

[321] Y Ikeda, B Grabowski and F Körmann. *Ab initio* phase stabilities and mechanical properties of multicomponent alloys: A comprehensive review for high entropy alloys and compositionally complex alloys. *Materials Characterization* 2019; **147**, 464-511.

[322] M Janbozorgi, KK Taheri and AK Taheri. Microstructural evolution, mechanical properties, and corrosion resistance of a heat-treated mg alloy

for the bio-medical application. *Journal of Magnesium and Alloys* 2019; **7(1)**, 80-89.

[323] S Liu, X Wang, Y Tao, X Han and C Cui. Enhanced corrosion resistance of 5083 aluminum alloy by refining with nano-CeB6/al inoculant. *Applied Surface Science* 2019; **484**, 403-408.

[324] J Liu, K Zhao, M Yu and S Li. Effect of surface abrasion on pitting corrosion of Al-Li alloy. *Corrosion Science* 2018; **138**, 75-84.

[325] D Nabhan, B Kapusta, P Billaud, K Colas, D Hamon and N Dacheux. Effects of pH, surface finish and thermal treatment on the corrosion of AlFeNi aluminum alloy. Characterization of oxide layers. *Journal of Nuclear Materials* 2015; **457**, 196-204.

[326] A Rostami and HA Nasr-El-Din. Review and evaluation of corrosion inhibitors used in well stimulation. *In*: Proceedings of the SPE International Symposium on Oilfield Chemistry, Texas, United States. 2009, p. 961-977.

[327] UM Angst, M Büchler, J Schlumpf, B Marazzani and M Bakalli. Long-term field performance of an organic corrosion inhibitor for reinforced concrete. *Material Performance* 2020; **55**, 36-40.

[328] LS Kuburi. Effect of flow velocity on the inhibition efficiency of low carbon steel corrosion in crude oil. *Journal of Applied Mechnical Engineering* 2013; **02(02)**, 2.

[329] M Fripp and Z Walton. Fully dissolvable frac plug using dissolvable elastomeric elements. *In*: Proceedings of the SPE Middle East Oil & Gas Show and Conference, Manama, Kingdom of Bahrain. 2017, p. 953-960.

[330] F Liang. *Hydraulic fracturing stimulation. In*: Q Wang (Ed.). Fluid chemistry, drilling and completion. Gulf Professional Publishing, Texas, United States, 2022, p. 421-465.

[331] RF LaFollette and RS Hurt. *Hydraulic fracturing. In*: GM Crawley (Ed.). Fossil fuels: Current status and future directions. World Scientific Publishin, Singapore, 2016, p. 229-288.

[332] Z Walton, M Fripp, J Porter and G Vargus. Evolution of frac plug technologies - cast iron to composites to dissolvable. *In*: Proceedings of the SPE Middle East Oil and Gas Show and Conference, Manama, Bahrain. 2019.

[333] Z Walton, J Porter, M Fripp and G Vargus. Cost and value of a dissolvable frac plug. *In*: Proceedings of the SPE/ICoTA Coiled Tubing and Well Intervention Conference and Exhibition, Texas, United States. 2017.

[334] M Fripp and Z Walton. Degradable metal for use in a fully dissolvable frac plug. *In*: Proceedings of the Offshore Technology Conference, Texas, United States. 2016, p. 3467-3475.

[335] Light Metal Age. Terves expands capabilities: New extrusion press for magnesium and other hard alloys, Available at: https://www.lightmetalage.com/magazine/2020/february-2020/, accessed July 2024.

[336] Canadian Geothermal Energy Association. *Potential for geothermal energy development from co-production in Alberta using existing oil and gas wells: Alberta geothermal opportunity overview*. CanGEA, Calgary, 2017.

[337] RE Wyman, SA Holditch and PL Randolph. Analyses of an Emworth hydraulic fracture in Alberta. *Journal of Petroleum Technology* 1980; **32(9)**, 1621-1630.

[338] B Hitchon and H Me. *Calcium and magnesium in Alberta brines*. Alberta Geological Survey, 1971.

[339] T He, W Chen, W Wang, S Du and S Deng. Microstructure and hydrogen production of the rapidly solidified Al-Mg-Ga-In-Sn alloy. *Journal of Alloys and Compounds* 2020; **827**, 154290.

[340] T He, W Chen, W Wang, F Ren and HR Stock. Effect of different Cu contents on the microstructure and hydrogen production of Al-Cu-Ga-In-Sn alloys for dissolvable materials. *Journal of Alloys and Compounds* 2020; **821**, 153489.

[341] C Wei, D Liu, S Xu, T Cui, Q An, Z Liu and Q Gao. Effects of Cu additives on the hydrogen generation performance of Al-rich alloys. *Journal of Alloys and Compounds* 2018; **738**, 105-110.

[342] W Wang, W Chen, XM Zhao, DM Chen and K Yang. Effect of composition on the reactivity of al-rich alloys with water. *International Journal of Hydrogen Energy* 2012; **37(24)**, 18672-18678.

[343] W Wang, XM Zhao, DM Chen and K Yang. Insight into the reactivity of Al-Ga-In-Sn alloy with water. *International Journal of Hydrogen Energy* 2012; **37(3)**, 2187-2194.

[344] TT He, W Wang, W Chen, DM Chen and K Yang. Influence of In and Sn compositions on the reactivity of Al-Ga-In-Sn alloys with water. *International Journal of Hydrogen Energy* 2017; **42(9)**, 5627-5637.

[345] MF Wang, DH Xiao, BR Sun and WS Liu. Microstructure, mechanical properties and corrosion behavior of Al-Cu-Mg-Sn-Ga-In alloy. *Journal of Alloys and Compounds* 2019; **776**, 172-180.

[346] VerTechs. A sustainable solution: Exploring the eco-friendly nature of dissolvable frac plugs, Available at: https://www.vertechs.com/news-detail/a-sustainable-solution-exploring-the-eco-friendly-nature-of-dissolvable-frac-plugs, accessed February 2025.

[347] BOE REPORT. Evolution of the dissolvable frac plug | BOE Report, Available at: https://boereport.com/2020/03/30/evolution-of-the-dissolvable-frac-plug/, accessed February 2025.

[348] SLB. Fully dissolvable frac plugs reduce time to production, Available at: https://www.slb.com/resource-library/case-study-with-navigation/co/reacxion-vista-energy-argentina-cs, accessed July 2024.

[349] M Li, L Chen, R Wei, C Liao and T Fu. The application of fully dissolvable frac plug technique in Weiyuan gasfield. *In*: Proceedings of the Society of Petroleum Engineers - SPE Kingdom of Saudi Arabia Annual Technical Symposium and Exhibition, Dammam, Saudi Arabia, 2018.

[350] SLB. Texas operator saves >6 days on cleanouts after fracturing, Available at: https://www.slb.com/resource-library/case-study-with-navigation/co/reacxion-complete-wolfcamp-cs, accessed June 30, 2025.

[351] Nine Energy Service. Case study - SRINGER dissolvable frac plug, Available at: https://nineenergyservice.com/completions-technologies/dissolvables/stinger-2, accessed July 2024.

[352] NOV. VapR frac plugs maximize a customer's efficiencies in the Appalachian basin, Available at: https://www.nov.com/about/news/vapr-frac-plugs-maximize-a-customers-efficiencies-in-the-appalachian-basin, accessed July 17, 2024.

[353] Halliburton. Enhanced characterization of reservoir, Available at: https://www.halliburton.com/en/resources/integrated-reservoir-characterization, accessed July 2024.

[354] EXPRO. BLACK gold™ and big easy® frac plugs perform successfully in harsh environment, Available at: https://www.expro.com/case-studies/black-gold-and-big-easy-frac-plugs-perform-successfully-in-harsh-environmen, accessed July 2024.

[355] INNOVEX. Frac plugs: Innovex, Available at: https://www.innovex-inc.com/our-products/well-completion/frac-plugs/, accessed July 2024.

[356] Vertechs Group. Case study - WIZARD THRU - tubing dissolvable plug, Available at: https://www.vertechs.com/completions/dissolvable-plug-wizard-thru-tubing-dissolvable-plug, accessed July 2024

Appendix A

Table A1 The chemical compositions of various steel alloys covered in this study.

Steel	Ref.	C	Mn	P	S	Ni	Cr	Mo	Cu	Si	Other
9A	[111]	0.12	0.49	0.013	0.006	0.16	9.78	1	0.13	-	
9B		0.12	0.454	0.013	0.003	0.15	8.95	0.95	0.13	-	
9C		0.124	0.454	0.01	0,005	0.171	8.93	0.99	0.13	-	
9D		0.11	0.454	0.01	0.0026	0.11	8.53	0.99	0.07	-	
410		0.128	0.83	0.017	0.002	0.39	13	0.02	0.06	-	
S13		0.01	0.38	0.016	0.002	5.25	12.6	2.02	nd	-	
Cr3-A	[113]	0.08	0.47	0.014	0.001	-	3.3	0.29	0.22	0.28	V 0.52, Nb 0.001, Ti 0.028
Cr3-B		0.08	0.47	0.013	0.001	0.043	3.1	0.25	0.248	0.32	Al 0.021, V 0.5, Nb 0.001, Ca 0.0012
L80		0.27	1.36	0.013	0.004	-	-	-	0.12	1.36	Nb 0.001, Ti 0.021
S13Cr	[149]	0.01	-	-	-	5.9	12.1	1.9	-	-	
S15Cr		0.03	0.28	-	-	6.3	14.6	1.9	0.97	0.36	
2507		0.017	0.8	-	-	6.93	25.17	3.87	0.4	0.28	N 0.27
2535		0.02	0.6	-	-	30.6	24.7	2.78	0.81	0.29	
29		≤ 0.02	≤ 2.5	-	-	31.5	27	4.4	1	≤ 1.0	
28		≤ 0.02	≤ 2.0	-	-	31	27	3.5	1	≤ 0.6	
C110	[91]	0.3	0.47	0.007	0.001	0.01	1.01	0.78	0.01	0.23	
1018	[112]	0.21	0.05	0.09	0.05	-	-	-	-	0.38	Al 0.1
A182		0.11	0.42	0.02	0.027	0.15	4.65	0.58	-	0.29	Al 0.029, V 0.05
S41000		0.13	0.49	0.012	0.005	0.112	12.74	0.017	0.009	0.23	Al 0.006, V 0.038, Sb 0.015
HS110S	[130]	0.37	0.42			0.002	0.51	0.75	0.073	0.23	Al 0.029, V 0.08, Nb 0.029
3Cr-80	[117]	0.19	0.32	< 0.01	< 0.006	0.17	2.93	0.39		0.32	
X65		0.12	1.6	0.025	0.015	0.5		0.5	0.5	0.45	
L415N		0.24	1.4	0.025	0.015	0.5	0.5	0.5	0.5	0.45	V 0.1, Nb 0.05, Ti 0.04
2507	[212]	0.017	0.8	-	-	6.93	25.17	3.87	0.4	0.28	N 0.27
S13Cr	[208]	0.01		-	-	5.9	12.1	1.9	-	-	
2535	[211]	0.02	0.6	-	-	30.6	24.7	2.78	0.81	0.29	
29		0.02	≤ 2.5	-	-	31.5	27	4.4	1	≤ 1.0	
CS (C110)	[91]	0.30	0.47	0.007	0.001	0.01	1.01	0.78	0.01	0.23	
CS (T95)	[110]	0.33	0.34	0.009	0.001	0.03	1.01	0.79	0.02	0.27	
CS (C110)		0.30	0.47	0.007	0.001	0.01	1.01	0.78	0.01	0.23	
CS (Q125)		0.26	0.49	0.012	0.001	0.04	0.91	0.26	0.03	0.21	
3Cr	[134]	0.16	0.51	0.009	0.002	0.05	3.02	0.35	-	0.22	Al 0.02
N80	[116, 135]	0.05	1.4	0.03	0.03	0.18	0.03	0.19	0.048	0.23	Al 0.015

Steel	Ref.	C	Mn	P	S	Ni	Cr	Mo	Cu	Si	Other
X70	[93]	0.054	1.53	0.011	0.0052	0.05	0.013	0.209	0.01	0.266	V 0.014, Al_s 0.019, Al_t 0.021, Ca 0.0015, Nb 0.039, Ti 0.015, Sn 0.017, N 0.0085, As 0.012
P110	[137]	0.28	0.60	0.012	0.0025	0.016	1.00	0.16	0.052	0.26	Nb <0.001, V 0.0046, Ti 0.0024, B 0.0003, Al 0.0021
3Cr*	[144]	0.37	0.51	< 0.02	< 0.009	0.03	3.37			0.48	Ti 0.01
X65	[145]	0.12	1.27	0.008	0.002	-	0.11	0.17	-	0.18	
5Cr		0.38	0.4	-	-	-	5.00	1.30	-	1.00	

* Compositions are given in atomic percent.

Table A2 Chemical composition of dissolvable Al-based alloys.

Alloys	Ref.	Zn	Mg	Cu	Sn	Ga	In	Al	Others
Alloy 1	[345]	-	6.00	6.00	5.00	3.00	0.00	Bal.	
Alloy 2		-	6.00	6.00	5.00	3.00	0.50	Bal.	
Alloy 3		-	6.00	6.00	5.00	3.00	1.00	Bal.	
Alloy 4		-	6.00	6.00	5.00	3.00	3.00	Bal.	
Alloy 5		-	6.00	6.00	5.00	3.00	5.00	Bal.	
DA13	[28]	8.00	2.40	7.55	0.25	0.88	0.37	Bal.	4.20 Ag, 0.19 Cr, 0.50 Zr, 0.03 Ti, 0.01 V
DA18		12.00	2.40	7.55	0.50	1.75	0.75	Bal.	0.70 Ag, 1.00 Cr, 0.03 Ti, 0.01 V
DA25		12.00	2.40	11.00	0.25	0.88	0.37	Bal.	2.14 Ag, 0.19 Cr, 1.00 Zr, 0.03 Ti, 0.01 V
DA27		12.00	2.40	11.00	0.25	0.88	0.37	Bal.	2.14 Ag, 1.00 Cr, 0.50 Zr, 0.03 Ti, 0.01 V

Table A3 Guidelines on corrosion allowance for different oilfield components [308].

Components	Corrosion allowance
Pipelines with dry gas or non-corrosive fluids	No CA
Carbon steel piping	CA typically 3 mm
Submarine pipeline systems	Max. CA 10 mm
Sour lines, vessels, and heat exchangers with pH_2S < 10 psi	CA 4.5 mm
Sour lines, vessels, and heat exchangers with pH_2S > 10 psi	CA 6 mm

Table A4 General guidelines for the use of CRA in oil and gas applications based on specific conditions [308].

Condition	CRA Material	Application/Notes
Sweet service, T < 100 °C	9Cr-1Mo [a]	Surface equipment or instrumentation
Sweet service, $[Cl^-]$ < 15 g/L	13Cr steel [a]	-
HT oxidation (e.g., *in situ* combustion injection)	13Cr steel	-
Sour service, pH_2S < 1.5 psi	13Cr steel	Suitable for any chloride and temperature conditions in oil and gas applications
Sulphur recovery handling	18Cr steel (SS304L)	Used in gas sweetening plants.
Handling wet CO_2 gas	SS316	
Sour service, pH_2S < 3 psi, $[Cl^-]$ < 100,000 ppm	Cold-worked duplex/super duplex steel	-
Sour service, pH_2S < 10 psi, $[Cl^-]$ < 100,000 ppm	Annealed duplex steel	-
Any pH_2S value, no sulphur	Ni-Cr-Mo alloys (Ni > 22 %), Alloy 28, Incoloy 825	-
Sour service, pH_2S < 70 psi, T < 204 °C	Incoloy 625	Suitable for any sulphur and chloride concentrations.
Severe conditions, pH_2S > 70 psi, T < 232 °C	C-276	Suitable for any sulphur and chloride concentrations.
Various (economic considerations)	CRA material cladding on carbon steel	Reduce project costs and improve feasibility
Sour service, beyond pH_2S > 1.5	Modified 13Cr alloys (2Mo-5Ni)	For environmental considerations, otherwise fit for duplex. Assessed case-by-case based on chloride level, *in situ* pH, and design temperature.
pCO_2 up to 1,500 psi, T 160 °C, 20 % NaCl	Modified 13Cr alloys (2Mo-5Ni)	Higher strength and toughness compared to API 5CT grade 13Cr steel
pCO_2 up to 1,500 psi. T < 198 °C, 20 % NaCl	15Cr steel	-

[a] conforming to API 5CT or API 5L